2021

PREDICTION OF NOISE EMISSIONS USING PANEL CONTRIBUTION ANALYSIS SUPPLEMENTED WITH SCALE MODELING

Gong Cheng
University of Kentucky, inter1908cg@gmail.com
Author ORCID Identifier:
https://orcid.org/0000-0002-2238-9489
Digital Object Identifier: https://doi.org/10.13023/etd.2021.115

Right click to open a feedback form in a new tab to let us know how this document benefits you.

STUDENT AGREEMENT:

I represent that my thesis or dissertation and abstract are my original work. Proper attribution has been given to all outside sources. I understand that I am solely responsible for obtaining any needed copyright permissions. I have obtained needed written permission statement(s) from the owner(s) of each third-party copyrighted matter to be included in my work, allowing electronic distribution (if such use is not permitted by the fair use doctrine) which will be submitted to UKnowledge as Additional File.

I hereby grant to The University of Kentucky and its agents the irrevocable, non-exclusive, and royalty-free license to archive and make accessible my work in whole or in part in all forms of media, now or hereafter known. I agree that the document mentioned above may be made available immediately for worldwide access unless an embargo applies.

I retain all other ownership rights to the copyright of my work. I also retain the right to use in future works (such as articles or books) all or part of my work. I understand that I am free to register the copyright to my work.

REVIEW, APPROVAL AND ACCEPTANCE

The document mentioned above has been reviewed and accepted by the student's advisor, on behalf of the advisory committee, and by the Director of Graduate Studies (DGS), on behalf of the program; we verify that this is the final, approved version of the student's thesis including all changes required by the advisory committee. The undersigned agree to abide by the statements above.

<div align="right">

Gong Cheng, Student

Dr. David W. Herrin, Major Professor

Dr. Alexandre Martin, Director of Graduate Studies

</div>

PREDICTION OF NOISE EMISSIONS USING PANEL CONTRIBUTION
ANALYSIS SUPPLEMENTED WITH SCALE MODELING

_____

DISSERTATION
_____

A dissertation submitted in partial fulfillment of the
requirements for the degree of Doctor of Philosophy in the
College of Engineering
at the University of Kentucky

By

Gong Cheng

Lexington, Kentucky

Director: Dr. David W. Herrin, Professor of Mechanical Engineering

Lexington, Kentucky

Copyright © Gong Cheng 2021
https://orcid.org/0000-0002-2238-9489

ABSTRACT OF DISSERTATION

PREDICTION OF NOISE EMISSIONS USING PANEL CONTRIBUTION
ANALYSIS SUPPLEMENTED WITH SCALE MODELING

Panel contribution analysis (PCA) can be used to predict machinery noise emissions, component contributions, and to assess the impact of sound reduction treatments. PCA is a measurement approach that is advantageous for complex machinery that is not easily modeled using conventional numerical analysis approaches. In this research, PCA is combined with scale modeling in order to speed up the necessary measurement work. It is demonstrated that the method can be applied to machinery and that noise emissions can be assessed prior to locating and installing the equipment. This eliminates the necessity to use voluminous anechoic chambers.

The machinery is first discretized into a collection of panels or patches. Volume velocities are measured for each patch with the machinery operating, and transfer functions are measured between patches and receiver locations with the machinery turned off. It is shown that transfer functions may be measured using a scale model. Then, the sound pressure level produced by the machinery is predicted. The method is first applied to a generator set and a 1/2 scale model is used to measure the acoustic transfer functions. It is demonstrated that PCA can be used to predict sound pressure levels in the far-field of a source even using a relatively small hemi-anechoic chamber. PCA was then used to assess the efficacy of barrier treatments.

The PCA and scale modeling combination were then applied to an interior acoustics scenario. The acoustic emissions from three similar air handlers positioned throughout a bakery were predicted at two locations. Transfer functions were measured between the panels and three different customer locations using a 1/10th scale model. Transfer functions were corrected to account for air attenuation and predicted sound pressure levels compare well with measurement. The described approach may be used to determine the sound pressure levels in large interior spaces before they are constructed so long as volume velocities on the source can be measured a priori. In addition, strategies, such as barriers and sound absorption, to reduce the noise by modifications to the acoustic path were accurately assessed prior to equipment installation.

PCA was then applied to a small unmanned aerial vehicle (UAV) and the sound pressure level was predicted 5.5 m away. In this case, both the panel volume velocities and sound pressures must be measured because the boundary encompassing the source is no longer semi-rigid. Measurements were performed on six measurement surfaces forming an imaginary box encompassing the UAV. A P-U Probe was utilized to measure both sound pressure and particle velocity on the imaginary surfaces. Acoustic transfer functions between the source and a receiver point were measured reciprocally. The noise level was predicted from measurements close to the UAV assuming both correlated and uncorrelated sources at the receiver point. The sound pressure level calculated by the correlated model compared well with direct measurement.

KEYWORDS: panel contribution analysis, vibro-acoustics reciprocity, transfer function, Microflown, P-U Probe, UAV

<div style="text-align: center">

Gong Cheng
Student's Signature

May 11, 2021
Date

</div>

PREDICTION OF NOISE EMISSIONS USING PANEL CONTRIBUTION
ANALYSIS SUPPLEMENTED WITH SCALE MODELING

By

Gong Cheng

Dr. David W. Herrin
Director of Dissertation

Dr. Alexandre Martin
Director of Graduate Studies

May 11, 2021
Date

ACKNOWLEDGEMENTS

TABLE OF CONTENTS

LIST OF TABLES

LIST OF FIGURES

Chapter 1   INTRODUCTION

1.1   Research Background

Industry is increasing their efforts to reduce noise emissions from their products. Low noise products are required by regulations in some industries and are essential for products to be competitive in others. Not surprisingly, the considerable academic and industrial effort has been invested in developing and then implementing noise reduction strategies. In the aerospace and automotive industries, dedicated engineering teams use simulation software to drive design for noise and several commercial diagnostic strategies are available after a prototype has been manufactured. However, noise expertise is lacking in other industries. Examples include power generation machinery, mining equipment, food preparation systems, and manufacturing equipment. In many instances, noise problems are not dealt with until the equipment is transported to and installed at the site.

Noise is assessed by making sound pressure level measurements with a microphone at locations in the field. Standards often call for the locations to be several meters away from the source. If that is the case, it is preferable if measurements are performed in a large, reflection free environment prior to siting. This requires special facilities such as hemi-anechoic chambers or outdoor test pads. In most cases, measurements are performed and then noise mitigation treatments are added to the equipment. It is not uncommon for equipment to be several meters in length or height. In that case, equipment must be transported

and installed at the facility which will need to be several times larger than the equipment itself. Facilities of this scale are uncommon and expensive.

In other cases, the industry is more concerned about limiting worker exposure to high sound pressure levels. Often, workers are not permitted to work a full shift without wearing noise protection gear such as ear plugs or ear muffs. It is in the economic interest of industry to reduce sound pressure levels to maximize worker effectiveness and to minimize the use of personal protective equipment which sometimes interferes with communication at the work site.

Reducing machinery noise in the early design stages requires dedicated experts, advanced simulation software, and expensive laboratory equipment. Noise and vibration engineering teams are well-established in high volume industries like automotive, aerospace, and climate control. However, these teams are non-existent elsewhere. Equipment is manufactured in small volumes and the commercial pressures do not exist which compel designing for low noise.

Consequently, these industries often manufacture equipment and install it at the site with little a priori effort at reducing noise in the earlier design stages. Due to the size and complexity of their equipment, there is little opportunity for using simulation to reduce the noise levels in advance. Hence, noise control measures must be implemented after the equipment is assembled.

For these industries, diagnostic approaches that can be applied in acoustically non-ideal environments are needed to both predict the sound pressure level after installation and to determine the contribution from different source

components. Unfortunately, treatments are less than ideal and are more expensive when applied on an ad hoc basis.

There are some commercially available noise diagnostic systems. Some of the more popular commercial systems combine planar beamforming methods (Bai et al., 1998) with near-field acoustic holography (NAH) (Cho et al., 2009). The former method is used to locate problem locations, and then the latter is used to visualize the vibration on the source surface. However, these systems are unable to predict the sound pressure level prior to installation at the customer site. Moreover, these methods cannot be used to assess the effect of treatments.

For large scale industrial equipment, noise assessments will continue to be performed after the equipment is built for the foreseeable future. Nevertheless, equipment can be evaluated before it is transported and installed at the site. The research in this thesis details an approach for performing sound pressure level predictions before locating the equipment. This approach is commonly referred to as panel contribution analysis.

Panel contribution analysis was primarily developed by Fahy (1995 and 2003) and Verheij (1997). Measurements are performed in two steps which can be performed in any order. 1) The source is discretized and volume velocities are measured with the source operating at each panel or patch. 2) Transfer functions are measured between the sound pressure in the field and the volume velocity of each patch. Once the measurements are performed in 1) and 2), the data can be used a) to determine the sound pressure level at the receiver locations and b) to determine the contributions from single patches or groups of patches.

Though the general procedure has been well established for decades, there has been minimal research to improve the method outside of the development and use of particle velocity sensors. Moreover, the success of panel contribution analysis depends on properly discretizing a system into patches and determining the volume velocities. Sound pressure levels may then be predicted assuming that patch sources are correlated or uncorrelated with respect to one another.

The research in this thesis aims to significantly enhance the procedure by demonstrating that acoustic transfer functions can be measured via the use of scale models. This eliminates the need to use large and voluminous anechoic chambers that are several times larger than the source. Moreover, this is a key development to being able to use the method to predict the sound pressure level and the impact of acoustic treatments like barriers and shielding prior to installing equipment at a customer site. Panel contribution analysis is first illustrated using a motorcycle engine. This is a relatively standard and straightforward application of the process.

The approach is then combined with scale models to investigate noise emissions from a generator set. The generator set is a typical exterior sound radiation case. Following this, the method is applied to determine the noise emissions from HVAC equipment in a bakery. This example is typical of many interior architectural acoustics problems. For both applications, modifications like barriers and adding sound absorption are considered.

The panel contribution analysis method is then applied to predict the sound radiation from an unmanned aerial vehicle or UAV. The UAV is a challenging

example because the volume velocities and sound pressures are measured on an imaginary box that encompasses the UAV. Since this imaginary box has no semi-rigid structure associated with it, both the sound pressure and particle velocity must be measured and corresponding transfer functions must be measured between the sound pressure and particle velocity on the source and the sound pressure at the receiver location.

1.2　Objectives of Research

The main objectives of this research are to:

1) Demonstrate that acoustic transfer functions can be measured using scale models. Doing so is critical to the ability to predict sound pressure levels prior to installation at a site.

2) Demonstrate that panel contribution analysis is applicable to both exterior and interior vibro-acoustics problems.

3) Demonstrate that panel contribution analysis can be used to assess the effectiveness of noise mitigation procedures such as introducing barriers or sound absorptive treatments. This will be shown using transfer functions measured on the actual equipment as well as scale models.

4) Demonstrate that contributions can be determined from different source components using both full-scale and scale models.

5) Apply panel contribution analysis to determine the noise emissions from a complicated source without a clear external structure. A UAV is selected as the test structure.

1.3   Outline of Dissertation

The dissertation is organized as follows.

Chapter 2 introduces PCA. Previous work on the method is reviewed and then the method is illustrated on a motorcycle engine.   This example shows the need to develop guidelines for selecting patch sizes and measuring volume velocities.   In addition, the ability of the procedure to determine component contributions is illustrated.

In Chapter 3, PCA is applied to a generator set. It is shown that scale models can be used to determine acoustic transfer functions and also to assess the effectiveness of barrier treatments.

Chapter 4 considers an interior acoustics case where PCA and scale modeling are applied to predict noise from the air handling system in a bakery. The effectiveness of sound absorbing treatments and barriers are investigated. In addition, the effect of air absorption is included in the calculation of scale modeled transfer functions.

Chapter 5 details a study where PCA is used to predict the sound pressure level from a hovering unmanned aerial vehicle (UAV).   This case is challenging because patches cannot be located on the surface of the UAV structure. Since patches are no longer located on an actual surface, the equations for PCA must be adjusted to included measurement of the volume velocity and sound pressure on the patch.

The thesis is summarized and future research directions are suggested in Chapter 6.

Chapter 2   BACKGROUND

The equations for panel contribution analysis (PCA) will be derived from first principles.   The subsequent development and history of the method will be summarized.   This will include an introduction to vibro-acoustic reciprocity: a commonly used strategy which speeds up PCA and makes it practical. In addition, combination sound pressure – particle velocity probes (P-U probes) are now commonly used in PCA and are useful to expedite the process. The workings of these probes are detailed explained. PCS is then demonstrated by applying it to a motorcycle engine on a test stand.

2.1   Panel Contribution Analysis (PCA) Derivation

The principles of panel contribution analysis are derived following Zheng et al. (1994) and Kim et al. (1997). The sound pressure in the far field can be expressed using the Helmholtz integral equation as

$$p(P) = \int_S \left(i\rho\omega v_n G(r) + p_s \frac{\partial G(r)}{\partial n} \right) dS \tag{2.1}$$

where v_n and p_s are the normal velocity and sound pressure on a vibrating surface. $G(r)$ is a suitable Green's function, n is the unit normal vector directed towards the acoustic domain, and r is the distance from a point on the surface of the vibrating surface to point P. If Equation (2.1) is used in the boundary element method, the free-space Green's function is used.   The free spaced Green's function is expressed as

$$G(r) = \frac{e^{-jkr}}{4\pi r} \tag{2.2}$$

8

where k is the acoustic wavenumber and r is the distance from a point source to a receiver position in the field. Equation (2.1) can be solved so long as the normal velocity, sound pressure or the relationship between them is known on each point on the boundary.

If a hard boundary is assumed, the first term on the right-hand side is the summation of all the volumetric velocity sources on the boundary and the second is the scattering effect from the rigid boundary on the acoustic field from each of the volumetric point sources. If a Green's function is instead chosen consisting of the direct field radiation term and the scattered sound from the remainder of the boundary, $\partial G(r)/\partial n$ is equal to zero. In that case, the sound pressure in the field can be expressed as

$$p(P) = \int_S i\rho v_n G_B(r)dS \qquad (2.3)$$

where $G_B(r)$ is a blocked Green's function. This blocked Green's function is easily measured. The blocked Green's function can be expressed in transfer function form as

$$G_B(r) = \frac{p}{v_n \delta S} = \frac{p}{Q} \qquad (2.4)$$

where δS is the surface area of a patch on the surface. The product of the normal velocity (v_n) and patch surface area (δS) is equal to the volume velocity (Q).

The blocked Green's function is most easily determined in a reciprocal fashion as illustrated in Figure 2.1 because it is easier to move sensors rather than the source.

Figure 2.1 is reproduced from paper of Fahy (2002) with permission. This idea can be expressed mathematically as

$$\frac{p_1}{v_n \delta S} = \frac{p_2}{Q}$$

(2.5)

where p_1 and p_2 are sound pressure responses identified in Figure 2.1, Q is the acoustic volumetric velocity, and δS is a differential area. These reciprocal transfer functions can be measured using a calibrated volume velocity source and a microphone. If the surface of the vibrating object is discretized, the total sound pressure at a point in the far field can be expressed as a superposition of the source velocity from each subarea having area ΔS_i as

$$p(P) = \sum_{i=1}^{n} (v_n)_i \Delta S_i \big(G_B(r)\big)_i$$

(2.6)

where $(v_n)_i$ and $\big(G_B(r)\big)_i$ are the normal velocity and blocked Green's function of the ith subarea respectively.

(a) Direct Measurement   (b) Reciprocal Measurement
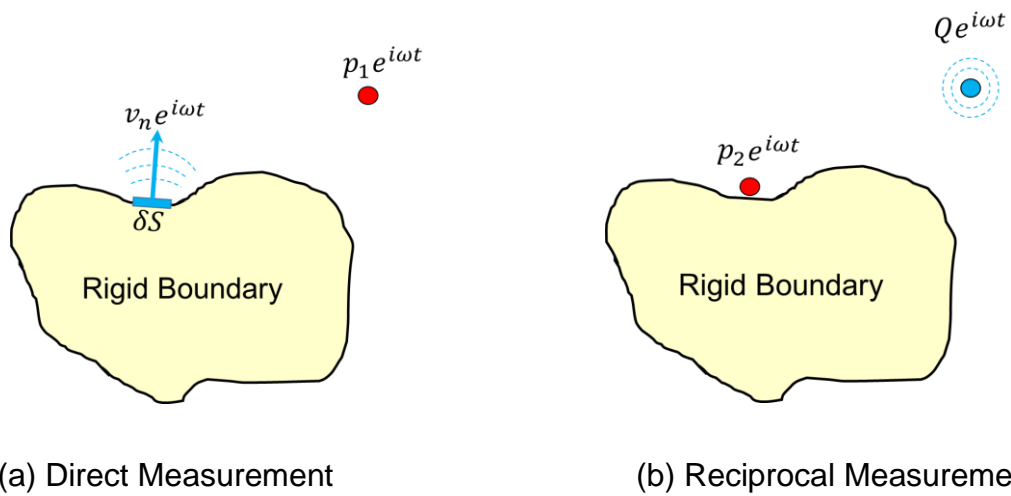
Figure 2.1 Reciprocal measurement of the Green's Function with zero normal derivative at the surface (Fahy 2002).

2.2   Correlated and Uncorrelated Source Assumptions

Equation (2.6) can be applied in two different ways (Fahy, 2002). First, the velocity of a patch can be measured and used directly. In that case, it is preferable that the phase be preserved so an appropriate phase reference should be selected. This approach is known as the correlated monopole assumption. Alternatively, the monopole sources may be assumed to be uncorrelated. It is assumed that the patch sources are located far enough apart so that phase effects can be ignored.

Assume a monopole source, the sound pressure is the superposition of the outbound and inbound wave superposition in the field and can be expressed as

$$p(r,t) = \frac{A_+}{r} e^{j(\omega t - kr)} + \frac{A_-}{r} e^{j(\omega t - kr)} \tag{2.7}$$

where r is the distance between source and the field point, A_+ is the wave amplitude of the outbound wave, A_- the amplitude of an inbound wave, and ω is the angular frequency. Assume that the reflected or inbound wave can be neglected and note that the wave amplitude A_+ includes the $1/4\pi$ term in Equation (2.7).

The particle velocity (u_r) at some distance r can be expressed in terms of the sound pressure as

$$u_r = \frac{j}{\rho \omega} \frac{\partial p}{\partial n} \tag{2.8}$$

via the momentum equation. The volumetric velocity (Q_r) can then be expressed as

11

$$Q_r = 4\pi r^2 u_r \qquad (2.9)$$

at some distance r. It follows that the complex amplitude of the volume velocity is

$$Q_r = 4\pi r^2 \frac{A_+}{\rho cr}\left(1 + \frac{1}{jkr}\right)e^{jkr} \qquad (2.10)$$

assuming that the source forcing function is harmonic with time. In the limit as $r \to 0$, the volume velocity Q_0 can be expressed

$$Q_0 = \frac{4\pi A_+}{j\rho ck} \qquad (2.11)$$

and is notably independent of r.

The sound intensity as a function of distance from the source for an outgoing wave can be expressed as

$$I(r) = \frac{1}{2}\,\mathrm{Re}(p'u_r) \qquad (2.12)$$

where p' is the complex conjugate of the sound pressure. Hence,

$$I(r) = \frac{1}{2}\mathrm{Re}\left(\frac{A_+^2}{\rho cr^2}\left(1 + \frac{1}{ikr}\right)\right) = \frac{A_+^2}{2\rho cr^2} \qquad (2.13)$$

The time averaged sound power through a spherical surface of radius r can then be written as

$$W = I(r)4\pi r^2 = 2\pi \frac{A_+^2}{\rho c} \qquad (2.14)$$

12

Inserting Equation (2.11) into Equation (2.14), the sound power for a point source can be expressed as

$$W = \frac{\rho c k^2}{4\pi} Q_0^2 \qquad (2.15)$$

and is also independent of distance r. The volume velocity amplitude for a patch i can be expressed in terms of the sound power

$$Q_{i0}^2 = \frac{W_i \cdot 4\pi c}{\rho \omega^2} \qquad (2.16)$$

after rearranging Equation (2.15)

For a monopole located close to a rigid baffle, the volume velocity Q_{eq} is

$$Q_{eq}^2 = \frac{Q_0^2}{2} = \frac{W 2\pi c}{\rho \omega^2} \qquad (2.17)$$

which is half the volume velocity for a point source in a free field. The average sound intensity from a patch (I_i) can be measured and the volume velocity (Q_i) can be expressed as

$$Q_i = (v_n)_i S_i = \sqrt{(I_i S_i) \frac{2\pi c}{\rho \omega^2}} \qquad (2.18)$$

since the sound power (W_i) from a patch i can be expressed as $W_i = I_i S_i$. Equation (2.18) can be inserted into Equation (2.6) where Q_i is equivalent to $(v_n)_i S_i$.

13

The uncorrelated approach roughly assumes that a patch is moving uniformly in phase. This assumption should be suitable if a patch is small compared to a structural wavelength. On the other hand, the uncorrelated assumption ignores phase and is likely more appropriate when a patch comprises several structural and/or acoustic wavelengths. If the volume velocities from the patches are assumed correlated, the acceleration for a patch can be measured using accelerometers. In addition, Holland (1997) and Fahy (1997) developed two volume velocity transducers. One consisted of a square cross-section tube, microphone, and anechoic impedance, and the other was comprised of an array of pressure difference microphones positioned in a perforated plastic sheet. More recently, particle velocity sensors or PU probes have been used. The primary advantages are that the volume velocity is directly measured and that the probe is noncontact.

If the uncorrelated assumption is used, the sound intensity is measured. Sound intensity can be measured using a sound intensity probe, which uses two microphones, by scanning or at a location in the center of a patch. More recently, P-U Probes (de Bree, 2003), which consist of a small microphone and particle velocity probe, have been used to measure sound intensity. The primary advantage is that the particle velocity probe is a truly directional sensor and should be less affected by external sources.

The P-U Probe is particularly advantageous for PCA because both the volume velocity and sound intensity are measured simultaneously. Accordingly, measurements can be performed and then both the correlated and uncorrelated

assumptions can be used. Hence, one method does not need to be selected over the other a priori.

2.3   Review Vibro-Acoustics Reciprocity and PCA

The extant literature on panel contribution analysis (PCA) and vibro-acoustics reciprocity will be reviewed in this section. Emphasis will be placed on how reciprocity can be applied to vibro-acoustics applications and PCA specifically.

Lord Rayleigh (1873) concluded that reciprocity need not be restricted to simple sources from which sound would radiate in all directions, and that reciprocity could apply to dissipative systems. However, the principle was not used for practical applications.

Ten Wolde (1973) used electrical network theory to suggest reciprocity relations for acoustical and vibro-acoustic systems. He also noted reciprocal measurements are often advantageous due to their ease because direct measurements often cannot be made due to the size of available sources (either structural or acoustics). Ten Wolde was interested in applying the methodology to marine applications but also suggested application to many other industries. In follow on work, Ten Wolde et al. (1975) demonstrated the method on laboratory examples where direct measurement is difficult. Specifically, transfer functions were determined between an underwater volume velocity source and accelerometers located on the outside of a tank.

Zheng et al. (1994) utilized the vibro-acoustics reciprocity approach to predict the sound pressure of an internal combustion engine and then usefully determined

the contribution from different engine components. This was an early example of PCA. In his measurement campaign, the uncorrelated assumption was used. A sound intensity probe was used to scan the engine surface in order to then determine the volume velocity using. The correlation between measured and PCA predicted sound pressure level was excellent. Moreover, they determined the contributions from the engine block, valve train, and gear box.

Fahy (1995) contributed further by detailing the various ways that the reciprocity principle can be applied. He also clearly laid out the PCA method for both correlated and uncorrelated sources and demonstrated the approach for sound radiation off a panel. Moreover, He dealt with the practicalities of the method by developing a crude volume velocity transducer to estimate the source strength from a patch. He proceeded to experimentally prove the viability of acoustic reciprocity by measuring transfer functions between a sound source inside and a sound pressure exterior to a scale model of an airplane fuselage.

In another application, Kim et al. (1997) utilized PCA and measured the transfer functions reciprocally. They conveniently differentiated the contribution from the tire sidewall and tread to a position on the interior of a vehicle. Conventional source identification approaches like beamforming and near field acoustic holography could not be used to determine the contribution since the receiver is separated from the source by the automobile structure.

Verheij (1997a, 1997b) summarized and further explored PCA in two companion papers that are well regarded. Verheij clearly differentiated between the correlated and uncorrelated monopole assumptions and helpfully detailed the

equations relating sound intensity or power to the volume velocity for use in the uncorrelated approach (Verheij, 1997a). Verheij (1997a, 1997b) also illustrated how a similar approach could be used to rank structural paths and determine an equivalent set of inverse forces called pseudo forces to represent the internal forces of a machine. This structural path ranking approach is often referred to as transfer path analysis and is the structural equivalent of the vibro-acoustical PCA.

Fahy (2002) reviewed the prior work and helpfully consolidated the essentials of the method in one place. Fahy began by reiterating the principle of reciprocity noting the applicability of the approach to vibrational, acoustical, and combination vibro-acoustical situations. Fahy then detailed several industrial applications.

Wolff and Sottek (2005) utilized PCA for vehicle cabin noise assessment and importantly demonstrated that a new combination sound pressure – particle velocity sensor (PU probe) could be used to expedite the procedure (Wolff et al., 2009). The agreement between reconstruction and measured sound pressure showed potential usage of this device for transient inputs. Later, Wolff et al. (2009) assessed the contributions to the interior noise in a passenger compartment while driving.

Hald and Mørkholt (2009) developed an array-based method for measuring the panel contributions in a vehicle cabin. Both the transfer function and the operational data were measured using a dual-layer microphone array. A statistically optimal near field acoustic holography (or SONAH) was used to determine the volume velocities on the surface and then PCA is used to reconstruct the sound pressure in the field and contributions of interest.

17

Comesaña et al. (2011) developed a similar scanning method for source visualization and transfer path analysis in an automobile. This approach used only a single P-U Probe with a camera tracking the sensor motion. This new method can preserve the relative phase information of a stationary sound field.

2.4 Summary of P-U Probe

The combination sound pressure – particle velocity sensor or P-U Probe is a sensor that has two separate transducers. One sensor is a small hearing aid type microphone while the other sensor is a hot wire sensor to measure particle velocity. While the microphone is standard but small, the particle velocity sensor is a novel device. H-E. de Bree (1996a, 1996b) introduced this micro-electronics mechanical sensor (MEMS) that consists of two very closely spaced wires parallel wires as is shown in Figure 2.2. This figure is reproduced from paper of de Bree (2003) with permission. The platinum wires are each 1 mm in length, and 200 nm in thickness. The wires act like resistors and are heated by electrical power. A temperature increase or decrease changes the resistance of the wires and the associated voltage drop. Perturbations in temperature can be related to the acoustic particle velocity.
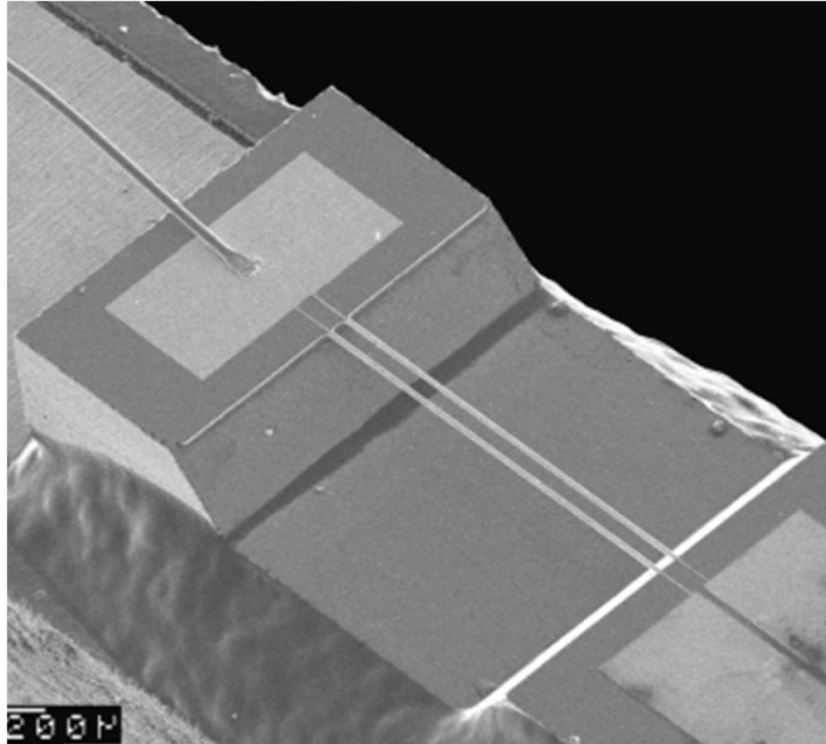
Figure 2.2 SEM photo of hot wires in a Microflown sensor (de Bree, 2003)

Figure 2.3 shows the construction of the PU probe (de Bree, 1997). Observe that the sensor consists of the hot wire probe and miniature microphone that are housed inside a cylinder so that they are reasonably durable. The sensor used in this research is the 1/2 inch (1.25 cm) diameter probe. There is also a windscreen that surrounds the sensors so that measurements can be performed in low steady flow environments. The operational temperature for the hot wires is approximately 300°C. Perturbations in hot wire temperature are particle velocity direction dependent, and the positive or negative character (i.e., phase) of the velocity can be identified. The specific directivity of the sensor forms a figure of eight as shown in Figure 2.4, so the transducer sensitivity drops off rapidly in other directions than the intended measurement direction.
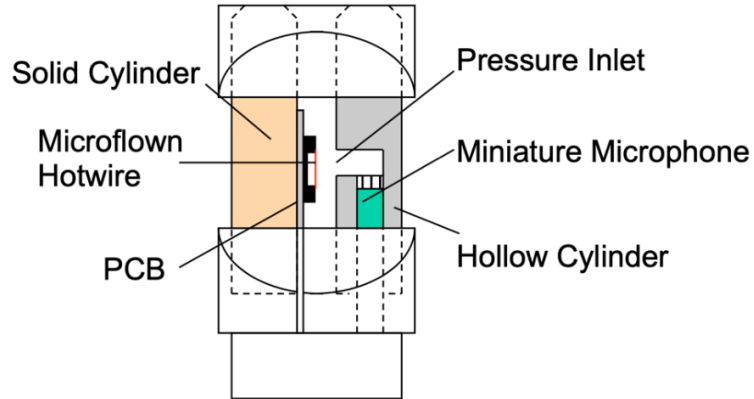
Figure 2.3 Layout of Microflown P-U Probe
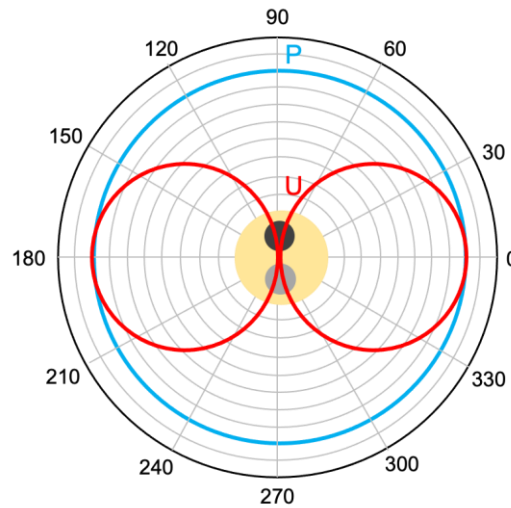
Figure 2.4 Directivity of microphone versus particle velocity sensor (Microflown Ebook 4A Standard Calibration Technique)

The sensor does respond linearly to increases in particle velocity for sound pressure levels up to approximately 135 dB (Microflown Ebook). However, the calibration of the probe is not constant with frequency. To calibrate the P-U Probe, a loudspeaker can be positioned facing up on the floor of a hemi-anechoic chamber (Jacobson et al., 2006). A P-U Probe and a measurement grade free-field microphone are placed very close to each other as shown in Figure 2.5. The

20

sensors should be located at some distance from the source and preferably in the acoustic far field. In this research, the sensors are located 1.14 m (45 inches) above a subwoofer and 2.03 m (80 inches) above a high frequency compression driver for calibration at low and high frequencies respectively.
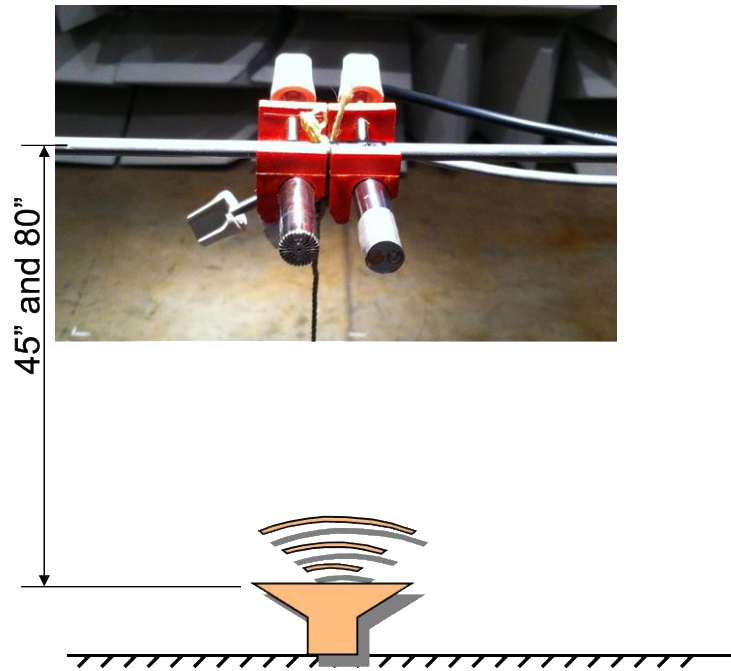
Figure 2.5 Calibration campaign of Microflown P-U Probe in a free-field

The free-field PCB pre-polarized condenser microphone (the left sensor in Figure 2.5) has a nearly flat sensitivity curve (PCB Manual) and is used as a reference sensor to calibrate the amplitude and phase of the sound pressure probe (embedded in the PU probe which is the right sensor in Figure 2.5). Once the pressure probe has been calibrated, the amplitude and phase of particle velocity sensitivity are obtained by knowing the impedance in a free field. The impedance can be written as

$$Z = \frac{p}{u} = \rho c \frac{jkr}{1+jkr} \qquad (2.19)$$

from which u can be solved.

Researchers at Microflown (de Bree, 1997, 2003) have developed calibration equations. Measurement data is used to adjust the parameters in order to obtain a calibration curve. The amplitude and phase correction of the microphone are expressed as

$$S_p[mV/Pa] = S_p@1kHz\frac{\sqrt{1+(f/f_{c3p})^2}}{\sqrt{1+(f/f_{c1p})^2}\sqrt{1+(f/f_{c2p})^2}} \qquad (2.20)$$

and

$$\varphi_p[deg] = \arctan\left(\frac{C_{1p}}{f}\right) + \arctan\left(\frac{C_{2p}}{f}\right) + \arctan\left(\frac{f}{C_{3p}}\right) \qquad (2.21)$$

respectively. The constants f_{c1p}, f_{c2p}, and f_{c3p} in Equation (2.20) and C_{1p}, C_{2p}, and C_{3p} in Equation (2.21) are all determined via a curve fit. A similar calibration curve is developed for the particle velocity sensor. The sensitivity for magnitude and phase are expressed as

$$S_u \left[\frac{mV}{Pa} \right]$$

$$= S_u @ 250Hz \left(\frac{1}{\sqrt{1 + \left(\frac{f_{c1u}}{f} \right)^2} \sqrt{1 + \left(\frac{f}{f_{c2u}} \right)^2} \sqrt{1 + \left(\frac{f}{f_{c3u}} \right)^2} \sqrt{1 + \left(\frac{f_{c4u}}{f} \right)^2}} \right) \quad (2.22)$$

and

$$\varphi_u[deg] = \arctan\left(\frac{C_{1u}}{f} \right) - \arctan\left(\frac{f}{C_{2u}} \right) - \arctan\left(\frac{f}{C_{3u}} \right) + \arctan\left(\frac{C_{4u}}{f} \right) \quad (2.23)$$

respectively. The calibration constants f_{c1u}, f_{c2u}, and f_{c3u} in Equation (2.22) and C_{1u}, C_{2u}, and C_{3u} in Equation (2.23) are all determined via a curve fit.

The following Figure 2.6(a) and Figure 2.6(b) show the calibrated correction curves for the sound pressure and particle velocity sensors respectively for the P-U Probe used in this research. After the correction curves are determined, the sound pressure and particle velocity are calculated using the equations. This P-U Probe calibration curve can be directly loaded into the Siemens Test.Lab software or can be programmed into Excel or MATLAB.
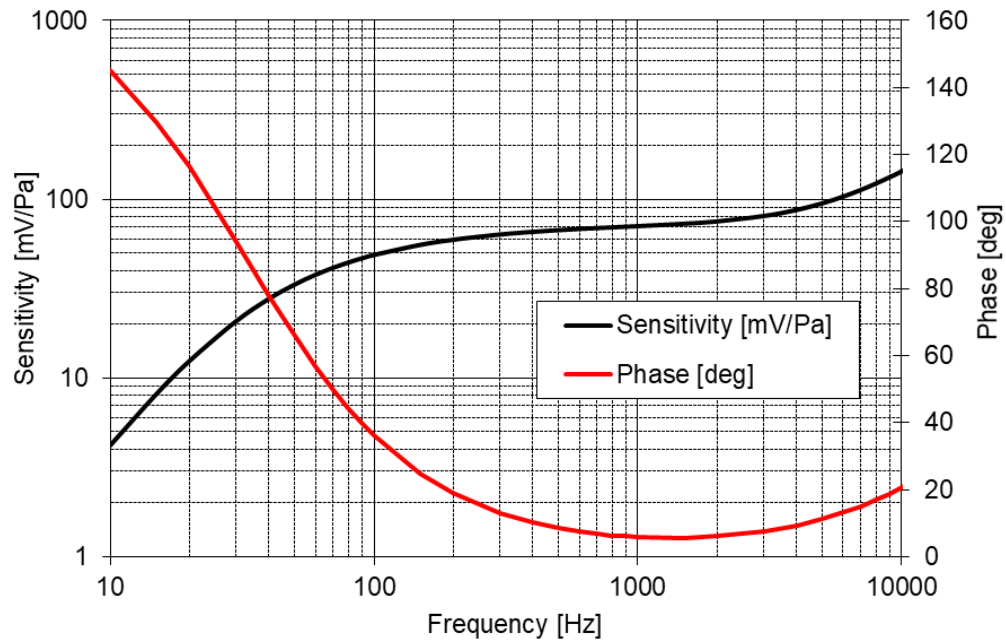
(a) Pressure probe sensor correction curve
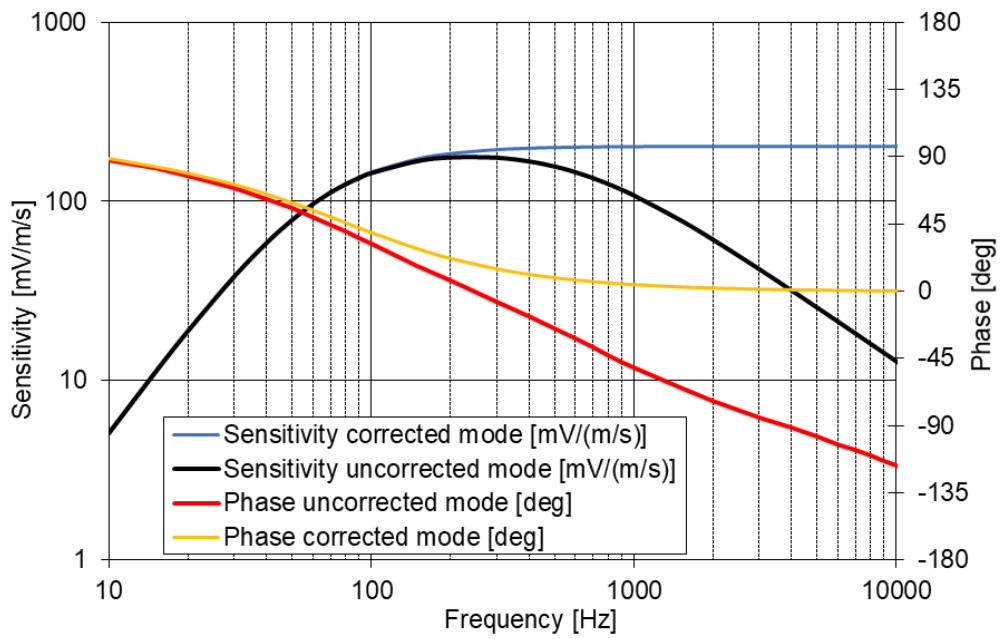
(b) Particle velocity probe sensor correction curve

Figure 2.6 Correction curve of Microflown P-U Probe (Microflown Regular P-U Probe Specification Sheet)

One advantage of the PU-probe is that it can be used to determine the sound intensity directly using Equation (2.12). The customary method for measuring sound intensity is to use two adjacent microphones where the spacing between them governs the frequency range of applicability. There are commercial devices called sound intensity or p-p probes for making these measurements and the algorithms for measuring the intensity are well established (HP application note). The time averaged sound intensity can be computed using the expression

$$\bar{I}_n = \frac{|\tilde{p}_1 \tilde{p}_2'|}{\omega \rho d} \sin(\varphi) \tag{2.24}$$

where $\tilde{p}_1$ and $\tilde{p}_2$ are root mean square sound pressures, d is the distance between the microphone sensors, and φ is the phase difference.

Sound intensity is measured in the direction of the line connecting the centers of the two microphones. If the microphones are phase calibrated, the sound intensity can be determined very accurately. However, measurement accuracy is degraded if there is a source to the side of the probe and perpendicular to the intended measurement direction. A strong signal from the side will introduce measurement noise that will make accurate determination of the phase difference between the two measured sound pressures difficult.

If the PU probe is used instead, the time averaged sound intensity is measured directly, and it does not seem to be very sensitive to phase issues. The key advantage of the PU probes is that the particle velocity probe is directionally sensitive and so data does not need to be processed to identify that directionality.

2.5   PCA Demonstration

(Note: Most of the research in this section has been previously documented in Cheng et al., 2015)

The procedure was demonstrated using a motorcycle engine on a test stand. All tests were performed in the hemi-anechoic chamber at the University of Kentucky with the motorcycle idling (~1050 RPM). The tailpipes were extended using long pipes in an effort to move the exhaust noise sources further from the engine and vent the exhaust. A photograph of the engine on the stand is shown in Figure 2.7 along with the extended exhaust pipes. The engine was divided into five parts: the engine proper, primary housing, transmission housing, exhaust, and other components. Each part was discretized into patches as shown in Figure 2.8.
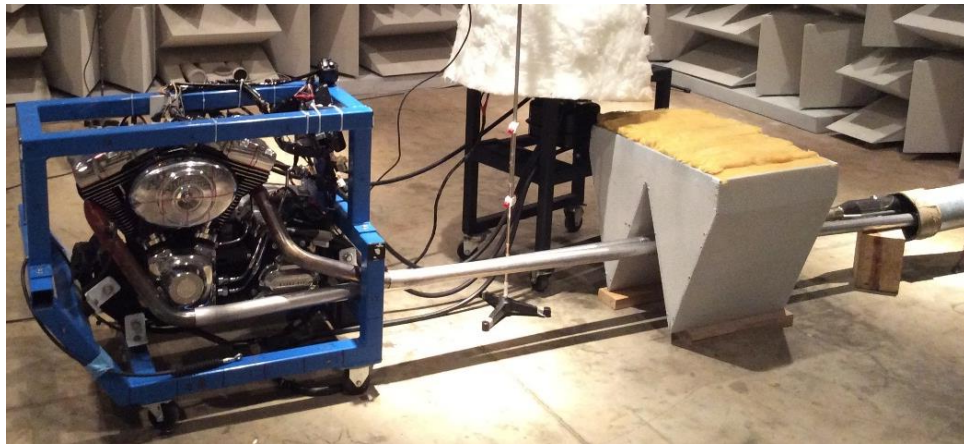
Figure 2.7 Photograph of motorcycle engine set

The transfer functions were measured with the engine turned off taking advantage of vibro-acoustic reciprocity. Two receiver positions were targeted for this demonstration. Target A was located 1.52 m away from the engine side and 1.07 m above the ground as shown in Figure 2.9 (a). Target B was close to the

driver's ear position as shown in Figure 2.9 (b). Accordingly, the volume velocity source was placed at these two positions, and the transfer functions were measured reciprocally.
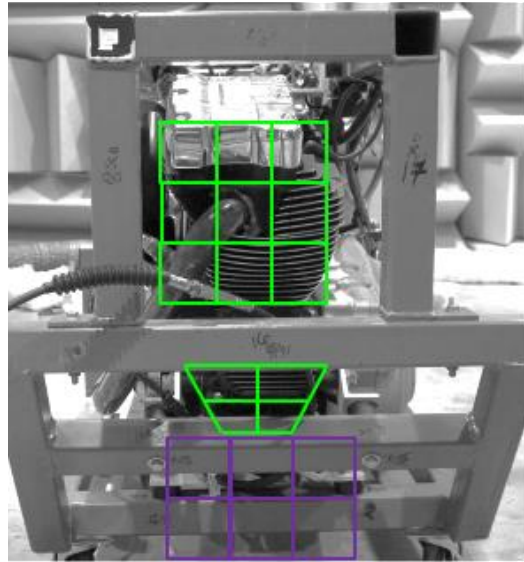
(a)
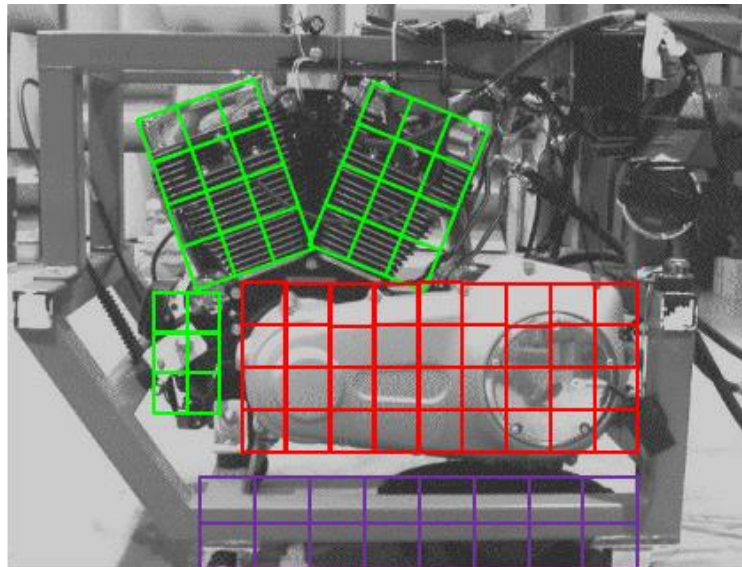
(b)
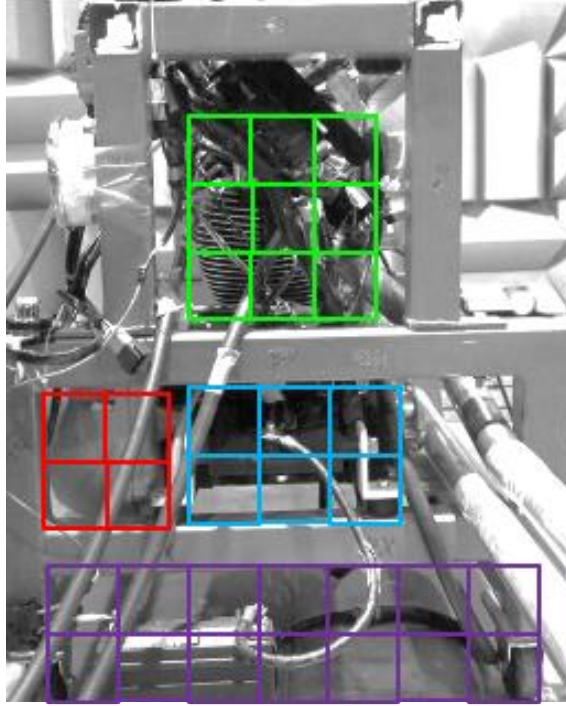
(c)
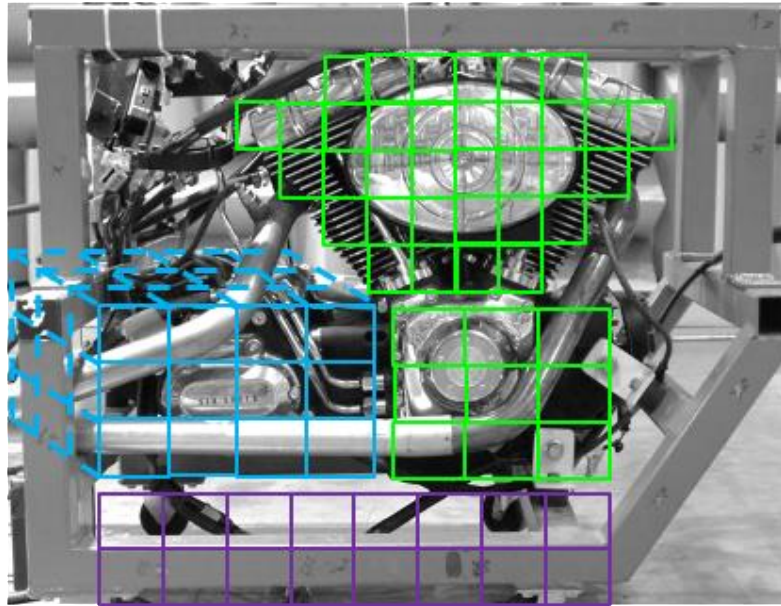
(d)
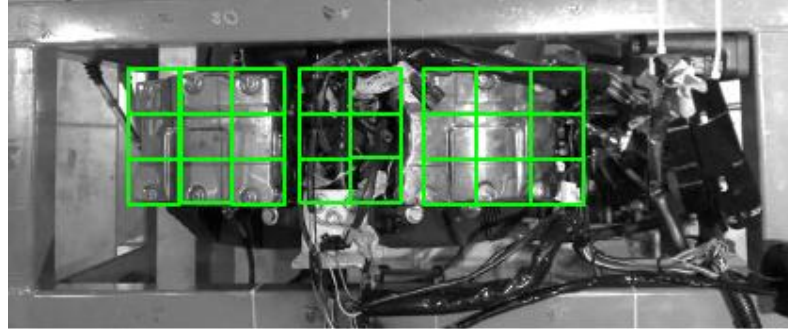
(e)
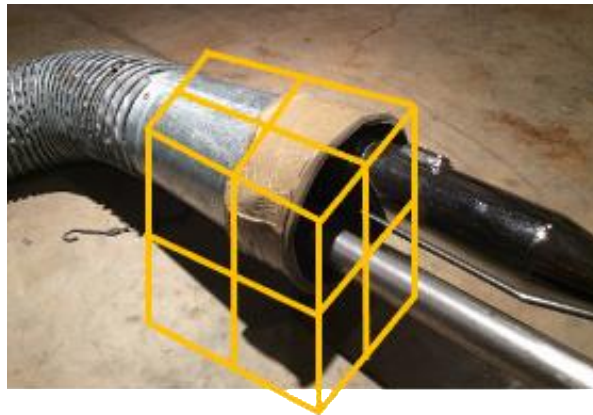
(f)

Figure 2.8 Engine discretization. The 5 components are identified: engine proper (green), primary housing (red), transmission housing (blue), exhaust (yellow), auxiliary components (purple)

For the transfer function measurements, two 1/2-inch free-field type microphones were used. One was placed approximately 1.25 cm from the center of the patch. The other microphone was placed 38 cm away from the volume velocity source and was used to calibrate the source. It was assumed that the source behaved as a point source.

The engine and components were divided into 266 patches. Each patch is approximately 7.6×7.6 cm^2 in size. The engine and other surfaces are curved so the sizing of each patch is approximate. The engine proper consisted of 120

patches, the primary housing of 40 patches, the transmission housing of 36 patches, the exhaust of 20 patches, and the auxiliary components of 50 patches. The exhaust pipes were ignored as a source so only the exhaust outlet was considered. The engine was isolated from the test rig stand using 7 rubber mounts. Since the stand is well isolated, the engine test stand can be neglected in the analysis.

After the transfer functions were measured with the engine turned off in the hemi-anechoic chamber, the engine was set to idle (~1050 RPM), and the P-U Probe was used to measure particle velocity and the sound intensity at the center of each patch. The P-U Probe sampling is shown in Figure 2.10.
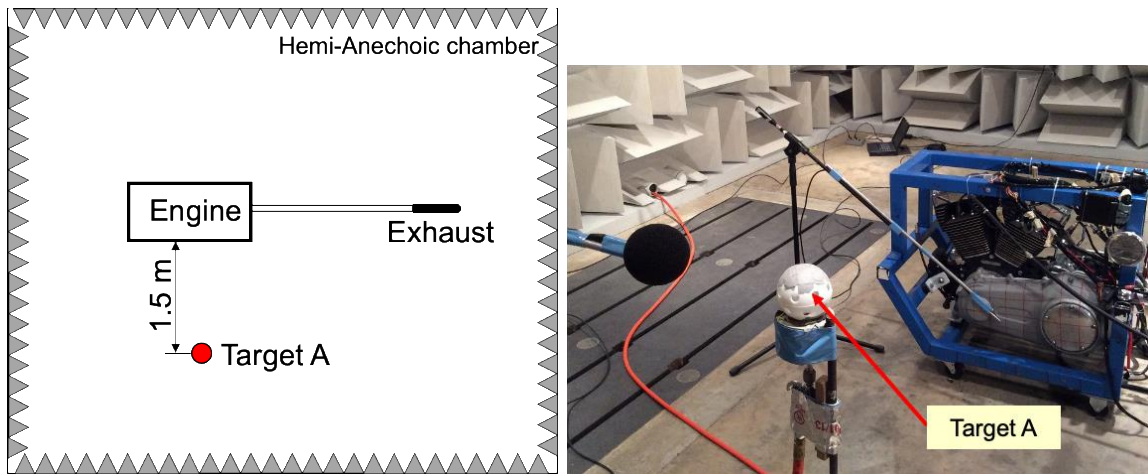
(a) Target A
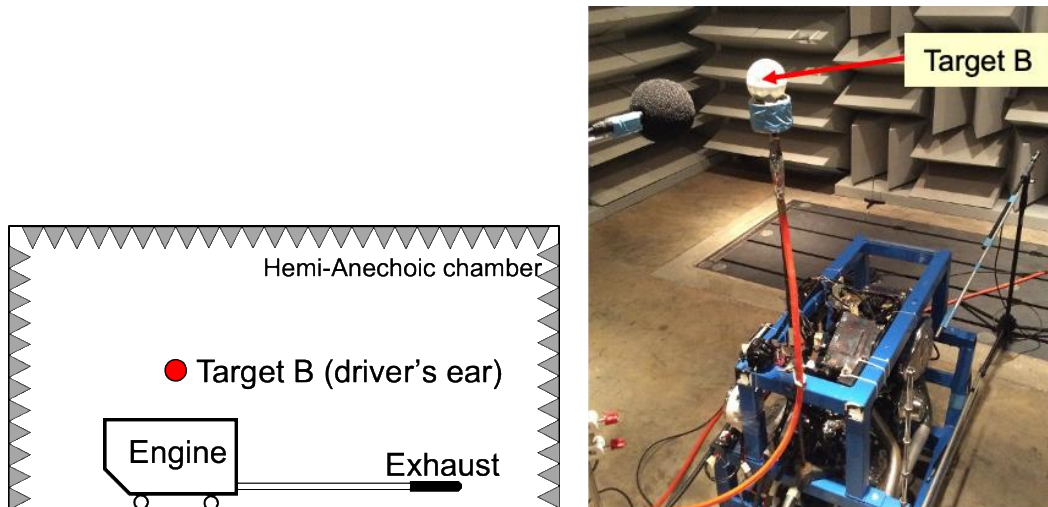
(b) Target B

Figure 2.9 Two sets of transfer functions measurement via reciprocity
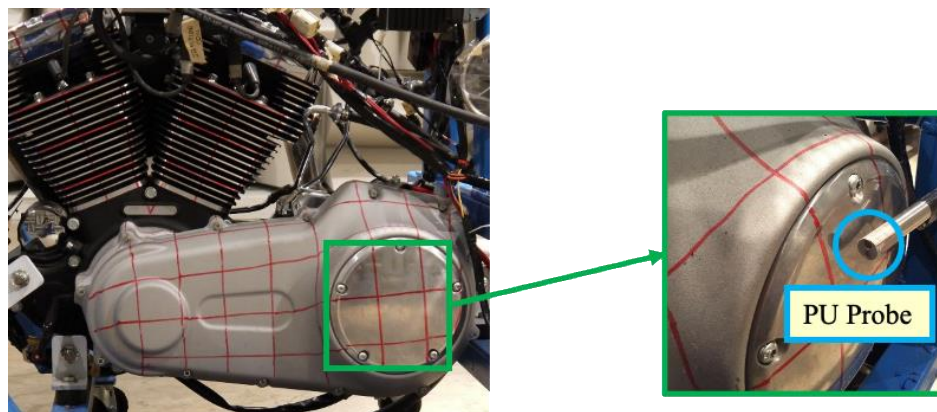
Figure 2.10 Measurement of particle velocity and sound intensity for each patch

Predictions were then made assuming correlated and uncorrelated sources. The reconstructed and measured sound pressures in narrow band and 1/3-octave bands at the Target A position are shown in Figure 2.11 and Figure 2.12 respectively. Results assuming uncorrelated sources compare better with measured results, especially at higher frequencies. The predictions are shown in 1/3-octave bands in Figure 2.12 and compare decently with the measured sound

pressure level, except for a few bands. In this experiment campaign, the P-U probe cannot be positioned closer to the engine surface than 3 cm due to the high temperature of the running engine.
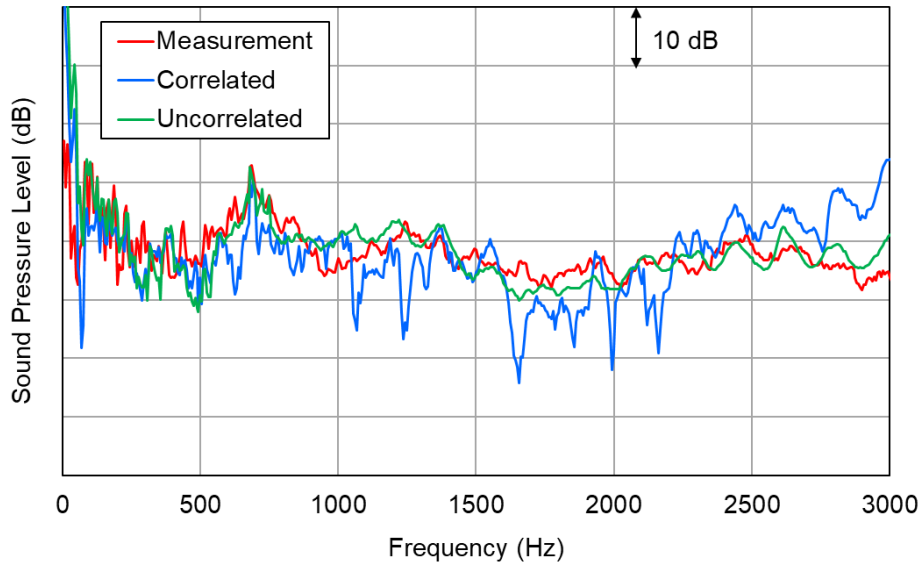
Figure 2.11 Comparison of reconstructed sound pressure at Target A in narrowband
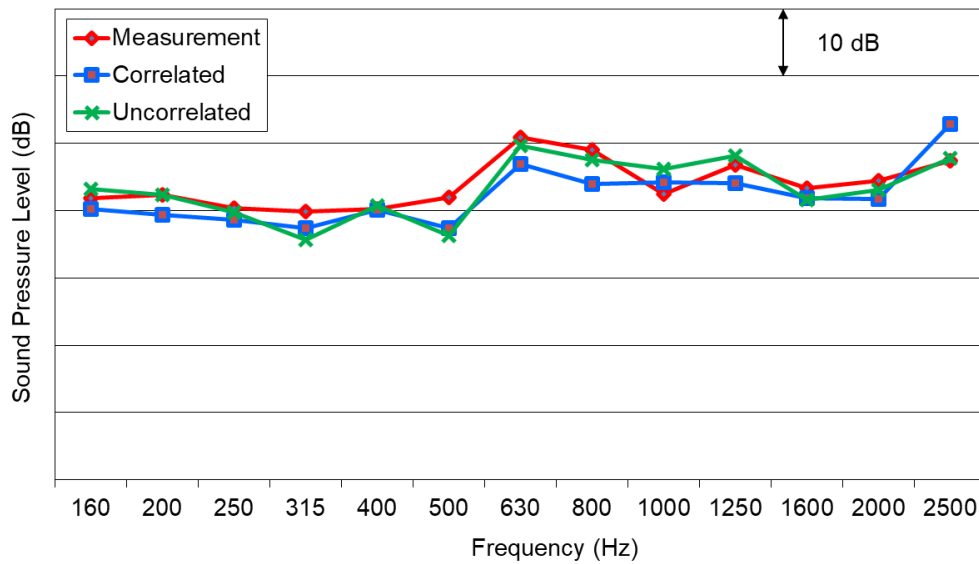
Figure 2.12 Comparison of reconstructed sound pressure at Target A in 1/3 octave band
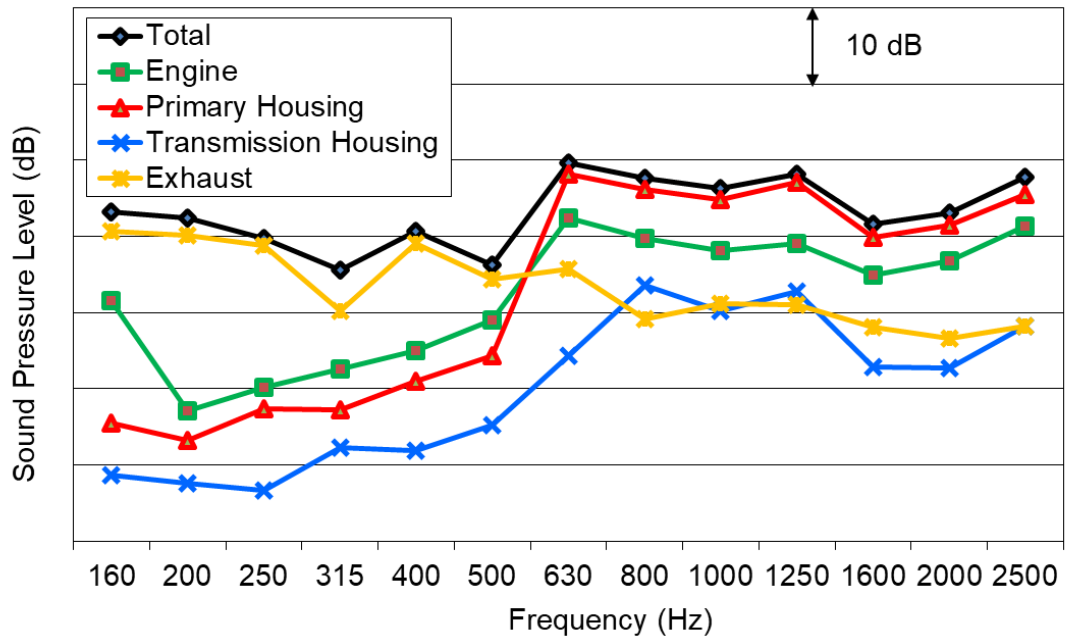
Figure 2.13 Patch contribution to Target A

The contributions to Target A from each of the primary sources assuming uncorrelated sources are shown in Figure 2.13. The approach predicted that the exhaust (even with pipe extended) was the primary source below the 500 Hz 1/3-octave band; while the primary housing dominated above the 630 Hz band. The contribution around the 690 Hz peak shown in Figure 2.11 is mostly from the primary housing. After checking the volume velocity of all the panels, Figure 2.14 shows the main contributory panels at the first firing frequency peak. Similar results are shown for Target B. The reconstructed and measured sound pressures are shown in 1/3-octave bands in Figure 2.15.
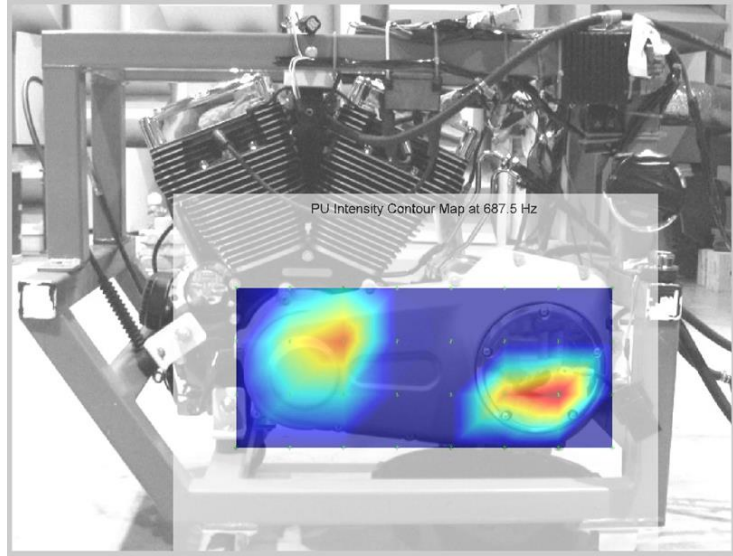
Figure 2.14 Pinpoint the Contributory Panels at Target A at the 1st Firing Frequency at 687.5 Hz
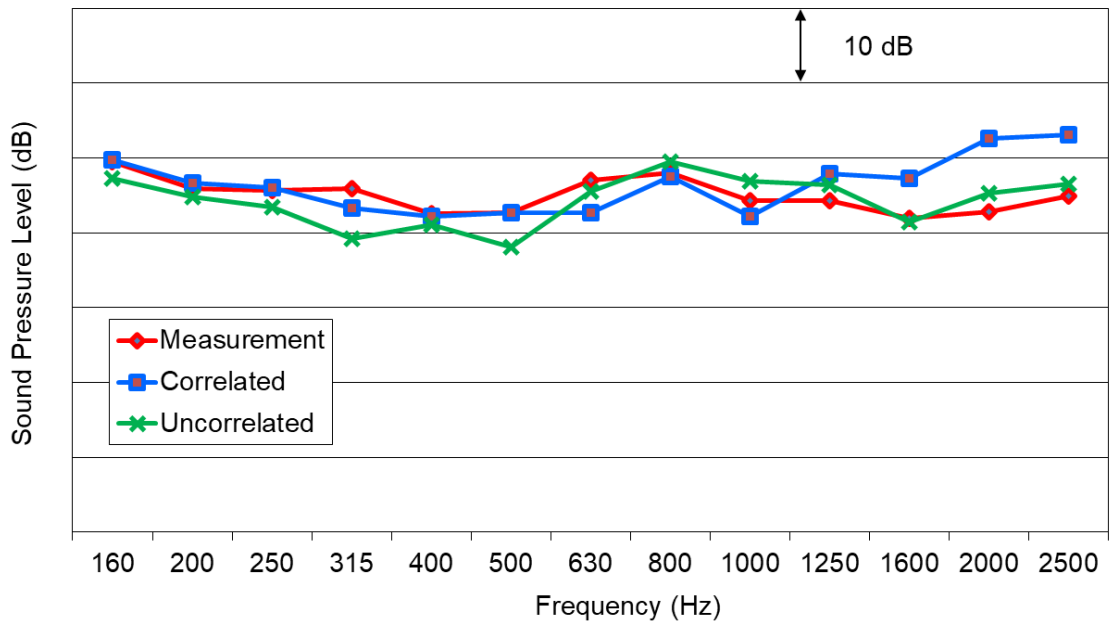
Figure 2.15 Comparison of reconstructed sound pressure at Target B in 1/3-octave bands
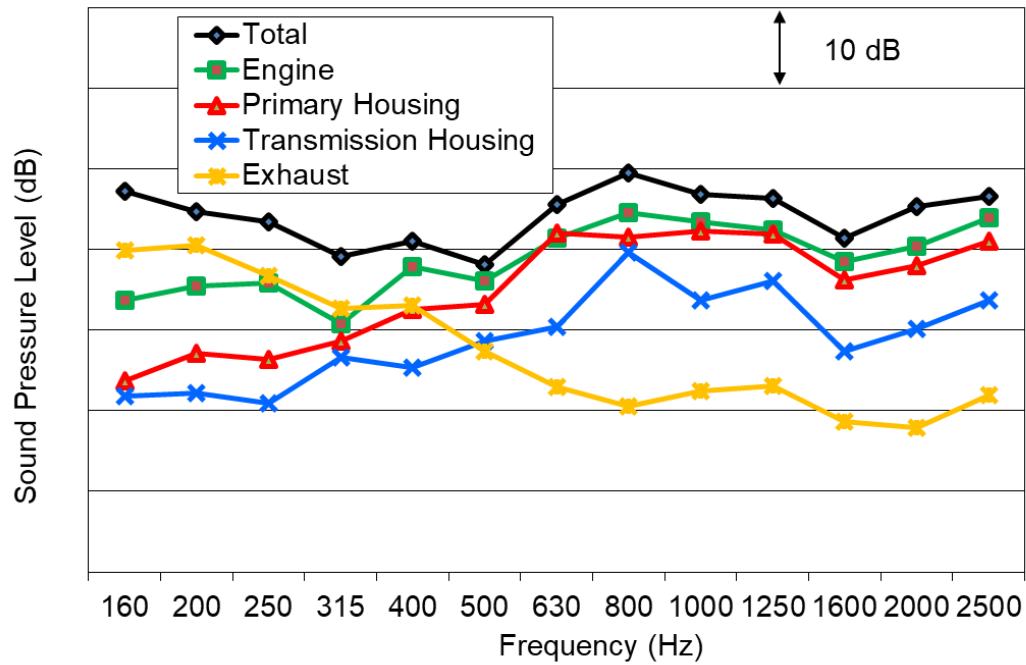
Figure 2.16 Patch contribution to Target B

Results assuming uncorrelated sources compare slightly better with measured results. The contributions to target B from each of the primary sources assuming uncorrelated sources are shown in Figure 2.16. Exhaust noise is dominant at low frequencies while engine noise is more important above 400 Hz.

In this section, Transfer functions were measured reciprocally using an inexpensive volume velocity source which could be utilized in most labs (Liu et al., 2011). The P-U probe proved convenient for determining the volume velocity either by measuring particle velocity directly or the sound intensity. Using the P-U Probe, measurements for particle velocity and sound intensity can be made simultaneously. After which, the sound pressure at points in the field can be reconstructed, and contributions from patches can be considered.

2.6   Summary

In this chapter, the fundamentals of PCA have been developed, and the important PCA literature has been reviewed. The applicability of using PCA in conjunction with vibro-acoustic reciprocity has been shown to be advantageous. PCA can be applied using correlated or uncorrelated sources by measuring particle velocity or sound intensity respectively. Moreover, it has been shown that a novel acoustic transducer, the P-U probe, can be used to make the source measurements for PCA. Specifically, the P-U probe can measure both the sound pressure and particle velocity simultaneously which permits direct measurement of either particle velocity or sound intensity. Hence, data collected is appropriate for both correlated and uncorrelated PCA assumptions.

PCA is then applied to characterize a motorcycle engine on a test stand.

The steps in the PCA process are detailed and it is shown that the PCA can be used to predict the sound pressure level at some distance from the source. Moreover, PCA is used to determine the contributions from different parts of the engine.

Chapter 3   PCA IN EXTERIOR ACOUSTICS AND SCALE MODELING

3.1   Introduction

Climate control, power generation, manufacturing, and other equipment is commonly delivered and assembled at the site where the equipment will be operated. Equipment is so large and complicated that noise tests prior to siting are infeasible due to lack of appropriate facilities by the manufacturers of the equipment. Moreover, noise simulation is ruled out due to the complexity and computational resources required. Hence, noise concerns are addressed after the equipment has been sited when noise mitigation measures are likely to be more expensive and less ideal.

Noise diagnostic approaches typically involve sound pressure level measurements at discrete locations. Sound mapping or beamforming are frequently used to identify major noise contributors. While certainly informative, neither of these approaches are useful for predicting the sound pressure levels or the effectiveness of mitigation methods like adding barriers around equipment prior to locating equipment.

PCA is a straightforward approach where a complicated source is first divided up into several panels or patches. In this chapter, the wording "patch" is used because that seems more descriptive of the approach. For each patch, the volume velocity with the machine operating is measured. The volume velocity may be measured directly using accelerometers or a particle velocity probe (Liu et al., 2011, Tijs et al., 2011, Comesaña et al., 2012). Alternatively, the volume velocity may be inferred by determining the sound intensity from a patch. Approached in

this way, phase is generally ignored, and patch sources are assumed to be uncorrelated with each other. With the source characterized, the missing linkage between the source and sound pressure level in the field are transfer functions relating the sound pressure to the volume velocity of a patch. The transfer function between each position and the receiver location may be measured reciprocally. Fahy (1995, 2003) and Verheij (1997a, 1997b) conducted the early research on PCA and used reciprocity to expedite measurement of the vibro-acoustic transfer functions. A point source is placed at the receiver and the sound pressure is measured at the center of each patch. The point source used at the University of Kentucky is a simple aeroacoustic source that can be inexpensively reproduced at most labs.

After collecting operating and transfer function data, the sound pressure can be predicted in the field. Other researchers have applied PCA to predict engine (Zheng, 1994), aircraft fuselage (Mason 1990), and tire noise (Kim, 1997). In this paper, PCA is applied to predict the sound pressure level in the field as well as the effectiveness of adding barriers to reduce the sound pressure level. This study is aimed at answering the following questions. 1) Can a combination of PCA and scale modeling be used to determine the sound pressure in the field from a source? If so, noise emissions can be predicted without the need to run equipment in voluminous and expensive anechoic chambers. 2) Can the combination of PCA and scale modeling assess the impact of placing barriers around the source? This is particularly pertinent to designing parapets around rooftop climate control or power generating equipment. If so, treatments can be assessed before the

equipment is installed at the site and the cost savings in doing so is anticipated to be significant.

A small generator set is used to test out the approach. Though the generator set is relatively small compared to larger equipment that the method would be used for, the equipment fits well in the hemi-anechoic chamber available and permitted a measurement several meters away from the unit. Moreover, the generator set is typical of much larger equipment. Frequently, regulations specify that the sound pressure emissions must be below a certain level at some predetermined distance from the source. It is demonstrated that a combination of PCA and scale modeling can be used to predict the sound pressure level in the field prior to siting of the equipment.

PCA is briefly reviewed and is then applied to the generator set. The procedures for developing a scale model are reviewed in detail. It is also shown that the procedure can be used to assess the efficacy of treatments and that the contribution from sets of patches can be considered for each treatment.

3.2   Transfer Function Measurement – Scale Model

Helmholtz equation can be used to describe the sound propagation in air and is expressed as

$$\nabla^2 p + \frac{\omega^2}{c^2} p = 0 \tag{3.1}$$

where p is sound pressure, c is speed of sound in the air, and ω is angular frequency. After combining with the equation of motion and continuity equations

(Schuring, 1977), the scaling rule for sound propagation in air can be developed based on Equation (3.1), and is expressed as

$$\frac{\gamma_L^2 \gamma_\omega^2 \gamma_T}{\gamma_c^2} = 1 \tag{3.2}$$

where γ are respective scaling factors, L is a characteristic dimension, T is temperature, and ω is the angular frequency. Assuming that the speed of sound and temperature are the same in both the full-scale and scaled model, Equation (3.2) can be simplified as

$$\gamma_\omega \gamma_L = 1 \tag{3.3}$$

where the scaling of the model is γ_L and is hereafter written as s. The procedure for relating scaled acoustic transfer functions to the full-scale model is now straightforward. Given a geometric scaling factor s, the frequency should be scaled as

$$\omega = \omega_S \cdot s \tag{3.4}$$

and the transfer or Green's functions as

$$G_B = (G_B)_S \cdot s^2 \tag{3.5}$$

where ω_s is the scaled frequency and $(G_B)_s$ is the scaled transfer function. There is no loss of phase information in scaling if Equations (3.4) and (3.5) are used. If the uncorrelated assumption is used, the magnitude of the transfer function $(G_B)_S$ is used in Equation (3.6) and phase is ignored.

These scaled blocked transfer functions can be inserted directly into the discrete form of the Helmholtz integral equation written as

$$p(P) = \sum_{i=1}^{n} (v_n)_i \Delta S_i \big(G_B(r)\big)_i \qquad (3.6)$$

where $(v_n)_i$ and $\big(G_B(r)\big)_i$ are the normal velocity and blocked Green's function of the subarea i respectively. The advantages of using scaled transfer functions is that the measurements of the airborne transmission paths for large equipment can be performed in relatively small anechoic chambers. For example, standards call for measurements to be performed at 7.5 m from the generator set. Performing this measurement in a large hemi-anechoic test chamber requires a voluminous chamber.

3.3   Point Monopole Source

For the scale model, a small volume velocity source was created using a compressed air source, a 3D printed throat, a 4 cm diameter whiffle ball, and duct tape. Compressed air was forced through a nozzle into the whiffle ball and the holes in the ball were shielded with duct tape opposite the nozzle. Figure 3.1 shows a photograph of the source. The source strength was calibrated by measuring the sound pressure at a given distance in the 120 m^2 hemi-anechoic chamber (150 Hz low frequency cutoff) at the University of Kentucky.
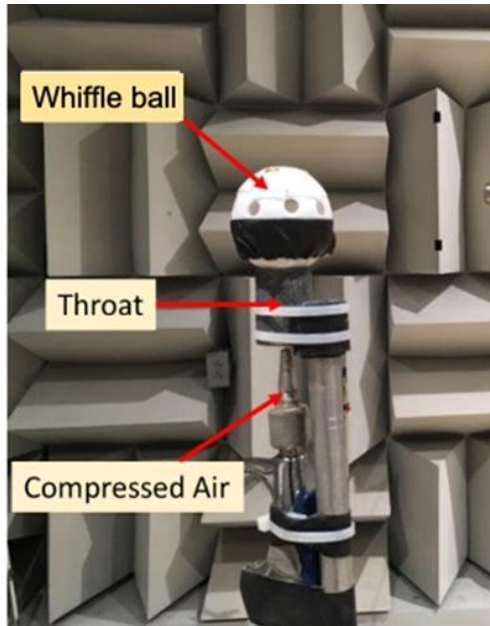
Figure 3.1 Volume velocity source
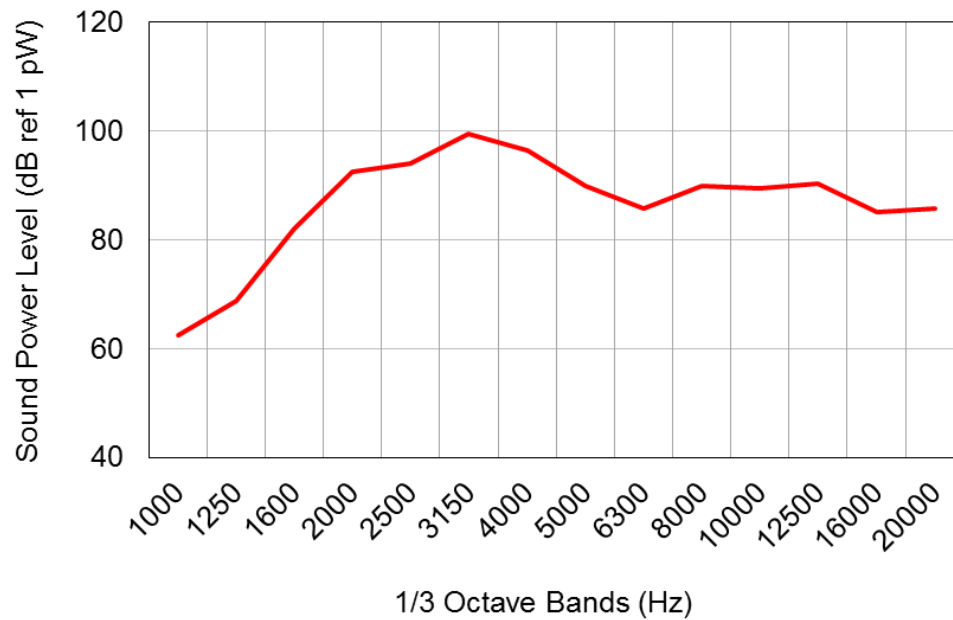
Figure 3.2 Sound power of volume velocity source shown in Figure 3.1

The source was qualified to 20 kHz which corresponds to a range to 2 kHz (see Equation (3.4)) at full-scale. The qualification was performed by centering the source in the room at a height of 1 m above the floor. Figure 3.2 shows the sound

power of the source and that it is over 70 dB in each one-third octave band above 1000 Hz which corresponds to the 100 Hz band at full-scale. Figure 3.3 shows the directivity of the source and compares it to the guidelines provided in ISO 140-4 and ISO 3745. Both standards call for measurements to be made at a distance of 1.5 m from the source along a circle parallel to the floor. Sound pressure level was measured in 30° increments, averaged, and the standard deviation was determined in each octave band. According to both standards, the maximum deviation from the average should be within the prescribed limits shown in Figure 3.3.
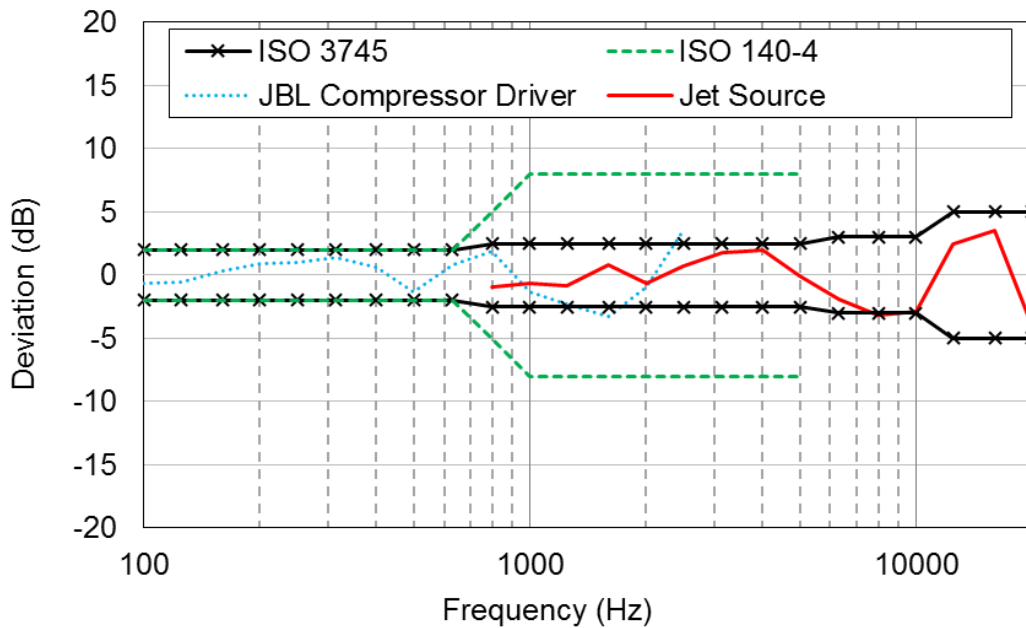
Figure 3.3 Comparison of compression driver and volume velocity source with ISO standards

3.4   Velocity/Intensity Sampling

Volume velocities may be directly measured using an accelerometer at the center of each patch (Liu et al., 2011) or using a sound intensity probe (i.e.,

two closely spaced microphones). In the past decade, a P-U Probe (de Bree, 1999) consisting of a particle velocity probe and built-in small microphone has been a preferred method. As implied by the name, a P-U Probe measures the sound pressure and particle velocity simultaneously. Particle velocity is directional, and the instrument is suitable for measurement in a non-anechoic environment. There are several advantages to using the probe. It is a non-contact sensor so it can be used to measure hot surfaces on engines or to measure air particle velocity; for instance, in the presence of leaks. In addition, quantities may be spatially averaged over a patch via scanning instead of fixed position sampling. Fixed position sampling may result in large errors especially at high frequencies (Holland et al., 1997).

At lower frequencies, the phasing between sources will be important and so phase should be considered for both the volume velocity and transfer function measurement. This is termed the correlated source assumption and the P-U probe is used to measure the velocity v_n directly. Phase may be referenced to an accelerometer or microphone measurement.

However, phase can be ignored in many cases. For example, it is more straightforward to only evaluate sound pressure level in 1/3 octave bands for most architectural applications. Moreover, the correlated assumption is invalid if patches are large or at least similar in size to a structural wavelength. Only volume velocity and transfer function amplitudes are needed for PCA and this approach is referred to as the uncorrelated source assumption.

In such cases, the volume velocity for a patch is estimated from the

sound intensity (I_i) as

$$(v_n S)_i = \sqrt{(I_i S_i) \frac{2\pi c}{\rho \omega^2}} \tag{3.7}$$

where ρ and c are the density and speed of sound of the medium respectively, ω is the angular frequency. Though sound intensity may be measured directly using a sound intensity probe, the P-U Probe is a truly directional sensor and should be less affected by external sources and can be placed closer to the object surface to obtain more accurate vibration information due to the compact size. Nevertheless, the most important advantage of the P-U probe for PCA is that particle velocity and sound intensity are measured simultaneously. This means that the specialist can select whether to use the correlated or uncorrelated source assumption depending on the frequency range and that choice need not be made a priori.

3.5   Measurement Procedure

A generator set was placed in one corner of a hemi-anechoic chamber located at the University of Kentucky. The hemi-anechoic chamber is approximately 6.1 m × 5.9 m × 3.5 m ($L \times W \times H$). The cutoff frequency for the chamber is approximately 150 Hz. The generator set uses gasoline as the fuel and is 0.86 m × 0.57 m × 0.56 m ($L \times W \times H$). The unit is placed in the corner of the chamber as shown in Figure 3.4. The receiver location is marked by the monopole source which is used for transfer function measurements. The distance between the generator set and the receiver location is 4.9 m. Though a distance exceeding 7 m that is typical of most standard acoustic measurements would be desirable, this is the maximum distance that can be used in the hemi-anechoic chamber available. It is also recognized that the anechoic chamber will not behave ideally at the lower frequencies since the equipment is not centered in the room.

Figure 3.4 Photograph showing unit and location of the receiver and receiver location

The primary sources of noise on the generator set are the exhaust, the engine, and the cooling fan. The exhaust is located outside of the generator set enclosure but is piped out to an exhaust disposal system located in another corner of the room. An acoustic wedge was laid over the exhaust pipe orifice so that it was largely eliminated as a sound source. Though the exhaust could be included if the measurement is made outdoors or if the method of ridding the exhaust from the room was more sophisticated, the focus of this work was on characterizing the sound emissions off the enclosure cover. The generator set enclosure is made of acrylic and plastic, and the interior surfaces of the enclosure are lined with a heat resistant glass fiber. It was observed that when the generator set was running, most of the sound energy is concentrated at the firing frequency and their harmonics.

Figure 3.5 shows a photograph of the unit. The receiving position (in Figure 3.4) is at the monopole location. Standard measurements used to qualify similar equipment in industry are typically performed on outdoor test pads where the microphone is located 7.5 m from the unit. Measurements are normally made on each side of the generator set. The configuration shown in Figure 3.4 is intended to roughly replicate standardized measurements of generator sets and other equipment. However, the generator set would preferably be positioned in the center of the room for a standard measurement. From the photo, it can be observed that the hemi-anechoic chamber will need to be voluminous for the standard measurement and on the order of $3 \times$ the size of the chamber at the University of Kentucky. Chambers of such size are

prohibitively expensive and are not commonplace even in industry. The measurement procedure demonstrated in this paper is intended to provide an alternative to such large chambers.

Figure 3.5 Generator set and half-scale model used for transfer function measurements

The application is also similar to rooftop heating and air conditioning units where sound is radiated into a free field. Barriers are often located around units to reduce the noise to those in neighboring buildings. The methods described in this paper can be used to assess barrier effectiveness prior to their construction.

Volume velocities were sampled using the P-U probe (Model No. PR 900490). Measurements of both particle velocity and sound intensity were

procured at the center of each panel or patch. Patches were 8 cm × 8 cm in size with 204 total patches spread over the surface of the generator set. The distance between the probe and the measurement surface was maintained at 7 mm. A microphone was placed near the unit and was used as a phase reference. In addition, the microphone served as way of ensuring that the operating condition of the unit did not change appreciably during the test.

The blocked Green's functions $(G_B(r))_i$ were measured using vibro-acoustic reciprocity. The volume velocity source was placed at the receiver location and the sound pressure was measured using a 1/2-inch microphone (PCB 377B02) at the center of each panel.

For the transfer function measurements, the generator set was turned off, and an 8-channel data acquisition (Siemens SCADAS SCM01) was used to collect transfer function data at 8 patch locations simultaneously by locating microphones at the center of multiple patches. Microphones were positioned as close to the center of each panel as possible. White noise (150 Hz~6400 Hz) excitation was used and the transfer function $TF_i = p_i/p_{ref}$ was measured between the sound pressure level at the center of each patch and close to the monopole source respectively. A microphone is located 0.38 m from the center of the monopole and is used for calibration of the source. Since the point source is located far from the generator set, the monopole can be assumed to be radiating in a free field for the purposes of calibration. The blocked Green's function can be expressed as

$$\left(G_B(r)\right)_i = \frac{p_i}{p_{ref}} \frac{p_{ref}}{Q_0} = TF_i \frac{\rho_0 i \omega}{4\pi r} e^{-ikr} \tag{3.8}$$

where r is the distance from compression driver to a reference microphone and the ratio p_{ref}/Q_0 is developed from Equation (2.7) and Equation (2.11). A moving average with 100 Hz Gaussian window is applied to $\left(G_B(r)\right)_i$ to smooth all transfer functions.

Transfer functions were also determined using a half scale model (i.e., $s = 0.5$). The scale model of the generator set is pictured in Figure 3.5 and the measurement setup for determining the vibro-acoustic transfer function is shown in Figure 3.6. The model is constructed from aluminum plating having a thickness of 0.95 mm. The interior of the scale model was filled with sandbags to eliminate any resonances from the plating. Vibro-acoustic reciprocity is used with the point monopole source located at the receiver position and microphone measurements are made at the center of each panel (i.e., patch).
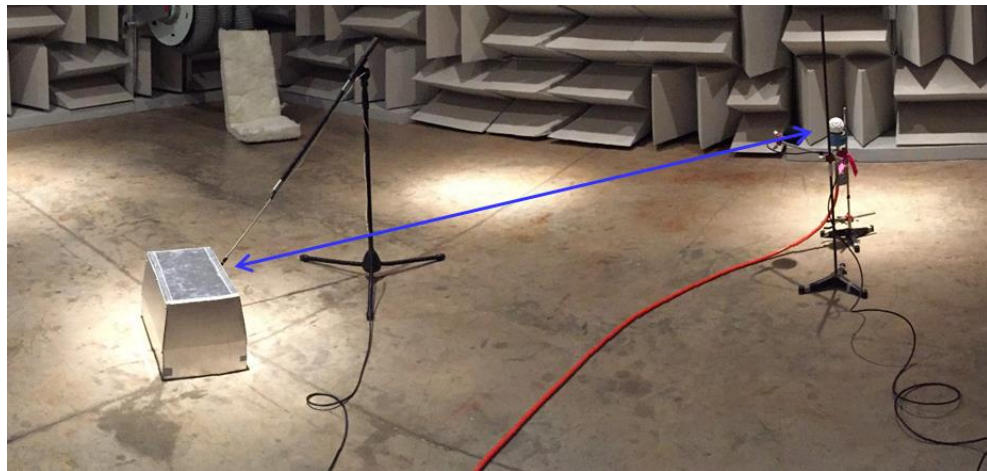
Figure 3.6 Half scale model transfer function measurement setup

Observe in Figure 3.4 that the generator set is nestled into one corner of the room in the full-scale case. This is clearly less than ideal since sources should be positioned in the center of the hemi-anechoic chamber and measurements are likely to be compromised by some reflections off the chamber walls at the lower frequencies. On the other hand, the half-scale model can be positioned in the middle of the hemi-anechoic chamber. Moreover, higher frequencies are of greater interest in the scaled model due to the frequency scaling introduced in Equation (3.4). For example, 400 Hz in the half scale model corresponds to 200 Hz in the full-scale case. Hence, small hemi-anechoic chambers should be more than adequate for scale models and the source used does not need to be especially powerful at low frequencies. Transfer function measurements for the scaled generator were measured in an identical manner to the full scale case except using a 1/4-in microphone (PCB 377C10). The uncorrelated assumption was assumed so that phase was not considered.

3.6   Sound Pressure Level Predictions

The sound pressure level was predicted using Equation (3.6) assuming both correlated and uncorrelated source superposition. Results are shown in 1/3-octave bands in Figure 3.7. It can be observed that both correlated and uncorrelated predictions track well with direct measurement though there are differences that exceed 5 dB in a few frequency bands. The overall sound pressure levels are also included in the legend and are within 2 dBA of each other. Results below the 200 Hz one-third octave band are not included since the hemi-anechoic chamber is not qualified below this frequency, and the generator set is

positioned in the corner rather than the center of the chamber. In addition, there is likely some contamination from engine exhaust noise at the very low frequencies.
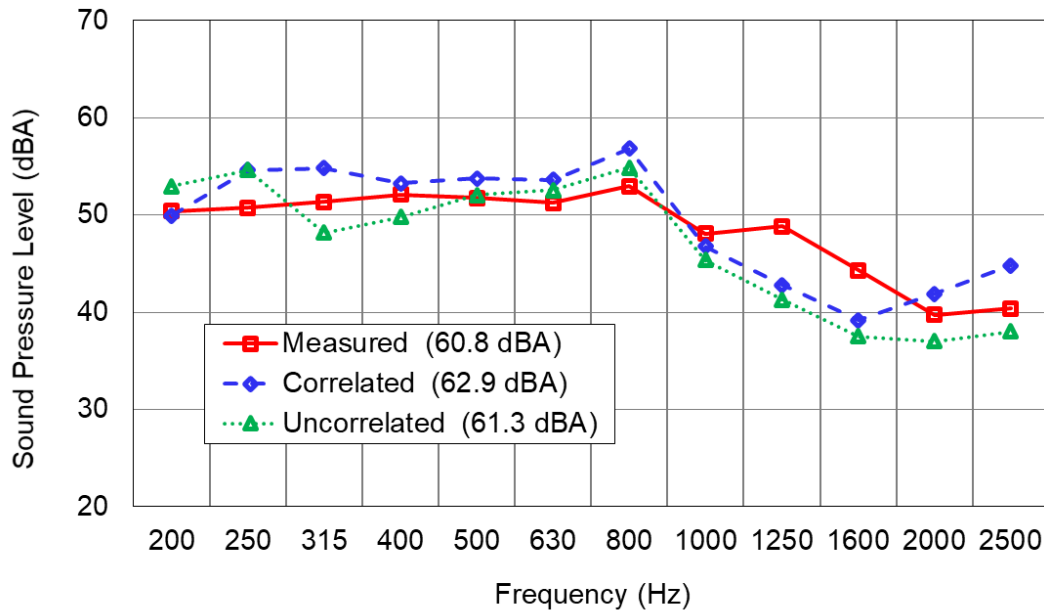
Figure 3.7 Comparison of measured to PCA predicted sound pressure at receiver location, using both correlated and uncorrelated approaches

Sound pressure level predictions are compared to direct measurement in Figure 3.8 for both full-scale and half-scale approaches. Results are shown for the uncorrelated assumption in each case. Observe that sound pressure level predictions using the half scale vibro-acoustic transfer functions are more accurate than for the full-scale prediction. There are several possible reasons why. First, the scaled generator set geometry is centered in the room rather than being placed close to a corner of the hemi-anechoic chamber. In the full-scale case, reciprocal transfer function measurements to patches on the generator set side nearest the wall are likely affected by the nearness of the generator set to the chamber walls. Secondly, sound pressure level measurements are made at the center of each

patch. Since the patches are much smaller in the scale model and measurements are made at higher frequencies, the sound pressure measurement is likely a more representative average at the center of the patch since the microphone is much larger relative to the patch size.
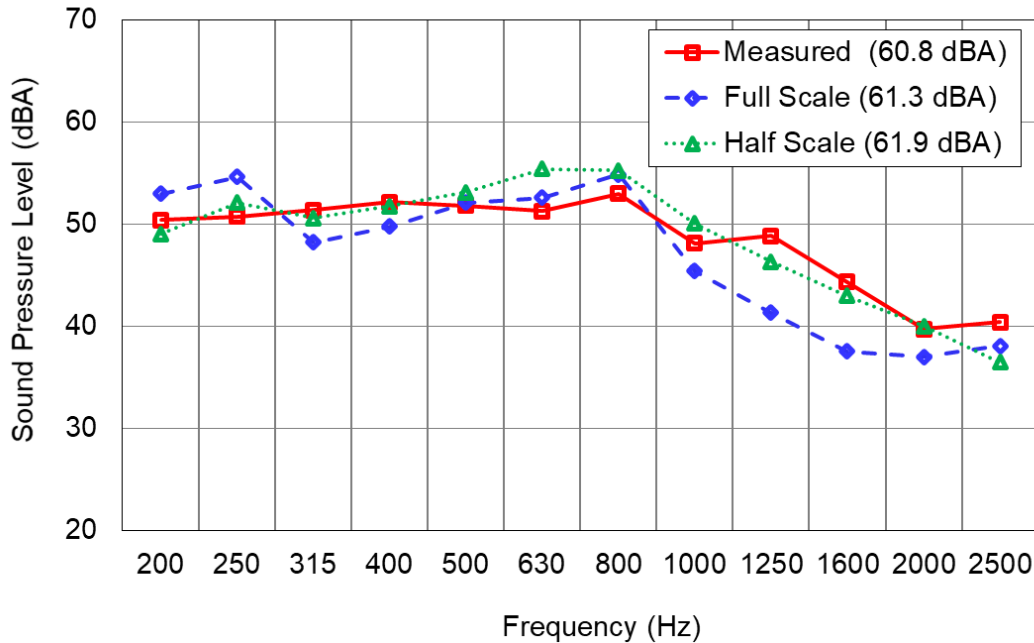
Figure 3.8 Comparison of measured to PCA predicted sound pressure at receiver location, using the uncorrelated approach with full and half scale transfer functions

A contribution analysis was also performed for each surface of the generator set. Figure 3.9 shows a schematic of the generator surfaces as well as the position of each surface relative to the receiver. Contributions from each surface are shown in Figure 3.10 using the full scale transfer functions and in Figure 3.11 using the half scale transfer functions. The uncorrelated source assumption is used for the calculations. First, observe that the overall contribution predictions are within 1 dBA of each other whether full or half scale transfer functions are used. Second, the trends in frequency are similar in each case.

Surface 1 is dominant in most frequency bands which is anticipated since Surface 1 faces the receiver location and is also large in surface area. The top of the unit, Surface 5, is similar in area but its contribution is 3 to 5 dBA lower because the noise is radiated upward. The contributions from Surfaces 3 and 4 are nearly the same because they are the same surface area and have similar directivities. Surface 2, which is opposite the receiver locations is also much lower. The contributions from Surfaces 3 and 4 are lower than from Surface 2 because the panel areas are smaller, and those surfaces are stiffer due to their small surface area. Table 3.1 summarizes the overall contributions assessed using full-scale and half-scale transfer functions. The conclusions are the same no matter which collection of transfer functions is used.

Table 3.1 Contributions determined using full-scale and half-scale transfer functions

Surfaces	Contributions using Full Scale Transfer Functions (dBA)	Contributions using Half Scale Transfer Functions (dBA)
All	61.3	61.9
Surface 1	59.1	58.9
Surface 2	52.8	53.4
Surface 3	49.6	50.2
Surface 4	50.3	51.1
Surface 5	54.9	55.4
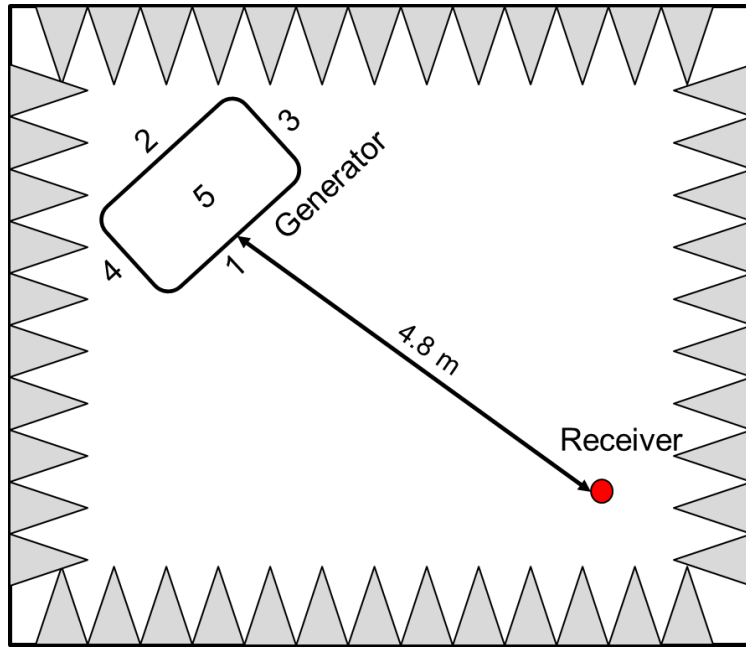
Figure 3.9 Schematic showing approximate locations of generator set and receiver locations. Surface identifiers are indicated for the generator set (not to scale)
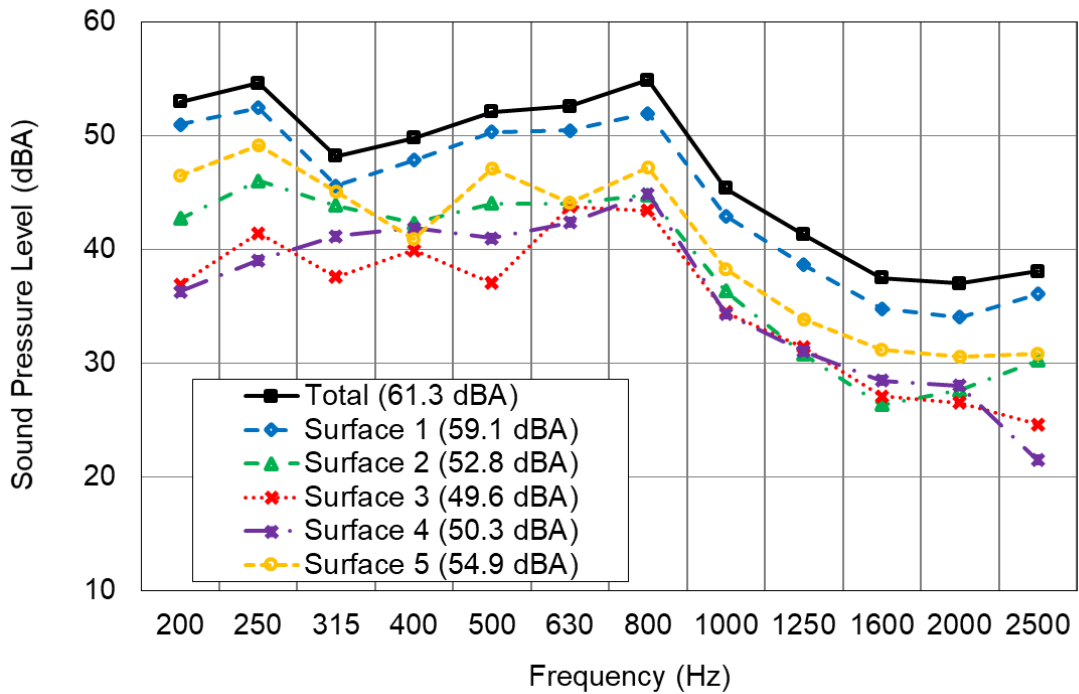
Figure 3.10 Contribution analysis from each surface at receiver location using full scale transfer functions
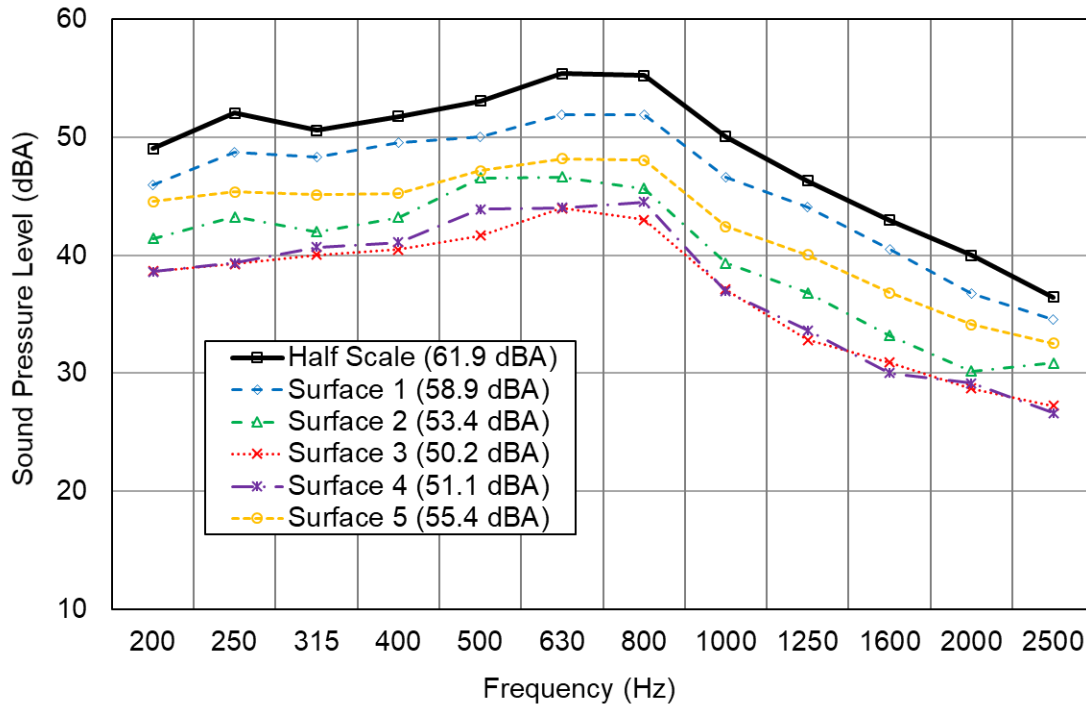
Figure 3.11 Contribution analysis from each surface at receiver location using half scale transfer functions

3.7 Barrier Treatments to Generator Noise Reduction

Machinery noise must often be reduced after placement. The most common approach is to use handbook equations to predict the possible impact of treatments. Treatments are then applied, and measurements are performed to verify the effectiveness which is often less than anticipated due to the complexities of the source. It would be beneficial to perform laboratory tests where the effectiveness of treatments is assessed prior to the equipment being installed. PCA is a means to that end. It provides an accurate representation of the source and approximates its directivity. Transfer functions may be measured both without and with barrier treatments and the effectiveness of the treatments can be determined.

56

If sources are large and sound pressure needs to be measured several meters from the source, it is more convenient to measure transfer functions using a scale model. PCA may then be used to predict the sound pressure level at a receiver location.

The combination of PCA and scale modeling was used to investigate the effectiveness of positioning barriers around the generator set. In this effort, the focus is on assessing the effectiveness of barriers for an outdoor case typical of power generation and rooftop climate control equipment.

The receiver position is located approximately 2.8 m from the center of the generator set and 2.3 m from the outside cover of the unit. This is relatively close to the unit compared to the measurements shown earlier in the paper. However, this permits placement of the unit in the center of the anechoic chamber. Transfer functions using both the full-scale equipment and a half-scale model were measured reciprocally. Eight different barrier treatments were considered. The full-scale treatments are shown in Figure 3.12 and the half-scale treatments in

Figure 3.13. In the half scale model, the thickness of the wood (~2.5 cm) was not scaled since it is relatively thin compared to a wavelength. Dimensions for each treatment are shown in Appendix A: Barrier Treatment Configuration Layout.
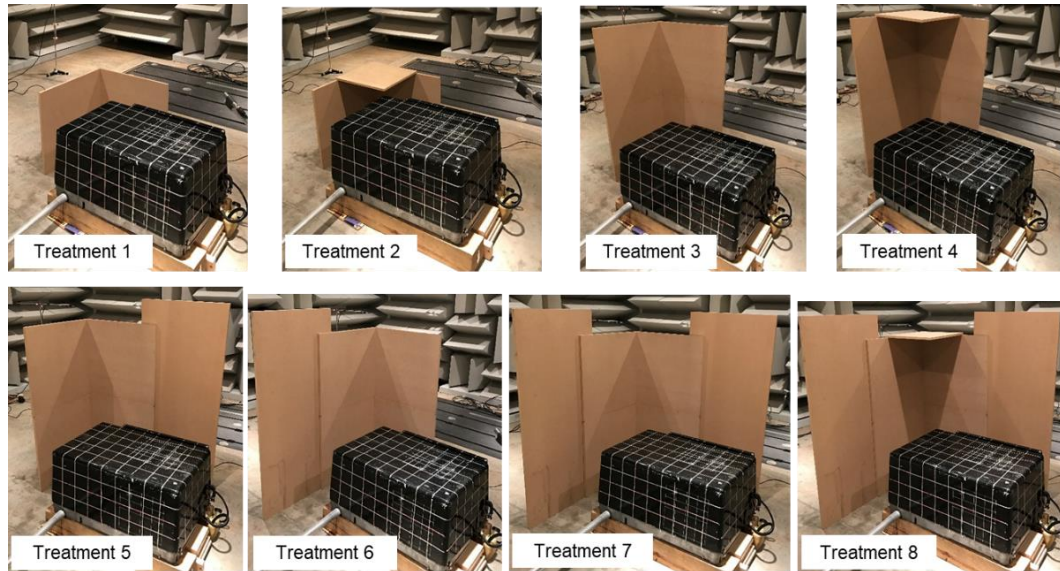
Figure 3.12 Photos showing 8 barrier configurations
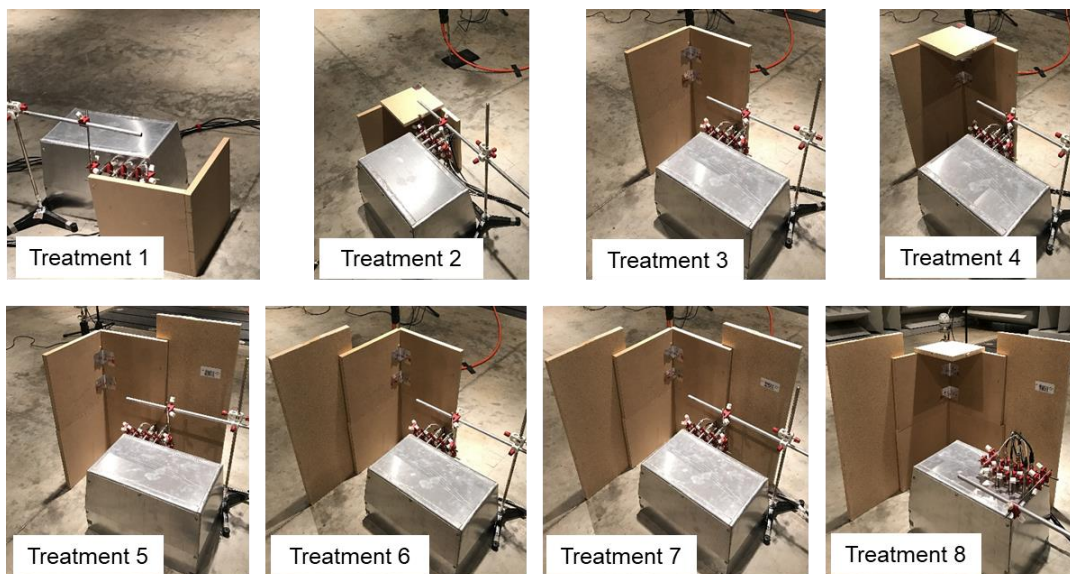
Figure 3.13 Photos showing 8 half scale barrier configurations

Sound pressure level predictions are compared to the direct measurement in Figure 3.14 and Figure 3.15 for Treatments 6 and 8 respectively. Overall A-weighted levels are indicated in the legend. For Treatment 6 in Figure 3.14, the overall sound pressure level in dBA is within 1 dBA though results may differ by as much 5 dBA in specific 1/3 octave bands. Nonetheless, the general low and high

frequency trends are well-predicted by the model. Results are similar for Treatment 8. The PCA full and half scale predictions are within 3 dBA of the overall level but differ by as much as 5 dBA in some 1/3 octave bands.
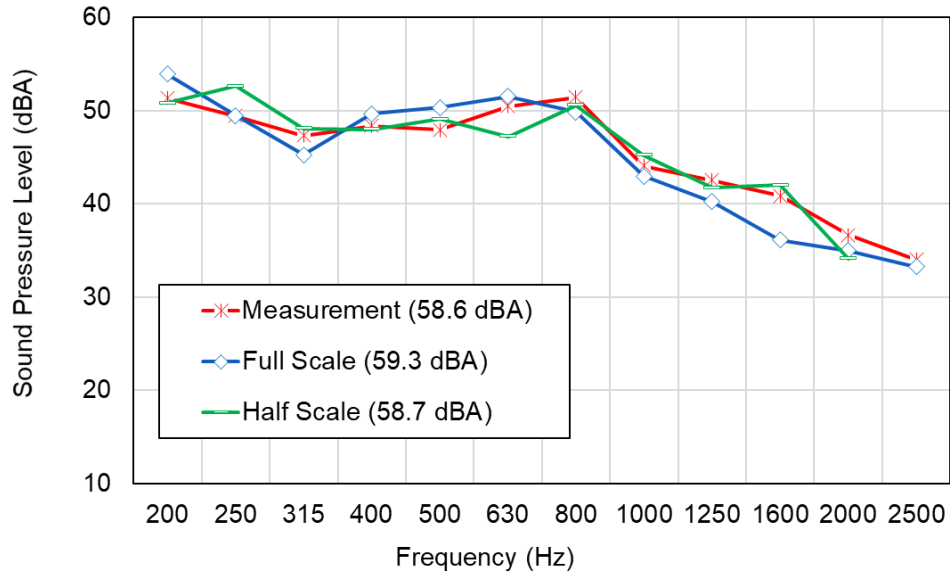
Figure 3.14 Comparison of sound pressure level at receiver location for barrier treatment 6
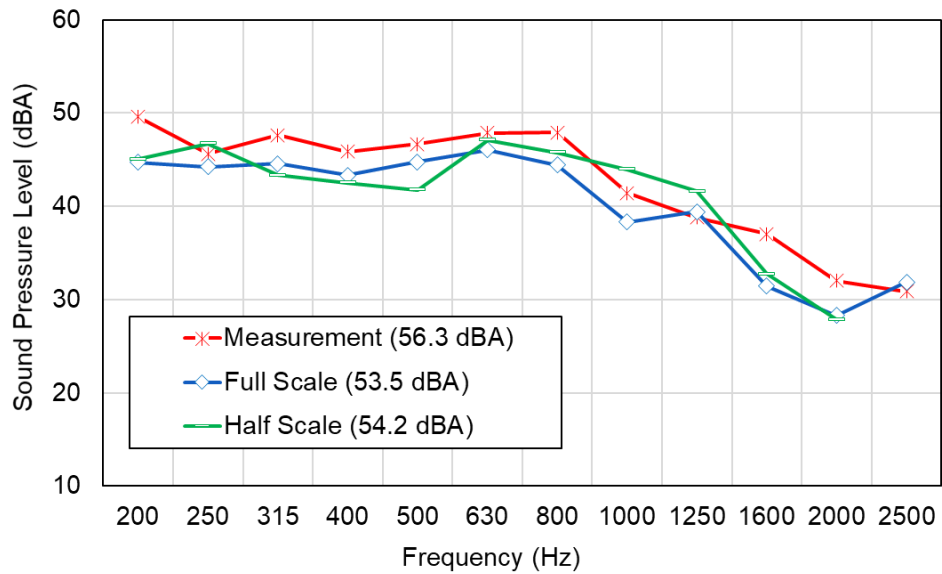
Figure 3.15 Comparison of sound pressure level at receiver location for barrier treatment 8

Results are summarized for all treatments in Table 3.2. Overall sound pressure level results are shown from 200 to 2500 Hz in dBA. Predicted results are within 3.1 dBA for all the treatments considered. Table 3.3 summarizes the predicted attenuations due to each treatment. For most treatments, predicted attenuations are within 2 dBA though there are a couple outlier predictions. Nonetheless, the PCA approach was successful at predicting the effect of the barrier treatments, and this was the case no matter whether the full or half scale transfer functions were used.

Table 3.2 Comparison between receiver location A-weighted sound pressure levels

Treatment	Measured SPL (dBA)	PCA Full Scale Prediction (dBA)	PCA Half Scale Prediction (dBA)
Baseline	65.1	64.5	62.2
Treatment 1	64.1	62.6	60.8
Treatment 2	63.7	61.8	60.2
Treatment 3	61.2	58.9	58.1
Treatment 4	60.3	61.8	60.8
Treatment 5	60.9	60.7	58.2
Treatment 6	58.6	59.3	58.7
Treatment 7	57.1	55.7	53.5
Treatment 8	56.3	53.5	54.2

Table 3.3 Comparison between directly measured and PCA predicted attenuations

Treatment	Measured Attenuation (dBA)	PCA Full Scale Attenuation (dBA)	PCA Half Scale Attenuation (dBA)
Treatment 1	1.0	1.9	1.4
Treatment 2	1.4	2.7	2.0
Treatment 3	3.9	5.6	4.1
Treatment 4	4.8	2.7	1.4
Treatment 5	4.2	3.8	4.0
Treatment 6	6.5	5.2	3.5
Treatment 7	8.0	8.8	8.7
Treatment 8	8.8	11.0	8.0

3.8   Summary

Panel Contribution Analysis has been combined with scale modeling to rank noise sources and assess treatments for a generator set. The generator set was discretized into patches and transfer functions were measured reciprocally on both the full-scale machine and a half-scale model. Surface vibration and sound intensity were measured by a P-U Probe while the machine was operating. The P-U probe is ideal for this usage because volume velocity and sound intensity may be measured simultaneously. PCA can then be applied assuming either uncorrelated or correlated sources. The correlated assumption is more appropriate at low frequencies whereas volume velocities are more likely to be

uncorrelated at middle and high frequencies, which was the case for most of the frequency range of interest for the generator set.

The sound pressure at the receiver positions was predicted using full-scale and half-scale transfer functions with good agreement. Barrier treatments were then investigated using the combination of PCA and scale modeling, and the comparison between them showed good agreement. Most importantly, the method successfully predicted the effect of the treatments used.

This approach can potentially be used to assess the effectiveness of barriers placed around sources such as building climate equipment, generator sets, and other equipment where barriers are applied to reduce noise emissions. Moreover, barriers can be designed prior to siting the equipment and the usage of voluminous anechoic chambers is not essential.

Chapter 4   PCA IN ROOM ACOUSTICS AND SCALE MODELING

(Note: Most of the research in this chapter has been previously documented in Cheng et al., 2019)

4.1   Introduction

Though great strides have been made in utilizing numerical simulation to predict acoustic emissions from machinery, simulation still falls short of the desired goal to predict sound pressure levels of most sited equipment. There are many reasons why this is the case. First, predicting accurate vibration levels of large machinery during design requires phenomenological models of vibrational and acoustic sources including detailed models of engine combustion, fans and surrounding enclosures, and geared transmissions. Even if sources are appropriately dealt with, machinery paths include welded and bolted connections that are over simplified in models. In addition, a model of the site where the machine will be placed is also required and such models have large numbers of degrees of freedom. Though the problems may not be intractable using simulation, the complexity is such that predictive computational models are only moderately successful at predicting noise levels of located equipment and require a great deal of time to develop, analyze, and validate.

In most cases, a measurement campaign is still required at the site and modifications after locating machinery are expensive. More sophisticated approaches like beamforming (Chiariotti et al., 2019) can be used for sound source identification once the machinery is in position. Nonetheless, approaches that can predict the sound pressure level before siting are desirable. This paper suggests

that a combination of panel contribution analysis and scale modeling is a promising strategy for predicting noise levels and assessing noise treatments of equipment prior to siting. The process is detailed and illustrated using a practical example.

PCA is a relatively simple process. A single source or multiple sources are discretized into panels or patches. Data collection consists of two parts: 1) the volume velocity is measured for each patch with the sources operating and 2) acoustic transfer functions are measured between the volume velocity for each patch and the sound pressure at receiver locations in the field with the sources not operating. The data collected can then be utilized for many purposes. The most direct use is to predict the sound pressure in the field by summing the volume velocities multiplied by corresponding acoustic transfer functions. If patches are grouped, sound pressure contributions from different source components or patch clusters can be determined. Moreover, treatments in the acoustic field can be investigated. For example, barriers or sound absorption are introduced in this paper and the impact of these treatments is assessed.

Foundational research on PCA was performed by Fahy (1995, 2003) and Verheij (1997). The principle has been successfully applied in this way to predict engine, rail, and aircraft fuselage noise. Most of the groundwork has been performed at the Institute of Sound and Vibration Research at Southampton, and there has been renewed interest due to the development and usage of P-U probes (de Bree, 1996, 2003, Jacobsen et al., 2006, Grosso et al., 2012) which are ideal devices for determining the volume velocity from patches.

In this chapter, it is demonstrated that the acquisition of acoustic transfer functions for interior problems can be further expedited by using scale models. Provided that volume velocities at the patches are well understood, the most obvious advantages of using scale models are: 1) acoustic transfer functions can be measured before large machinery is located at a site or even before a site is constructed, 2) acoustic transfer functions are more easily measured using a scale model due to the reduced size, and 3) modifications and treatments to the acoustic path may be considered and evaluated much less expensively via the scale model. This work anticipates that future developments in 3D printing will make scale model development easier for machinery and the environment in which they are installed.

The current work details a measurement study where the sound pressure level produced by three air handlers was predicted in a bakery using this combination of panel contribution analysis and scale modeling. The procedure used is described in detail. Emphasis is placed on the use of the P-U probe to assess volume velocity using correlated and uncorrelated source assumptions, and corrections to the transfer functions for dealing with air dissipation if a scale model is used for an interior problem. Each step of PCA is detailed and the contributions of this study are reviewed in the concluding section.

4.2   Floor Layout of Bakery

The acoustic space investigated in this paper is the bakery pictured in Figure 4.1. The room is approximately 25 m in length, and 7 m in width, with a total floor space of approximately 175 m^2. There is a loft above the reception area with a floor area of 45 m^2. The bakery floor is smooth concrete, the

ceiling is metal, one wall is painted concrete block, and the other gypsum board. There are windows at the store front and in the garage door at the bakery rear. The bakery has an industrial aesthetic typical of many food and drink establishments in use currently where most surfaces could be considered hard.
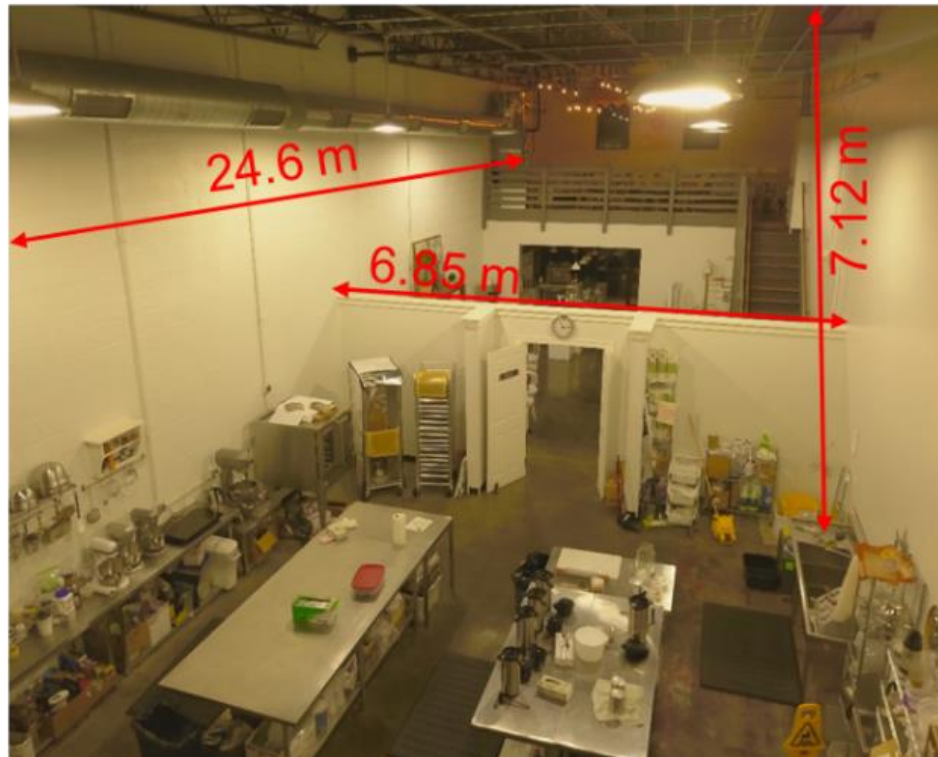
Figure 4.1 Photograph of bakery studied

The primary sources of noise are three air handling units. One unit (AH 3) is located in the loft area while the other two units are located under the stairs near a customer area (AH 1) and in the kitchen (AH 2). The floor plan for the space is shown in Figure 4.2. Two locations in Figure 4.2 were identified as receiver locations of interest. Receiver locations 1 and 2 are in the loft and main floor, respectively, in seating areas.
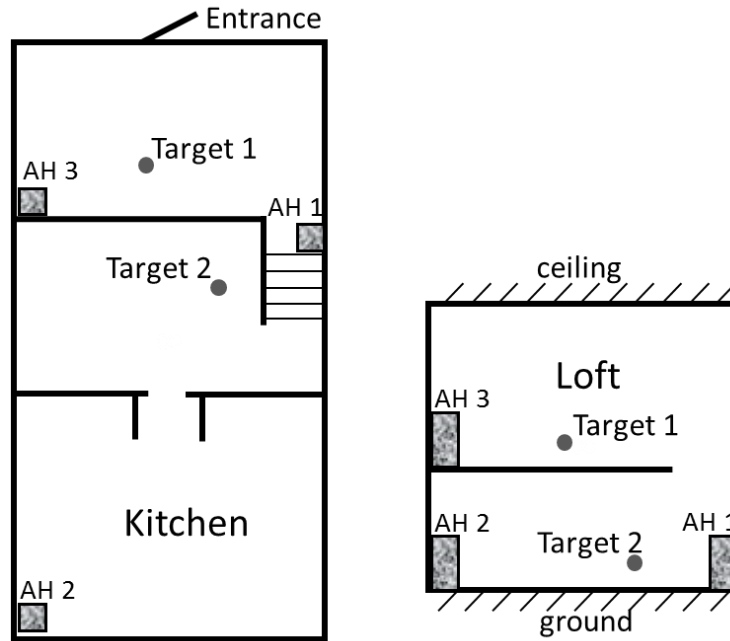
Figure 4.2 Floor layout showing source and receiver locations in bakery

During the measurement campaign at the bakery, a P-U probe (Model No. PR 900490) was used to sample the surface velocity and sound intensity. The patches were divided into the two groups shown in Figure 4.3.

Figure 4.3 Patch discretization on air handler

During pre-test, it was found that the main component of vibration on the upper air handler panels was in the low frequency range, whereas air intake noise was broadband and more important at higher frequencies. For the flat metal panel portion, patches were 30×20 cm^2 in size whereas a finer patch size of 15×15 cm^2 was used for the air intake. There were 85 total patches on the 3 air handlers.

Each unit was turned on one by one, and the P-U probe was used to scan each patch to measure both particle velocity and sound intensity. The distance between the probe and surface was maintained at 7 mm, which is close enough for vibration sampling (Holland et al., 1997).

A microphone was placed near the unit and used as a reference for phase measurement.

4.3 Transfer Function Measurement – Full Scale

In Equation (2.4), the blocked Green's functions $\left(G_B(r)\right)_i = p_i(X)/Q(Y)$ or transfer functions are typically measured using reciprocity rather than moving the source from patch to patch. Lord Rayleigh was the first to state the principle of vibro-acoustic reciprocity and Lyamshev in 1959 published a formal mathematical proof of the principle some 80 years afterward. The principle is general and applicable to both mechanical and acoustical source and response variables. Fahy tabulated several cases suggested by Rayleigh (2003), and Verheij (1997) added others. The reciprocity principle states that the transfer functions between a source and receiver are identical if their positions are interchanged. This is especially convenient when measuring acoustic transfer functions because a

monopole source can be centered at one or several receiver positions and sound pressure measured at the center of each patch on the source.

In this study, transfer functions were measured in the bakery using a compression driver (JBL 2447H) as the volume velocity source. The omni-directional nature of the source was tested based on ISO 140-4 and ISO 3745 and these results are shown later in the paper. The compression driver was placed at the target point (i.e., at ear level, 1.2 m above the ground) and a microphone was placed 1.3 m above the speaker and used to calibrate both the strength and phase of the volume velocity source.

Transfer functions were measured with all units turned off, and an 8-channel data acquisition (Siemens SCADAS SCM01) was used so that several transfer functions were measured at the same time by placing microphones (PCB 377B02) at the center of multiple patches. From prior experience at our lab, it is recommended that the microphone be positioned as close as possible to the patch center. White noise (150 Hz~5000 Hz) excitation was used and the transfer function TF_i between the patch surface and calibration microphone was measured. By assuming the calibration microphone is placed in the free field, the blocked Green's function can be expressed as Equation (3.8). A moving average with 50 Hz Gaussian window was applied to $\left(G_B(r)\right)_i$ to smooth all transfer functions.

4.4   Sound Pressure Level Predictions – Full Scale

Sound pressure level predictions using Equation (2.6) were performed assuming both correlated and uncorrelated assumptions. The predicted and directly measured sound pressures at the target positions are shown in Figure 4.4.
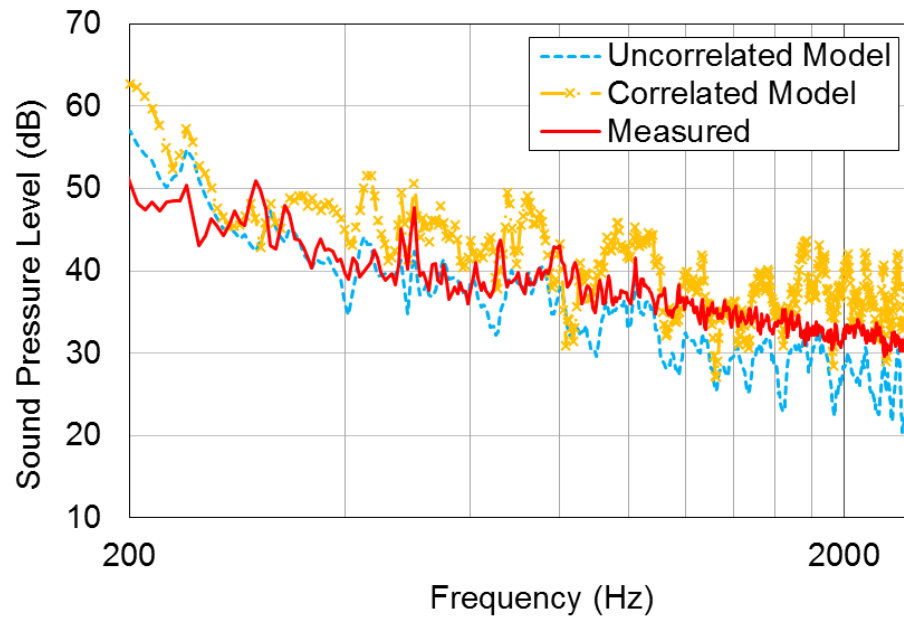
(a) Target 1
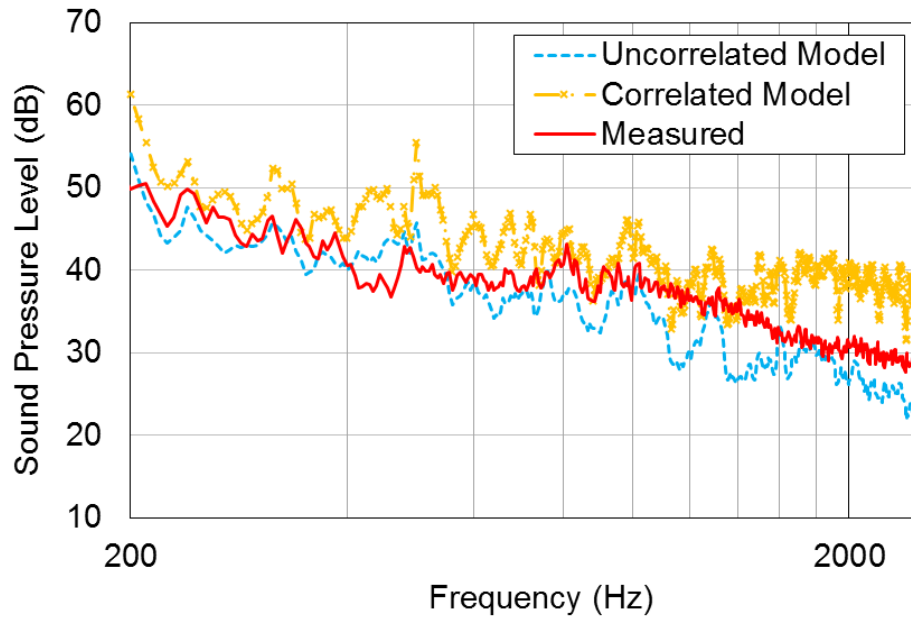
(b) Target 2

Figure 4.4 Comparison of measured to PCA predicted sound pressure at (a) Target 1, and (b) Target 2

Predictions using the uncorrelated assumption were more accurate especially above 1000 Hz where the correlated model overpredicts the sound pressure level. This is anticipated because all points on a patch are assumed to be moving in phase with the correlated assumption. However, this approximation is only valid when the patch size is small compared to a structural wavelength and is inappropriate for the thin panels of the air handler except at very low frequencies.

Note that correlation is very good between measurement and PCA at low frequencies. PCA predictions, even for the uncorrelated assumption, fall below measured sound pressure levels. Results might be improved upon if the air handler was discretized into more patches or if a better volume velocity source were used.

A contribution analysis was also performed. Figure 4.5 shows the flat panel and air intake contributions at target location 1 in 1/3 octave bands. Calculations were performed using the uncorrelated assumption. The results show that below the 315 Hz band, the contribution from the flat panels is dominant whereas the air intake panels are more important above 1000 Hz.
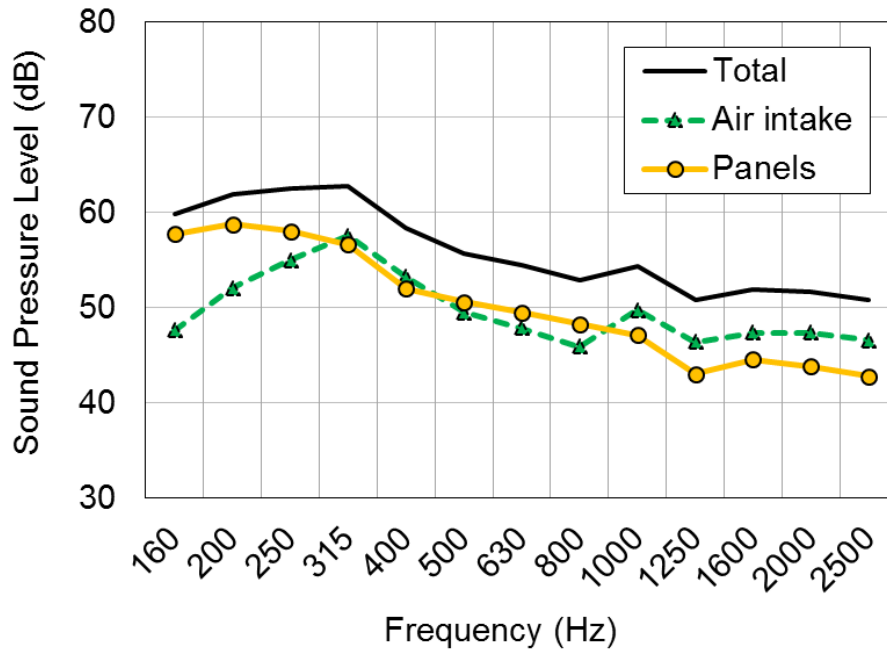
Figure 4.5 Contribution analysis from different sections of AH 3 at Target 1

Figure 4.6 shows the contribution for each of the air handler units assuming uncorrelated sources. The results show that, below 315 Hz band, AH 2 located in the corner of the kitchen, dominates at both target locations 1 and 2. This is in agreement with the observation in situ that AH 2 has distinct low frequency noise components compared to AH 1 and 3. Above 315 Hz, AH 3 is the primary source at target location 1. For target location 2, AH 1 is the principal source. These results are expected since units nearest to the respective target positions contribute greatest.
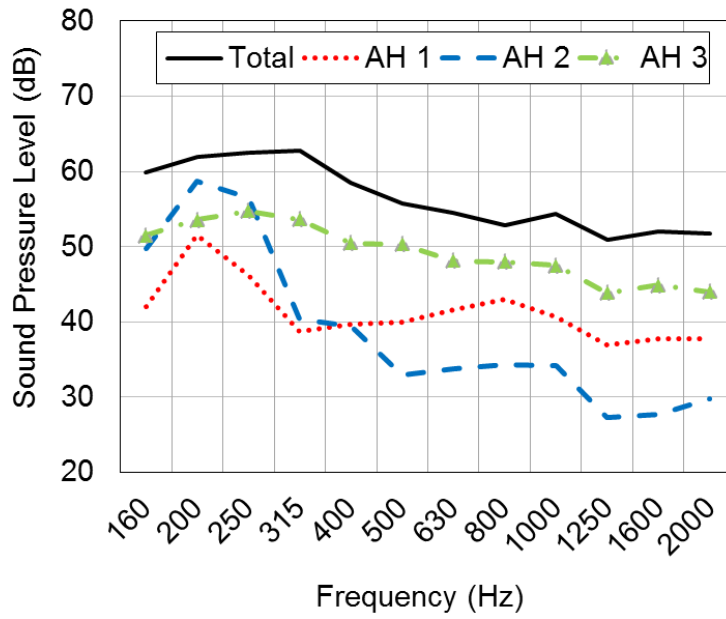
(a) Target 1
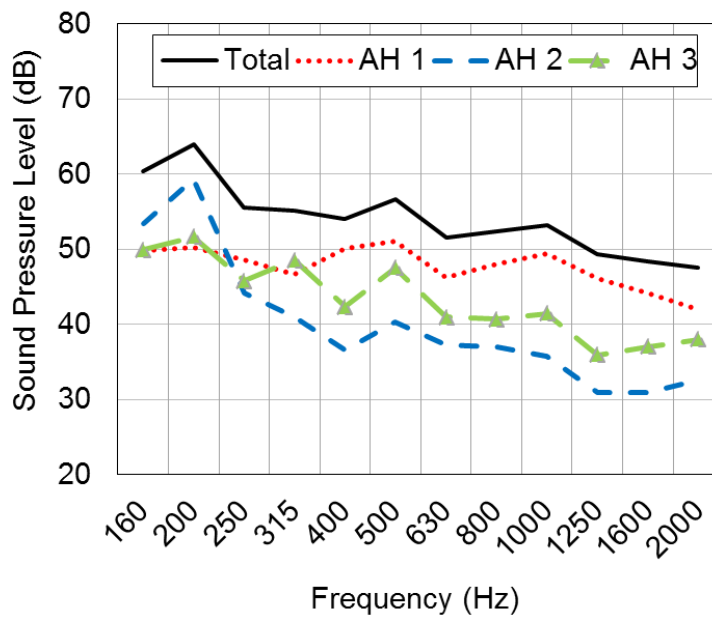
(b) Target 2

Figure 4.6 Contribution from each air handler to sound pressure level at (a) Target 1 and (b) Target 2

4.5   Transfer Function Measurement – Scale Model

The prior example was a typical application of PCA though application to interior problems is considerably less common than for radiation problems. The example demonstrated the utilization of PCA for prediction of sound pressure and assessment of source contributions.   One drawback of the approach was that transfer functions were measured in the bakery itself. Hence, measurements were performed after the equipment was installed. Treatments might be investigated as well but that would necessitate installation of the full-scale treatment in the room. It is preferable to instead measure or estimate acoustic transfer functions before installing the sources or treatments in the room. Fahy (2002) noted that use of a scale model may be helpful for determining transfer functions but did not utilize the approach. In work in our laboratory, Liu et al. (2011) used a scale model to determine the acoustic transfer functions (i.e., blocked Green's functions) in a laboratory experiment.

A scale model of the bakery with $s = 1/10$ was constructed as shown in Figure 4.7.   The model was constructed from dense particleboard with a thickness of 1.9 cm except for the ceiling constructed from transparent polycarbonate. Since the walls, ceiling, and floor in the bakery are hard with minimal sound absorption, the scale model is constructed from hard materials as well.   In some cases, it may be important to ensure that the sound absorption of each surface correlates well with the actual room though no effort was made to do so in this case. Some details of the construction are

included which may affect the sound propagation from the AH units including partition walls, large tables, stairs, and several other details as shown in Figure 4.2 and Figure 4.7.

Figure 4.7 1/10-Scale model of bakery

The compression driver used as the volume velocity source in the full-scale case is also shown in Figure 4.8 for comparison. It can be seen that the compression driver and small jet source are satisfactory at most frequencies in the range of interest.

Measurements in the scaled bakery were performed in the hemi-anechoic chamber though this is not necessary. Reciprocal transfer functions were measured in a similar way as in the full scale bakery, with a 1/4-in microphone (PCB 377C10) positioned at the center of each patch as shown in Figure 4.8. The volume velocity of the small jet source was measured outside of the scale model. The uncorrelated assumption was assumed so that phase was not considered.
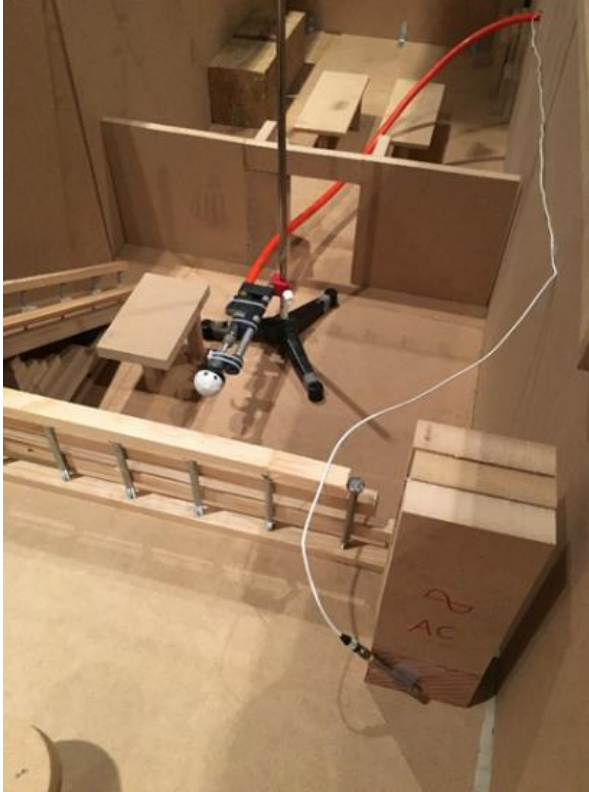
Figure 4.8 1/10-scale model transfer function measurement setup

Based on the scaling rule, the transfer functions measured in the scale model were adjusted by squeezing the frequency from 0 to 20 kHz to 0 to 2 kHz. Figure 4.9 compares transfer functions between full-scale and 1/10-scale model between a typical patch of AH 1, AH 2 and Target 1. Figure 4.9 (a) shows a good agreement of transfer functions between full- and 1/10-scale model. However, Figure 4.9 (b) shows significant deviation between the full-scale and scaled transfer functions for a patch on AH 2. This deviation is caused by the air attenuation in the bakery due to its large dimension, which is underestimated in the scale model.
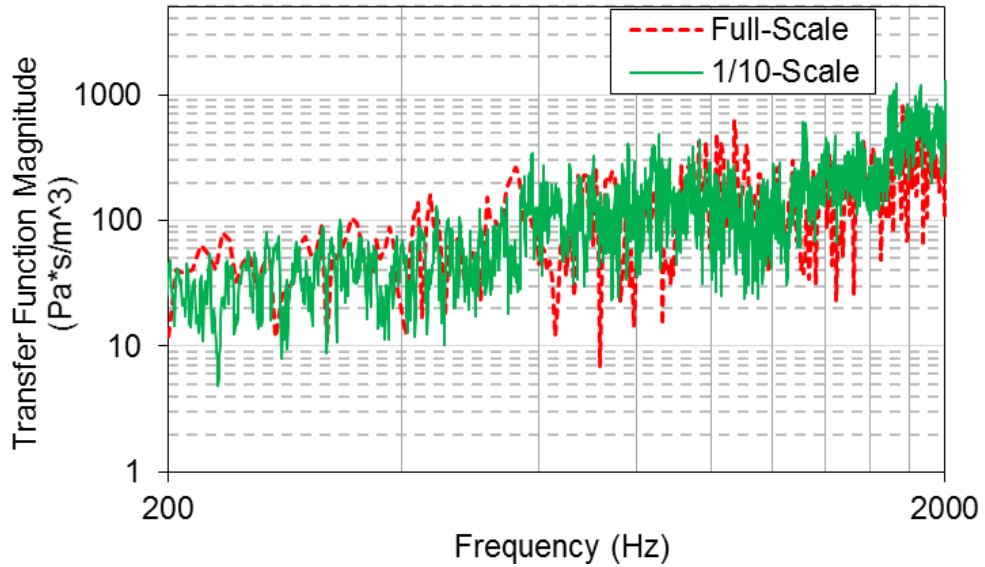
(a) AH 1 to Target 1
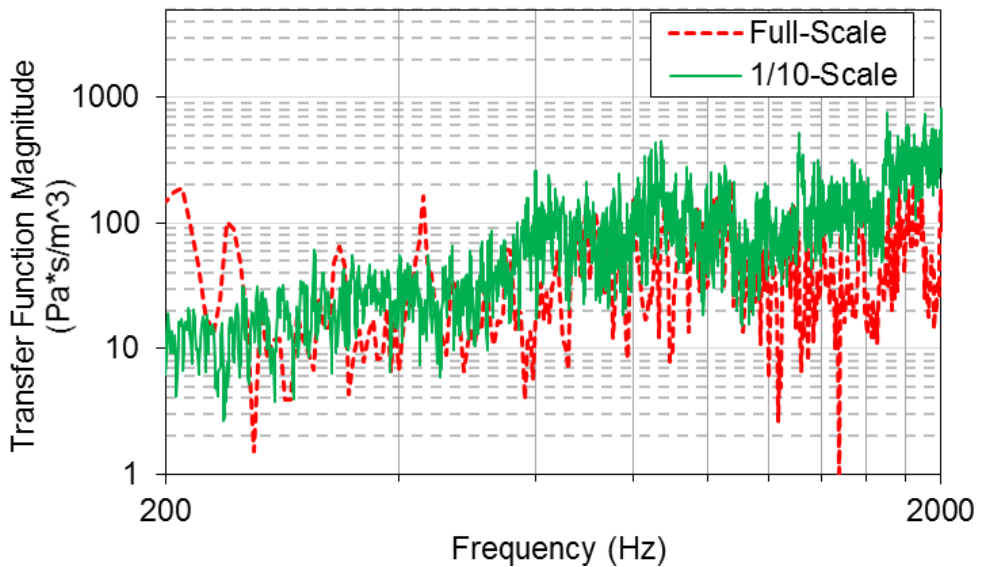
(b) AH 2 to Target 1

Figure 4.9 Transfer function comparison between full-scale and 1/10-scale model from (a) AH1 to Target 1, and (b) AH 2 to Target 1

To correct the air absorption term in the scale model, room acoustics theory is used to adjust the transfer function. For the transfer function from a patch on AH 2 to Target 1, the distance between the positions is approximately 20 m. The

77

distance, sometimes referred to as the echo radius (Wallin et al., 2011), where the reverberant and direct field strengths are approximately equal is 4.5 m. Note that the target location is in the reverberant field of AH 2.

In room acoustics theory (Bies et al., 2018), the acoustic response due to a source may be divided into two terms, i.e., the direct field and the diffuse field or reverberant field. The rms sound pressure ($\tilde{p}_{tot}^2$) from a source in the room may be expressed as

$$\tilde{p}_{tot}^2 = \rho_0 c W_{dir} \left[\frac{\Gamma}{4\pi r_F^2} + \frac{4}{R_F} \right] \tag{4.1}$$

where W_{dir} is the sound power of the source, r_F is the distance between source and receiver in the full-scale model, R_F is the room constant of the full-scale model, and Γ represents the directivity index. Since $W_{dir} \propto Q^2$, the transfer functions of the full-scale and scale models can be written as

$$TF_F = C \left[\frac{\Gamma}{4\pi r_F^2} + \frac{4}{R_F} \right]^{\frac{1}{2}} \tag{4.2}$$

and

$$TF_S = C \left[\frac{\Gamma}{4\pi r_S^2} + \frac{4}{R_S} \right]^{\frac{1}{2}} \Bigg|_{\omega=\omega_S \cdot s, G_B=(G_B)_S \cdot s^2} \tag{4.3}$$

respectively where C is a constant. In Equation (4.3), R_S is the room constant of the scale model. If the receiver point is located far outside the direct field, the direct field term can be ignored and simplified as

$$TF_{corrected} = TF_S \cdot \left.\left[\frac{R_S}{R_F}\right]^{\frac{1}{2}}\right|_{\omega=\omega_S \cdot s; \, G_B=(G_B)_S \cdot s^2} \qquad (4.4)$$

where the room constants R_F and R_S are expressed as

$$R_F = \frac{\langle \alpha_F \rangle \cdot S_F}{1 - \langle \alpha_F \rangle} \qquad (4.5)$$

and

$$R_S = \frac{\langle \alpha_{wall} \rangle \cdot S_F}{1 - \langle \alpha_{wall} \rangle} \qquad (4.6)$$

with S_F the room surface area and $\langle \alpha_F \rangle$ the average sound absorption of the room. The sound absorption of the room was determined by measuring the reverberation time. The average sound absorption of the walls of the room is α_{wall}. The reverberation time of the scale model room is difficult to measure using the current source. A rough approximation was assumed instead by assuming that the sound absorption of the walls for the scale model is the same as that for the full-scale case. The wall absorption for the full-scale room is estimated using

$$\langle \alpha_{wall} \rangle = \frac{55.3 V_F / T_0 - 4 V_F m}{c \cdot S_F} \qquad (4.7)$$

where the wall absorption is the difference between the total sound absorption and the absorption due to air attenuation. The atmospheric absorption constant m in Equation (4.7) can be determined based on the standard, ANSI/ASA S1.26 (2019). Bies et al. (2018) provided a table of m in octave bands dependent on humidity

and temperature. For a large space with hard walls, the air attenuation effect is dominant so the approximations used should be appropriate. If wall absorption is more important, a better fidelity approximation of the acoustic characteristics of the walls may be more important.

Figure 4.10 compares transfer functions between the full-scale and 1/10-scale model after the air attenuation has been included. It can be observed that agreement is improved after the transfer function has been corrected. Both target locations 1 or 2 are within the echo radius of AH 1 and 3 and no air attenuation correction is needed for these transfer functions.
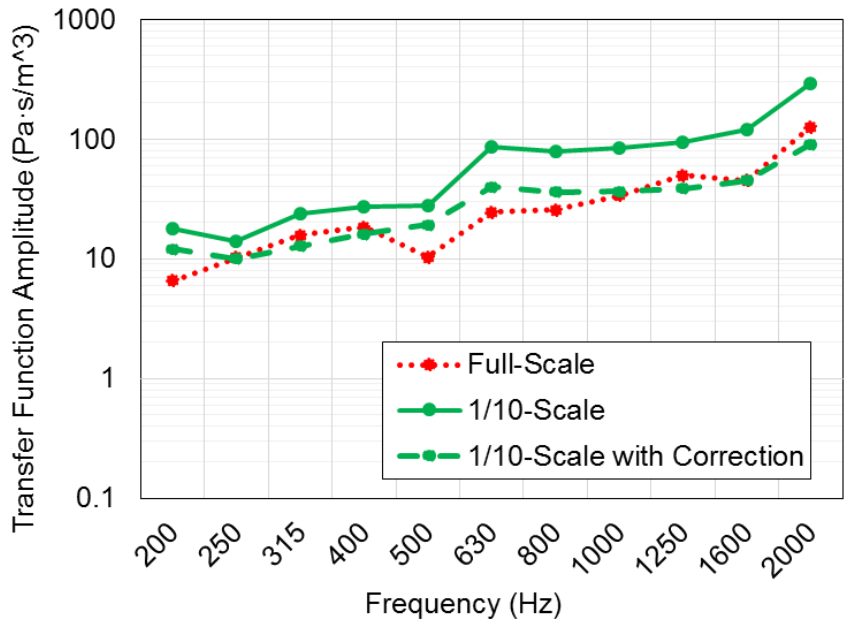

Figure 4.10 Transfer function comparison between full-scale and 1/10-scale model from AH 2 and Target 1 including adjustment with air attenuation

4.6 Inclusion of Sound Absorption in Scale Model

Sound absorption was considered as a treatment in the bakery and was incorporated into the scale model in a rudimentary fashion. Sound absorbing

materials are frequently characterized by their complex wavenumber and characteristic impedance, often referred to as bulk properties. Several well-known empirical equations have been developed relating the bulk properties to the flow resistivity σ of a material (Bies et al., 2018). The characteristic impedance Z_c and complex wavenumber k_c are expressed as

$$Z_c = \rho_0 c \cdot (1 + C_1 X^{-C_2}) - jC_3 X^{-C_4} \tag{4.8}$$

and

$$k_c = \frac{\omega}{c}(1 + C_5 X^{-C_6}) - jC_7 X^{-C_8} \tag{4.9}$$

where $X = \rho_0 \omega / 2\pi\sigma$ and ρ_0 is the medium mass density. The coefficients C_i where $i = 1$ to 8 are empirical coefficients and are available for many different material types. In this research, the empirical model suggested by Dunn and Davern (1986) is used, and this empirical model is accurate in the flow resistivity range $\sim 10^3 - 5 \times 10^4$ Rayls/m. It follows that scaling of the complex wavenumber, characteristic impedance, and resulting properties like the sound absorption should be valid if X is scaled correctly. If the same medium (i.e, air) is assumed, the scaling rule for sound absorption can be expressed as

$$\gamma_\omega \gamma_\sigma^{-1} = 1 \tag{4.10}$$

where γ_ω and γ_σ are the scaling factors for frequency and flow resistivity. In a very rudimentary sense, it can be assumed that the flow resistance is proportional to

the material density as the absorber is compressed. In that case, the relationship between the frequency scaling and thickness of the absorbing material can be expressed as

$$\gamma_\omega \gamma_d = 1 \qquad (4.11)$$

where γ_d is the thickness scaling. From Equations (4.10) and (4.11), it can be concluded that the sound absorption can be scaled in an approximate sense by simply compressing the foam and reducing the thickness by the geometric scale factor s.

For this research, 7.5 cm (3 inch) polyurethane foam was installed in the loft of the bakery. The flow resistivity of the polyurethane foam was 4100 Rayls/m measured according to ASTM C522 (2016).

The foam was compressed to approximately 1/10 of the original thickness, shown in Figure 4.11, and the flow resistivity was measured. The material was compressed to several different thicknesses until the flow resistivity was close to a factor of 10 times the original. After some trial and error, the thickness and flow resistivity of the compressed foam were 0.9 cm (0.35 inch) and 40,600 Rayls/m respectively.

| (a) Full-Scale | (b) 1/10-Scale |

Figure 4.11 Sound absorptive material (polyurethane foam) in (a) full-scale, and (b) 1/10-scale model

The normal incident sound absorption was measured in impedance tube using ASTM E1050 (1998).

The sound absorption is compared for the uncompressed and compressed foam in Figure 4.12. The compressed foam is plotted with the scaling rule applied on the frequency axis. Since the compressed foam is measured in the same impedance tube, the impedance tube cut-off frequency is reduced from 5500 Hz to approximately 550 Hz. Both measured results compare well up to the cutoff frequency for the compressed material. The sound absorption predicted using the empirical model for the compressed foam is also included and compares well to the uncompressed foam to 2000 Hz which is the maximum frequency of interest.
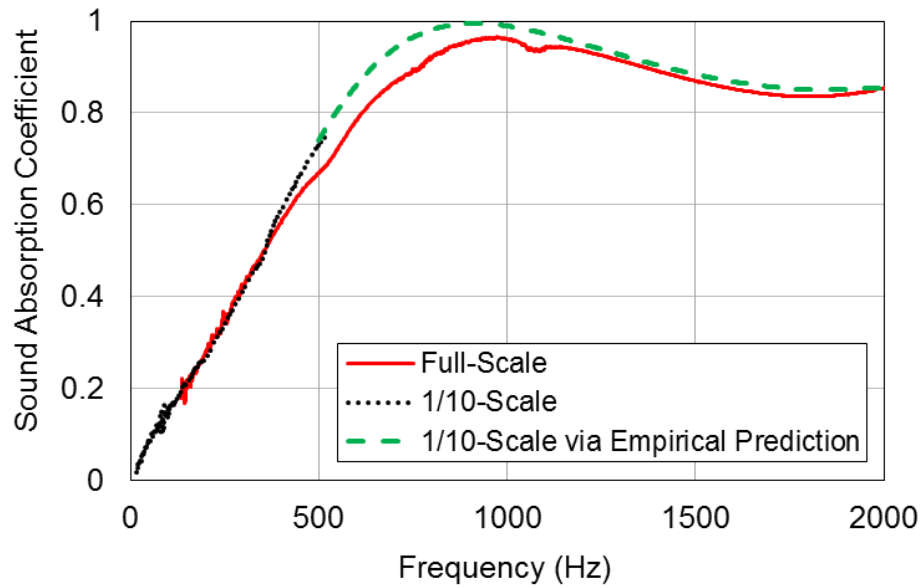
Figure 4.12 Sound absorption coefficient comparison between full-scale and 1/10-scale model. Empirical prediction from flow resistivity is also included for comparison

4.7   Treatments Considered to Reduce Air Handler Noise

Several treatments were considered to reduce the noise from the air handlers in the bakery. Air handler noise was especially bothersome in the loft and so treatments were applied close to AH 3. The effect of the treatments was assessed using the scale model and then compared to the full-scale case.

The three treatments considered are shown in Figure 4.13 and are listed below.
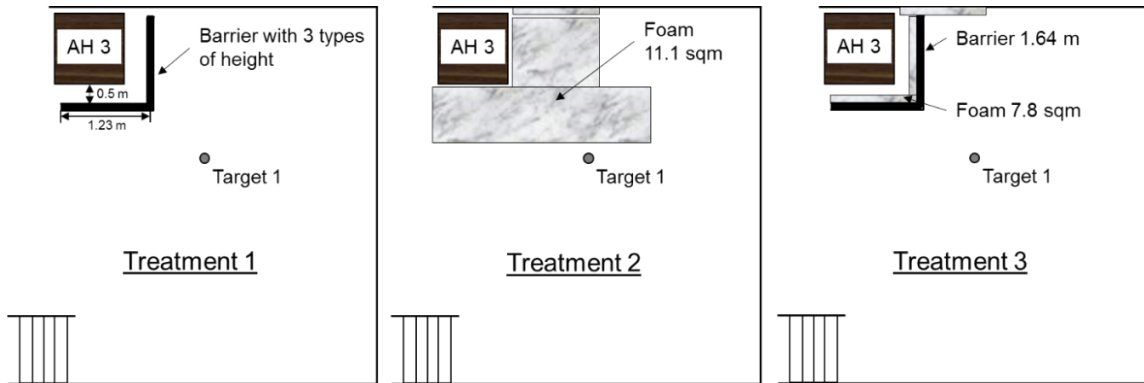
Figure 4.13 Floor layout showing treatments applied to AH 3 in loft area

1) <u>Treatment 1</u> – A barrier placed on two sides of the air handler was constructed. The primary noise source at higher frequencies is from the air intake which is on the lower part of the unit. Barrier heights of 0.82 m, 1.64 m, and 2.46 m were considered. The barrier was 1.9 cm thick and was positioned 0.5 m from the unit. The same thickness barrier was used in the scale model. Note that barrier thickness was not scaled, but this effect proved to be relatively minor in this example. Photographs of the full-scale and 1/10-scale models for the different height barriers are shown Figure 4.14.

2) <u>Treatment 2</u> – The acoustic foam measured earlier was placed on the wall and floor near the unit. The total surface area of the 7.5 cm foam was approximately 11.1 m². Photographs of the full-scale and scale model treatments are shown in Figure 4.15.

3) <u>Treatment 3</u> – The 1.64 m height barrier was lined on the two inner sides with 7.5 cm foam. Foam was also added to the wall adjacent to the unit and barrier. The total surface area of sound absorption was approximately 7.8

m^2. Photographs of the full-scale and scale model treatments are also shown in Figure 4.15.
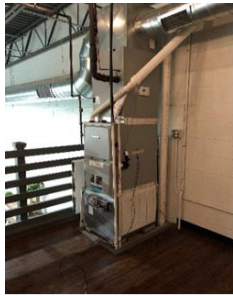
| a) Baseline | b) 0.82 m Barrier | c) 1.64 m Barrier | d) 2.46 m Barrier |

| e) Baseline | f) 0.82 m Barrier | g) 1.64 m Barrier | h) 2.46 m Barrier |

Figure 4.14 Photos showing barrier treatments for full-scale a) – d) and 1/10-scale model e) – h)

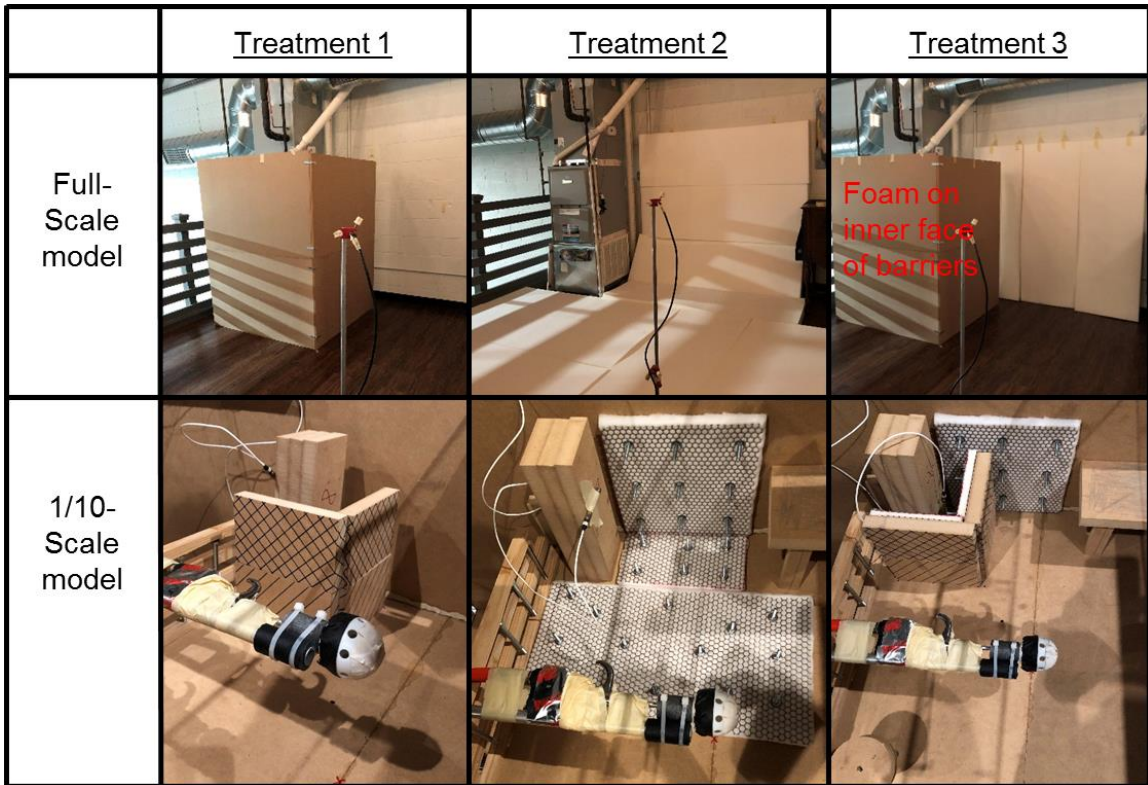|	Treatment 1	Treatment 2	Treatment 3
Full-Scale model			Foam on inner face of barriers
1/10-Scale model			

Figure 4.15 Photos showing Treatment 1, Treatment 2, and Treatment 3 in full-scale and 1/10-scale model

4.8   Sound Pressure Level Predictions – Scale Model

The sound pressure was predicted at the receiver locations using the 1/10-scale model and results were compared to direct measurement for the baseline case without any treatments. Figure 4.16 compares the sound pressure level predictions in 1/3 octave bands with direct measurement for target location 1. Both the full-scale and 1/10-scale model results were computed assuming sources were uncorrelated. The air attenuation correction has been included in the scale model. It can be observed that agreement is acceptable with the measured sound pressure at the target locations though the sound pressure level is overpredicted at the low frequencies. There was noticeable variation in the sound pressure level

of the air handlers at low frequencies and this is the most likely reason for the discrepancy.
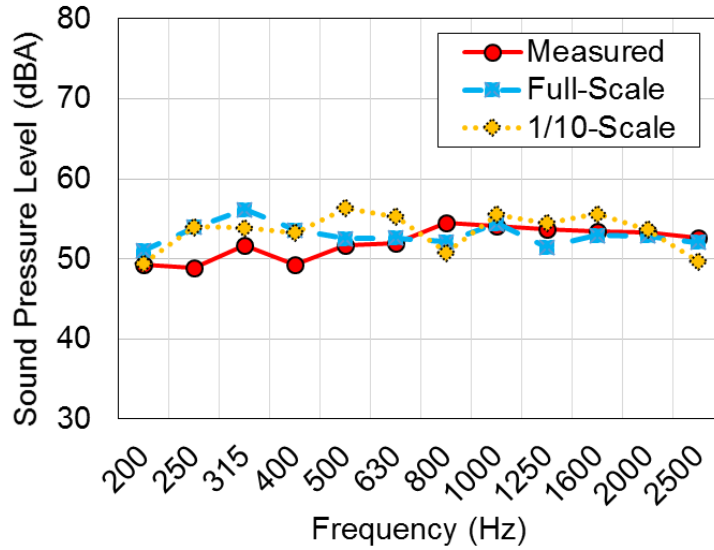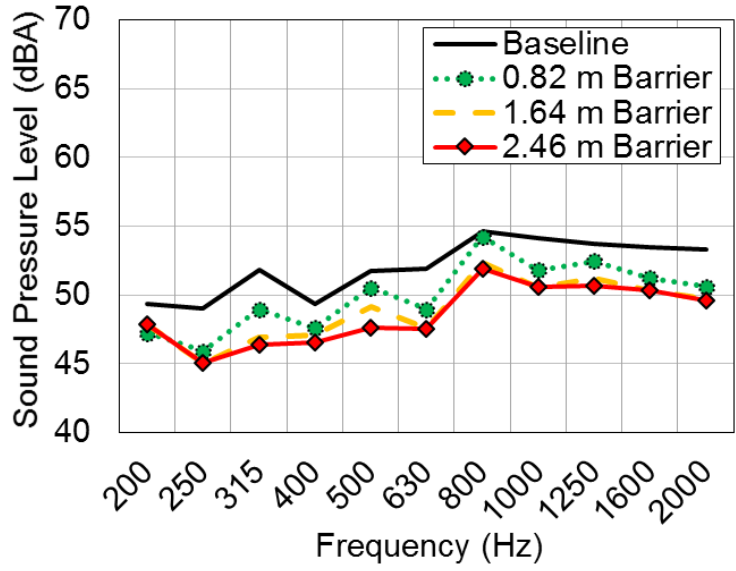

Figure 4.16 Sound pressure level comparisons at Target 1 for the baseline case. Measure results are compared to PCA predictions for full-scale and 1/10-scale model

The addition of barriers (Treatment 1) was considered next. To simplify the testing, only AH 3 was operating since AH 1 and AH 2 contribute much less at Target 1 and will not be affected by the barriers. Since the barriers were unlined, they were not anticipated to greatly reduce the noise at the receiver.
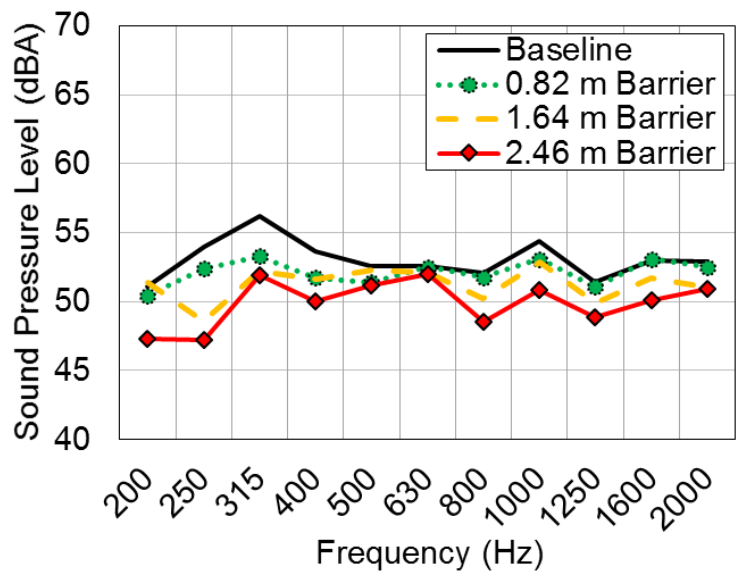
Table 4.1 Sound pressure level measurements and PCA predictions for different barrier heights

|	Overall SPL (dBA)		
Testing Cases	**Measured**	**Full-Scale**	**1/10-Scale**
Baseline	61.4	61.8	63.2
0.82 m Barrier	60.0	60.8	62.0
1.64 m Barrier	58.7	60.0	60.7
2.46 m Barrier	58.3	58.8	60.1

Table 4.1 compares directly measure sound pressure levels in dBA to full-scale and 1/10-scale PCA predictions. The effect of adding the barriers on the A-weighted sound pressure level is modest. For the tallest barrier (2.46 m), noise is reduced about 3 dBA. Though 1/10-scale model PCA predictions are approximately 2 dB high, reductions due to the barriers are successfully predicted using both full-scale and 1/10-scale PCA predictions. Results are shown in 1/3 octave bands in Figure 4.17 and show similar trends between measurement and PCA (full-scale and 1/10-scale) predictions as the barrier height is increased.

(a) Measurement

(b) Full-Scale
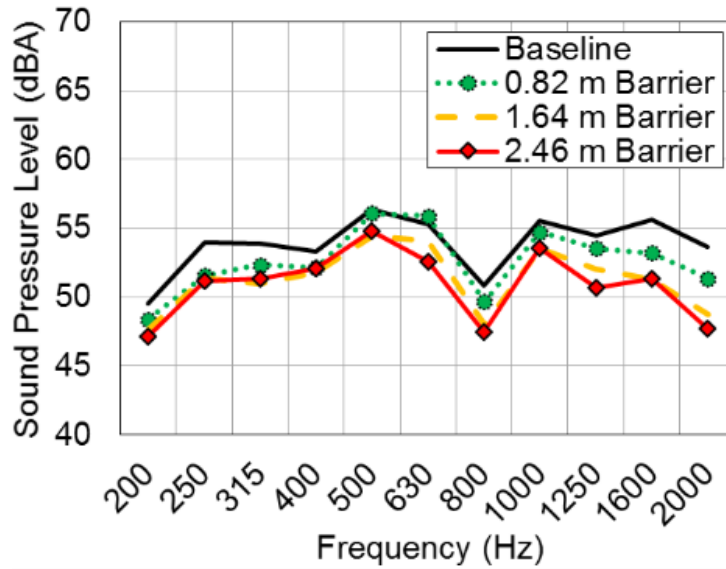
(c) 1/10-Scale

Figure 4.17 Sound pressure level comparisons at Target 1 for the different barrier heights of (a) Measurement, (b) Full-Scale, and (c) 1/10-Scale

The noise may also be reduced by adding sound absorption to the wall and floor close to the unit. Treatment 2 is strictly sound absorptive whereas Treatment 3 combines sound absorption with the 1.64 m barrier.   Figure 4.18(a) and Figure 4.18(b) compare the measured sound pressure level with the1/10-scale model predictions for Treatments 2 and 3 respectively. In both cases, correlation between direct measurement and prediction is acceptable.

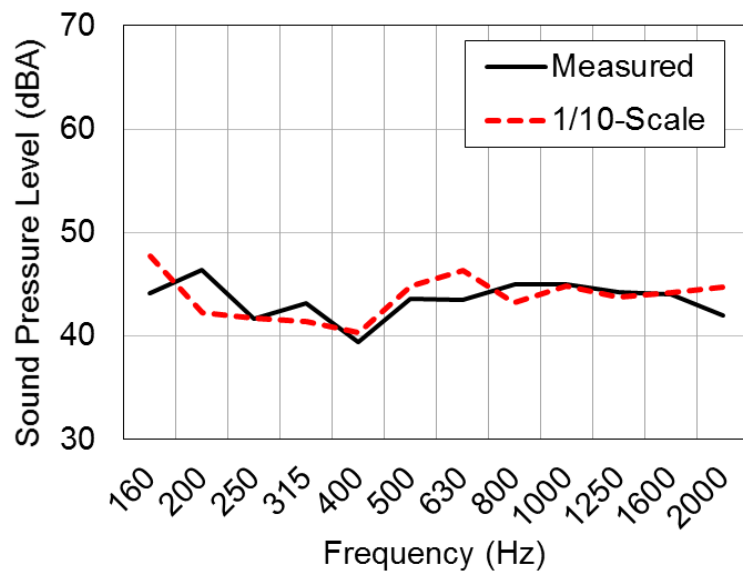Table 4.2 Sound pressure level measurements and 1/10-scale model PCA predictions for Treatments 1, 2, and 3

Testing Cases	Overall SPL (dBA)	
	Measured	1/10-Scale
Baseline	61.4	63.2
Treatment 1 (1.64 m Barrier)	58.7	60.7
Treatment 2	58.0	59.5
Treatment 3	54.9	56.4

Table 4.2 compares the A-weighted measured sound pressure level with PCA predictions. Treatment 2 provides approximately a 2.5 dBA noise reduction which is similar to the noise reduction achieved with the 2.46 m tall barrier. If sound absorption is combined with the 1.9 m barrier (Treatment 3), a noise reduction of 6.5 dB is achieved. PCA predictions for the 1/10-scale model compare well with measurement. Differences are less than 2 dBA and trends are predicted very accurately. (b) 1/10-scale model

Figure 4.19 shows that the 1/10-scale model PCA predictions compare well to measurement in 1/3-octave bands as well.
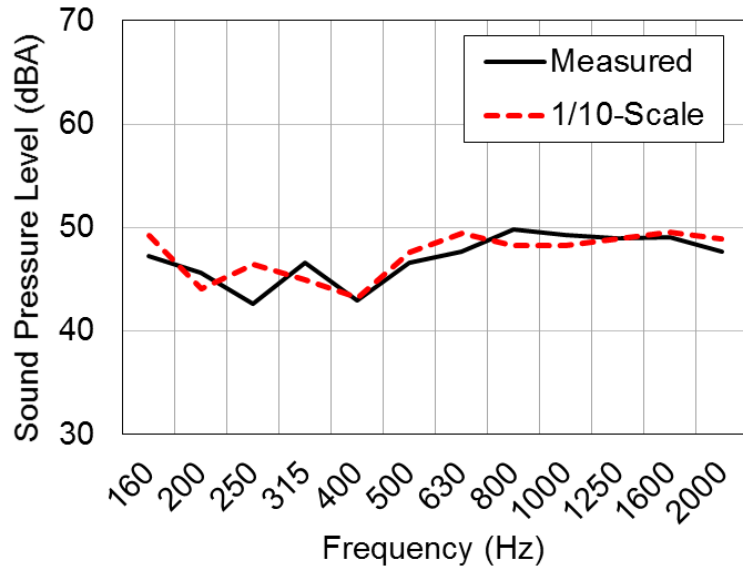
(a) Treatment 2

(b) Treatment 3

Figure 4.18 Sound pressure level comparisons between direct measurement and 1/10-scale model prediction for (a) Treatment 2, and (b) Treatment 3
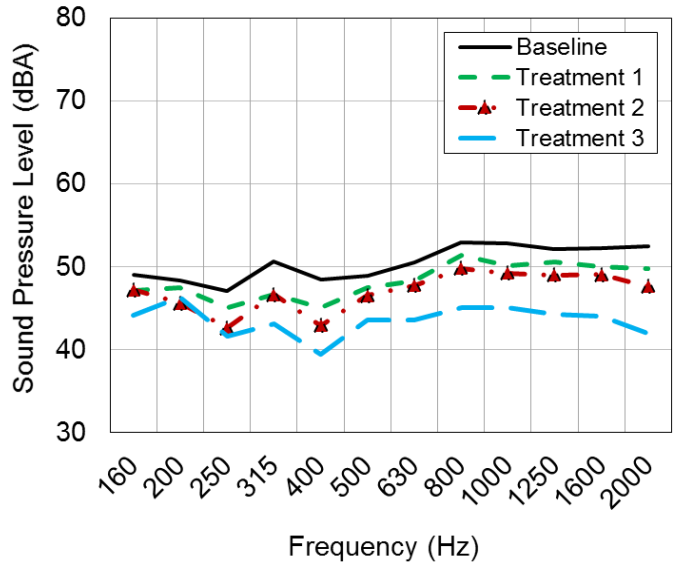
(a) direct measurement
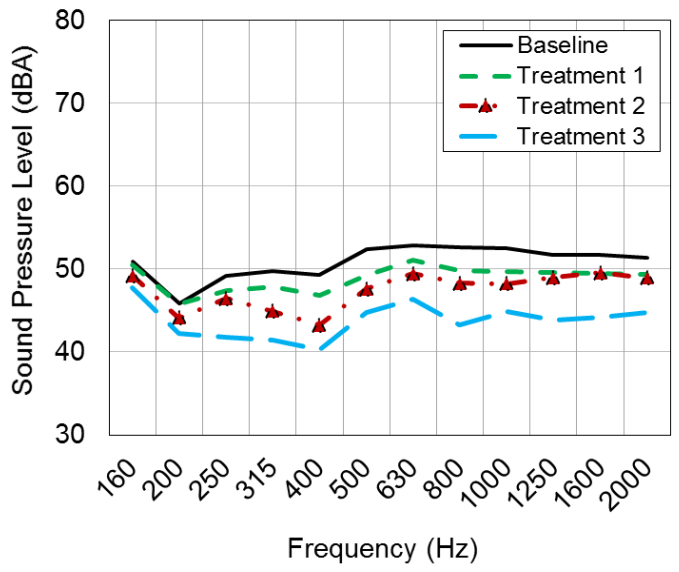
(b) 1/10-scale model

Figure 4.19 Sound pressure level predictions at Target 1 for different treatments using (a) direct measurement, and (b) 1/10-scale model

Contributions were predicted from the panels and air inlet using the 1/10-scale model PCA predictions and results are shown in Figure 4.20 for both the baseline case and for Treatment 3. PCA predictions reveal that the noise treatments reduce noise transmitted from both the air intake and the panels of the

air handler, but most of the improvement is a result of blocking and absorbing the noise from the air intake opening. This example demonstrates that PCA with scale modeling can be used to assess treatments as well as the effectiveness of treatments for specific paths of interest.
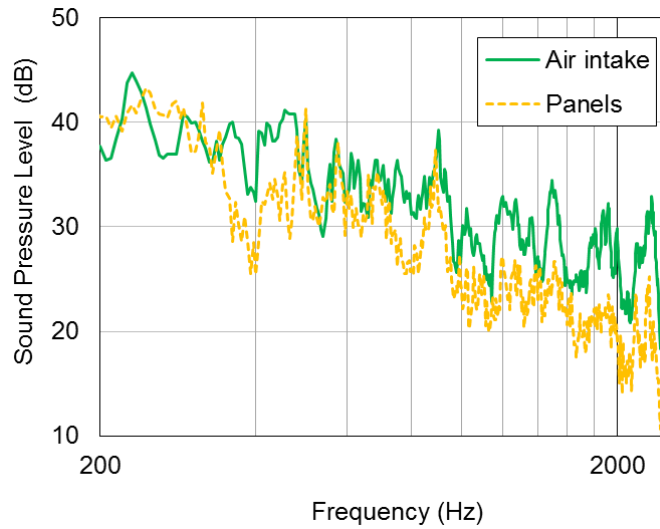
(a) Baseline
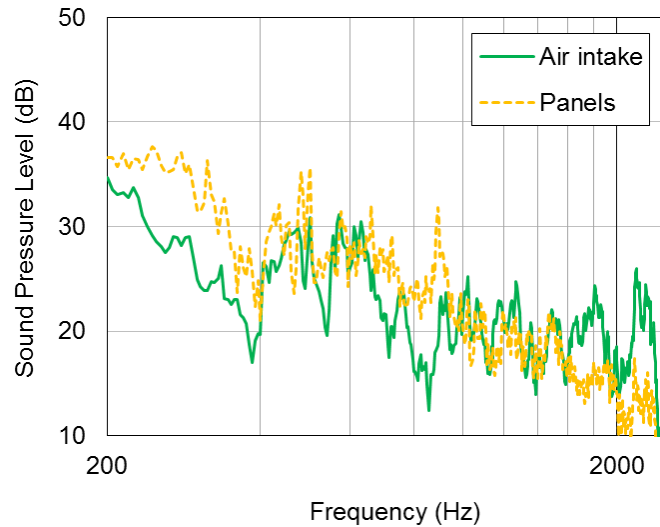
(b) Treatment 3

Figure 4.20 Sound pressure level contribution analysis using the 1/10-scale model for (a) Baseline, and (b) Treatment 3

4.9   Summary

PCA has been combined with scale modeling to rank noise sources and assess treatments in a large bakery. Though applied to a building acoustics case, the approach detailed and used in the paper is amenable for use in predicting noise emissions from large machinery and equipment. Most importantly, modifications to the path can be assessed prior to installation so long as volume velocities from source panels or components can be measured a priori. If implemented, this procedure can provide great benefit by permitting prediction of sound pressure levels from airborne paths in buildings or other environments prior to large machinery being installed.

For the bakery considered, the primary noise sources were three air handler units. Each unit was discretized into patches and transfer functions were measured reciprocally on both the full-scale case and a 1/10-scale model. Surface vibration and sound intensity were measured by a P-U Probe while the machine was operating. The P-U probe is ideal for this purpose because volume velocity and sound intensity may be measured simultaneously. PCA can then be applied assuming uncorrelated or correlated sources. The correlated assumption is more appropriate at low frequencies whereas volume velocities are more likely to be uncorrelated at middle and high frequencies, which was the case for most of the frequency range of interest for the three air handler units. The sound pressure at the receiver positions was predicted using full-scale and 1/10-scale predictions, and then compared to direct measurement with good agreement.

Barrier and sound absorptive treatments were then assessed using the combination of PCA and scale modeling.

Future efforts should investigate selecting the patch size and best practices for measuring volume velocities and transfer functions. In addition, it would be of great interest to investigate the fabrication of scale models using 3D printing.

Chapter 5   PCA APPLIED ON UNMANNED AERIAL VEHICLE

(Note: Some parts of the research in this chapter has been previously documented in Cheng and Herrin 2018)

5.1   Introduction

Recreational use of small unmanned aerial vehicles or UAVs has increased greatly because of groundbreaking improvements in technology along with decreased cost.   Similarly, commercial applications are becoming more widespread due to the ability to easily maneuver a payload without a pilot onboard including cameras and sensors for use in agriculture, film making, 3D mapping, wildlife ecology management, logistics, and other applications (Xiang et al,, 2011, Anderson et al., 2013).   As the use of UAVs in public areas has increased, noise has been recognized as problematic (Berglund et al., 1999) and the FAA is becoming increasingly concerned (Burleson, 2017).

Research on noise related UAV topics is increasing with the evident need. For example, Cannard et al. at University of Southampton in his paper (2019) validated that changing the shape of leading edge slits is a promising technology to control the broadband Aerofoil-Turbulence Interaction noise (Chaitanya, 2017), which just requires a small modification on the blade design. Hasheminejad et al. from the same institution, concluded in his paper (2019), that the serrations of leading edge of the blades can disrupt the vortex shedding phenomenon and therefore reduce the associated noise emission.

Ning et al. (2017) introduced serrated edges to attenuate the trailing edge induced noise at low Reynolds numbers (Re≈53,000). Gur et al. (2009) presented three different optimization schemes to design quiet propellers for an electric mini UAV subjected to power and structural constraints. The design variables include propeller radius, number of blades, blade geometry and cone angle, and rotational speed. Kloet et al. (2017) used a microphone array to map the sound signature of a small UAV in a laboratory and field under hovering conditions. Most of this acoustic related research involves measuring the sound pressure level in the far field. However, it is also important to make measurements closer to the UAV in order to better discriminate between source mechanisms.

The objective of the current research is to make a series of measurements close to the UAV and then to predict the sound pressure level at some distance away. Once a source model is developed, it is relatively simple to predict the sound pressure level at any distance away from the source in any environment including both outdoor and indoor applications.

The approach used is a simple and approximate method commonly referred to as panel contribution analysis or PCA. Seminal research in the area was performed by Fahy (1995, 2003) and Verheij (1997) over 20 years ago. It has been applied in a number of different industries (Zheng et al., 1994) including aerospace (Mason et al., 1990). PCA consists of the following steps.

1. A source is discretized into a collection of panels or patches. These patches should surround a source but need not be on the source.

2. Acoustic transfer functions are measured between the patch volume velocity and the sound pressure and sometimes particle velocity at the receiver position. These transfer functions are most easily measured reciprocally.

3. The volume velocity and sometimes the sound pressure is measured for each patch.

4. The sound pressure in the field can be predicted by summing the products of volume velocities (and sound pressures) and the respective transfer functions.

In this chapter, the relevant theory is discussed, and then it is applied to a small UAV of the type commonly used by hobbyists.

5.2   The Primary Noise Sources of a Small UAV

Propeller noise is the dominant noise source for small UAV (Marte et al., 1970, Self, 2010). In the frequency domain, the noise signature induced by blades or propellers consists of both harmonic tones and broad band components (Sinibaldi et al., 2013, Intravartolo et al., 2017). The harmonic tonal noise is caused by the rotational blade and occurs at the blade pass frequencies, while the broadband noise results from the flow structure convection along the leading or trailing edges of the blades.

Both analytical predictions and measurements show that the maximum value of sound pressure levels is in the proximity of the blade tip (Marino et al., 2010), where the high intensity of the trailing vortex is expected. In the research

of this dissertation, the P-U Probe sensor was located above the blade tip (Figure 5.2) in an effort to capture the most important noise sources.

A small UAV (DJI Mavic Pro) is considered in this chapter. Propeller noise is the dominant noise source for small UAV (Rod, 2010). Tonal noise components dominate at lower frequencies with broadband noise due to turbulence becoming more important at higher frequencies. The reason is that the propeller speed is not excessively high. The tips of the propellers are moving at ~60 m/s while hovering (~6000 RPM). The propeller diameter is 0.2 m. Hence, the first several harmonic components due to the blade pass frequencies are dominant (Marte 1970). Figure 5.1 shows a measurement of the sound pressure level at 5.5 m away from the UAV. The blade pass frequency is ~200 Hz and there are important harmonics at ~400, 600, and 800 Hz.
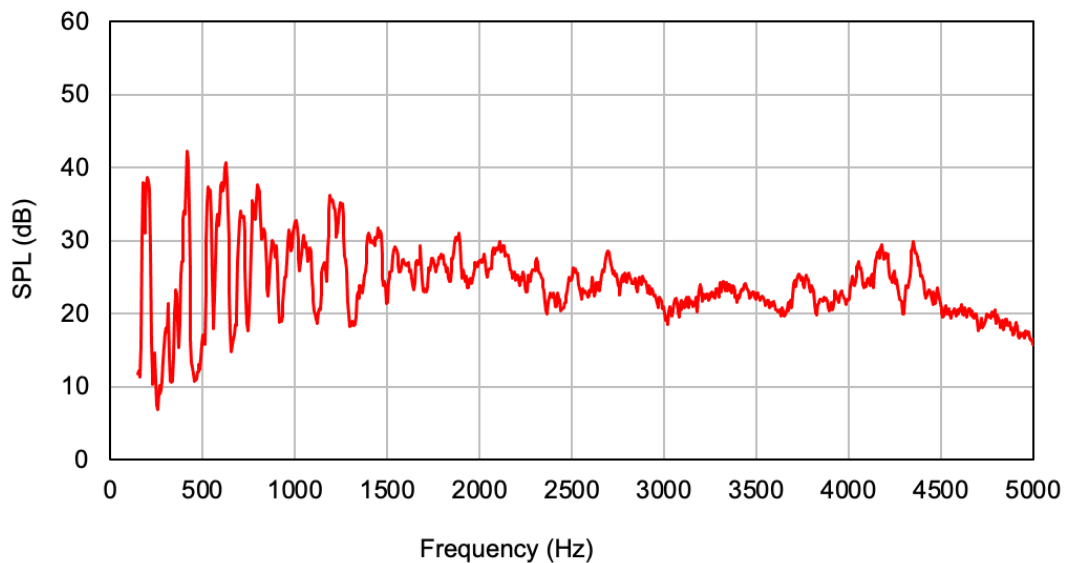
Figure 5.1 Sound pressure level of a small drone

5.3   Panel Contribution Analysis for Non-rigid Surfaces

A discrete version of the Helmholtz integral equation can be used to express the sound pressure at a receiver point in the field ($p(P)$) at position P. This is expressed as

$$p(P) = \sum_{i=1}^{N} \left[(v_n)_i \left(\frac{p_i}{Q_R} \right)_{TF_i} - p_i \left(\frac{(v_n)_i}{Q_R} \right)_{TF_i} \right] \Delta S_i \qquad (5.1)$$

where $(v_n)_i$ is the normal velocity and p_i is the sound pressure at the center of a patch. Transfer functions $(p_i/Q)_{TF_i}$ and $((v_n)_i/Q)_{TF_i}$ are measured reciprocally by placing a volume velocity source Q_R at the intended receiver position in the field and measuring the sound pressure and particle velocity at the center of each patch. The UAV should be in the correct position but not operating. For most applications, the second term on the right-hand side in Equation (5.1) can be neglected. If a source is relatively rigid, the transfer function $((v_n)_i/Q)_{TF_i}$ will be small since the source will vibrate little when insonified. However, it is included in this case because patches surround the source but are not on the source.

The next phase of the measurement campaign is to identify the volume velocity $(v_n)_i \Delta S_i$ and sound pressure p_i for each patch i with the UAV operating. If phase is not ignored, the volume velocity and sound pressure at the center of each patch can be measured directly using a P-U Probe or a traditional intensity probe. Phase is preserved in the measurements so long as there is an appropriate reference signal. Alternatively, sources may be assumed to be uncorrelated with

respect to one another. In that case, the average sound intensity from each patch I_i is measured and the volume velocity Q_i expressed as
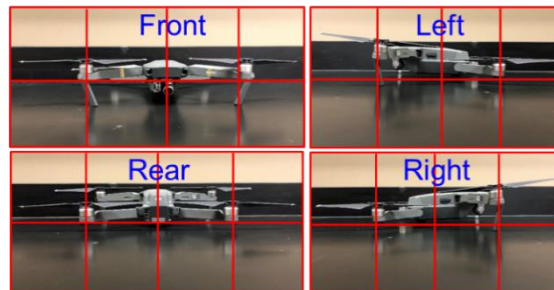
$$Q_i^2 = (I_i \cdot \Delta S_i) \frac{2\pi c}{\rho \omega^2} \tag{5.2}$$

5.4 Sound Pressure Level Prediction of UAV

An imaginary rectangular cuboidal surface was constructed around the UAV and discretized into patches. The discretization is as shown in Figure 5.2 with each patch having an area of 10 cm × 10 cm for a total of 64 patches.
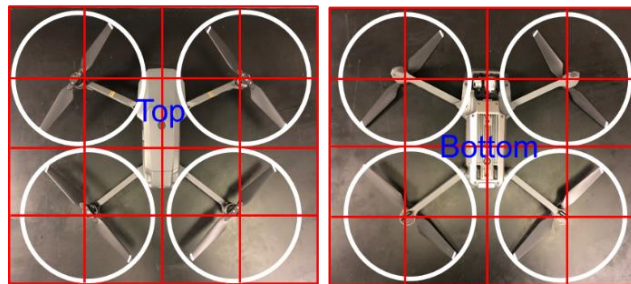

(a) Top and Bottom Surface

(b) Front, Rear, Left and Right Surface

Figure 5.2 Patch Discretization on the imaginary box

Transfer functions were measured with the UAV suspended from a metal frame in the hemi-anechoic chamber at the University of Kentucky as shown in

103

Figure 5.3.   The UAV is turned off and is positioned 0.8 m above the floor of the chamber. The volume velocity source was placed at a receiver point 5.5 m away from the UAV, and 1.5 m above the ground (i.e., approximately ear level). A microphone positioned 0.8 m away from the source is used to calibrate the sound source.   The sound source consists of a shop air connected to a metal throat attached to a whiffle ball.   With the P-U probe at the center of each patch, transfer functions $(p_i/Q)_{TF_i}$ and $((v_n)_i/Q)_{TF_i}$ were measured.
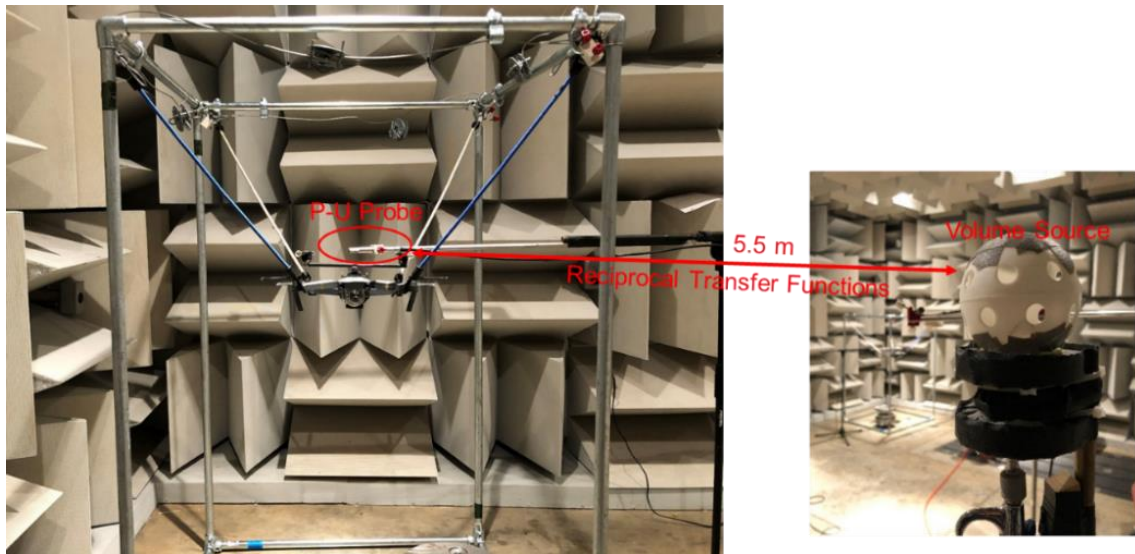

(a) Measurement Setup
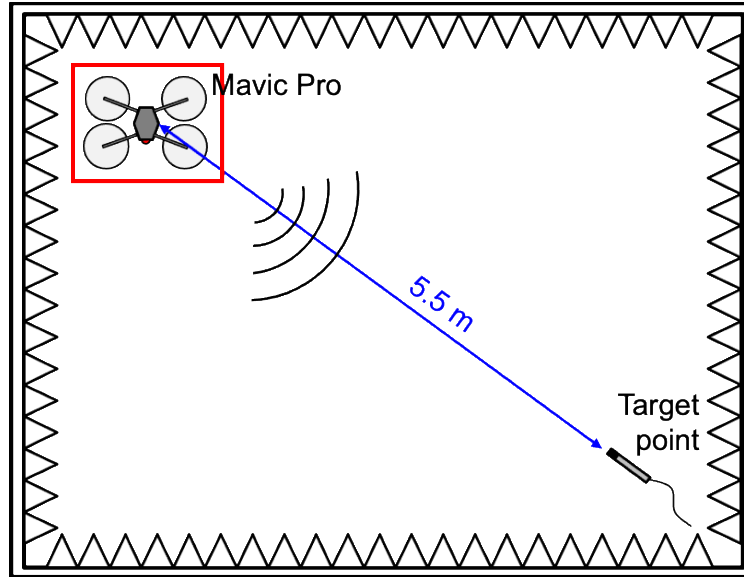
(b) Schematic showing layout of testing environment

Figure 5.3 Transfer functions measurement

For the operating measurements shown in Figure 5.4, the UAV was flown to the same position where it had been suspended in the prior step. The P-U Probe was then used to measured particle velocity, sound pressure and sound pressure at the center of each patch on the rectangular cuboidal surface. With the help of a forward and downward vision sensor and motion sensor, the UAV hovered very precisely and steadily. Figure 5.5 shows the spectrogram for one patch during a 15 second testing period. As the spectrogram shows, the signal was very consistent in the testing window with very little fluctuation in frequency. Hence, measurements were made without the benefit of any holding stand.

Figure 5.4 Particle velocity and sound pressure measured on imaginary box
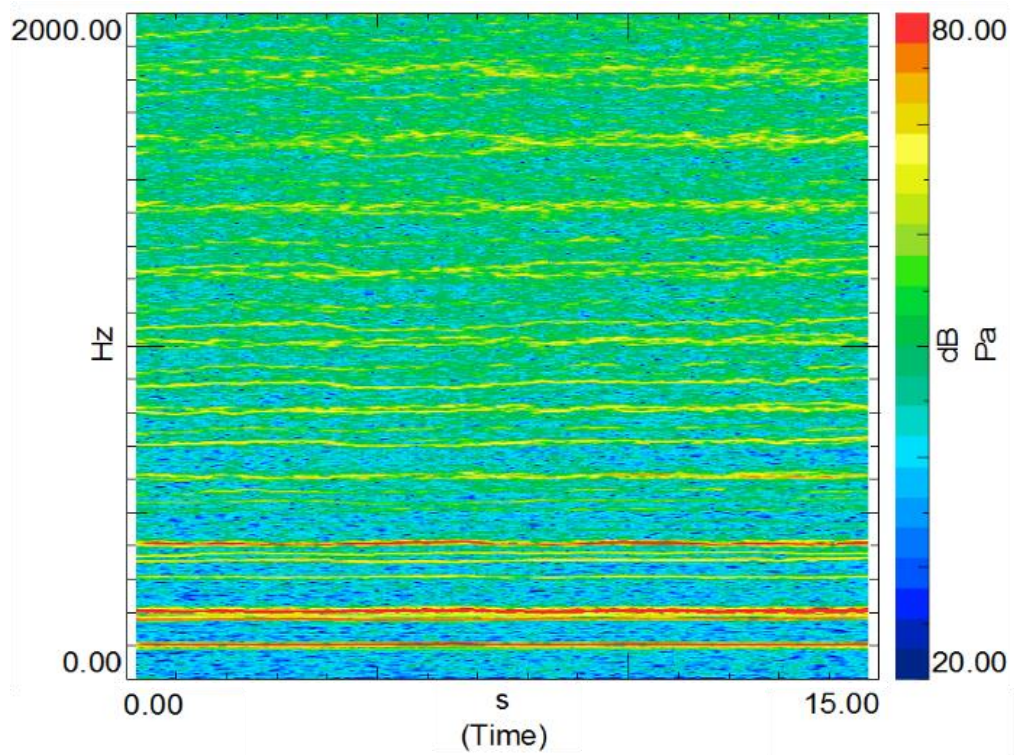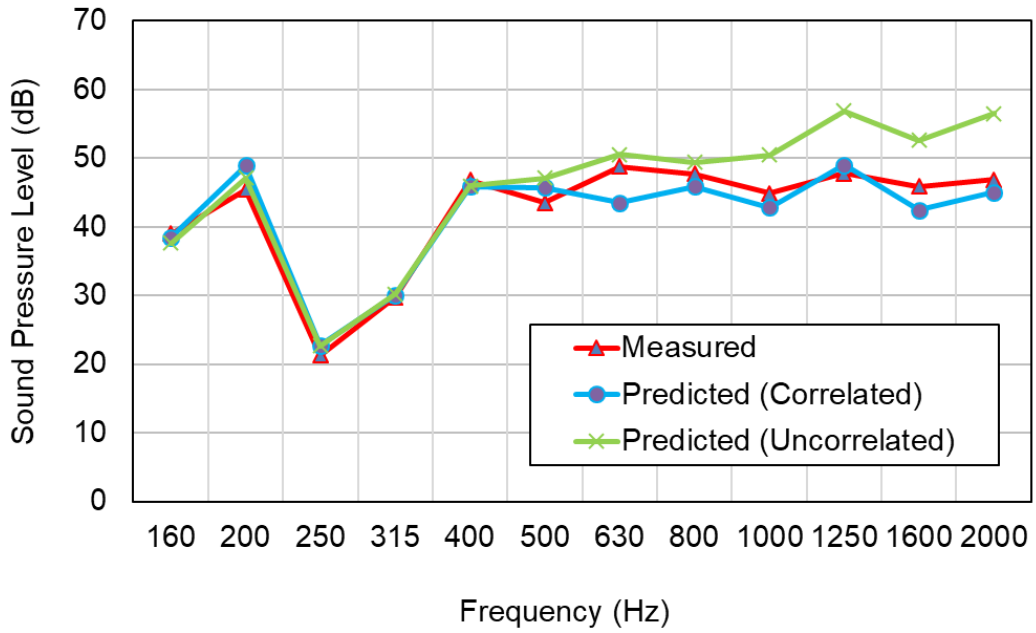

(a) Sound pressure
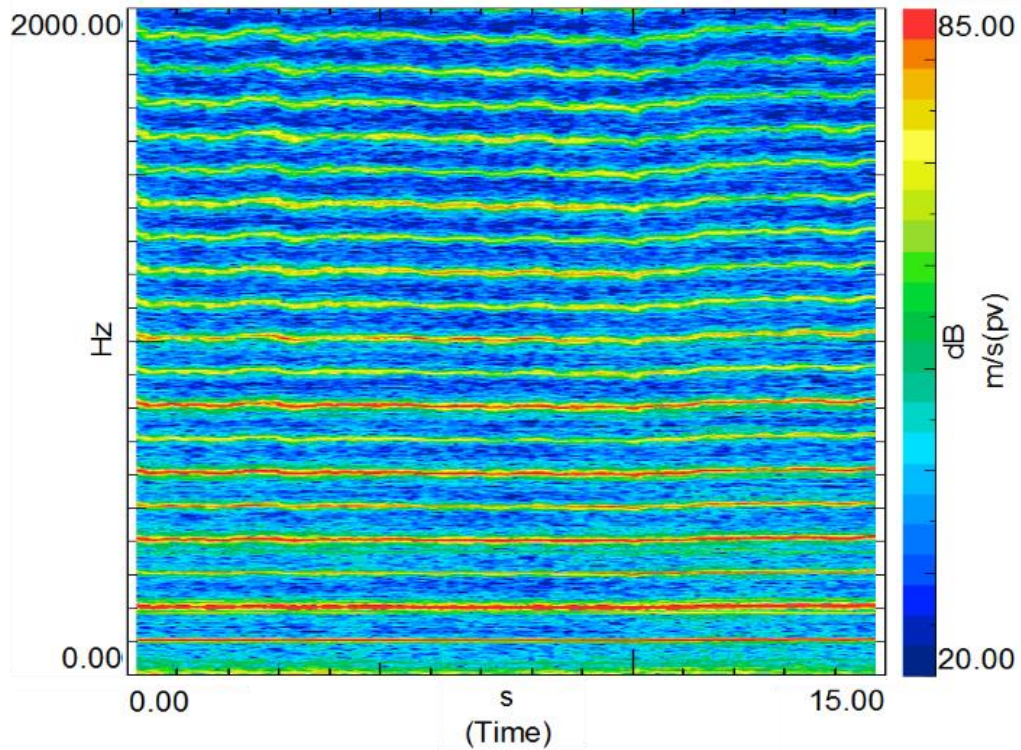
(b) Particle velocity

Figure 5.5 Spectrogram by P-U Probe

Predictions were then made for both correlated and uncorrelated assumptions. The reconstructed and measured sound pressures in narrow band and 1/3 octave bands at the receiver point are shown in Figure 5.6. Results based on the correlated source assumption compare better with measured results. This was as anticipated since blade pass noise produces a strong dipole pattern (Marte et al., 1970). It follows that phase information cannot be ignored. Note also that the predictions using the correlated assumption also capture the information at the harmonics which is most important.
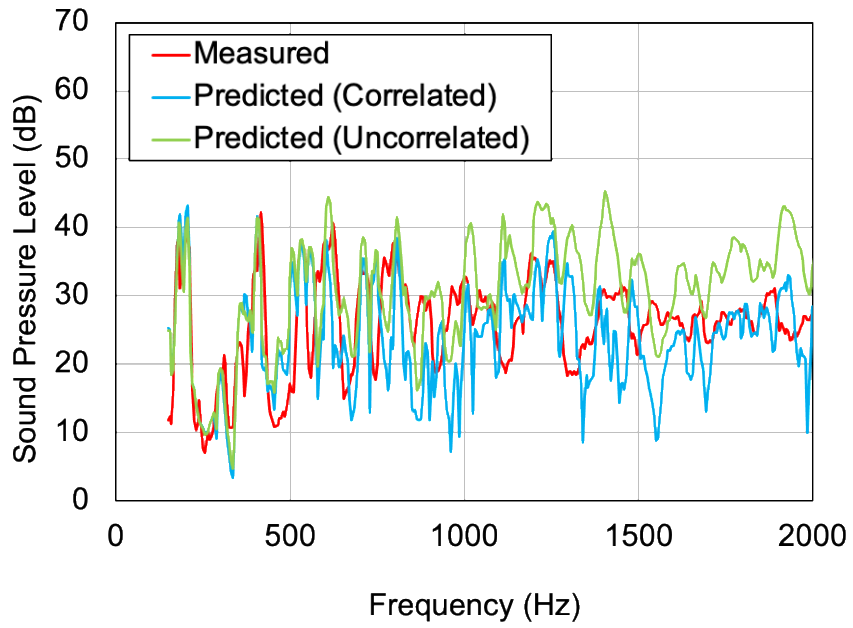
(a) Narrow band

(b) 1/3 Octave bands

Figure 5.6 Sound pressure level prediction by PCA

5.5 Contribution analysis of the UAV

The sound pressure level contributions from each surface assuming correlated sources are compared in Figure 5.7. It can be seen that the top face is the primary contributor. This result agrees with microphone measurements which showed the sound pressure level to be ~5 dB higher on the top compared to the bottom surface. The sound pressure level comparison is shown in Figure 5.8.
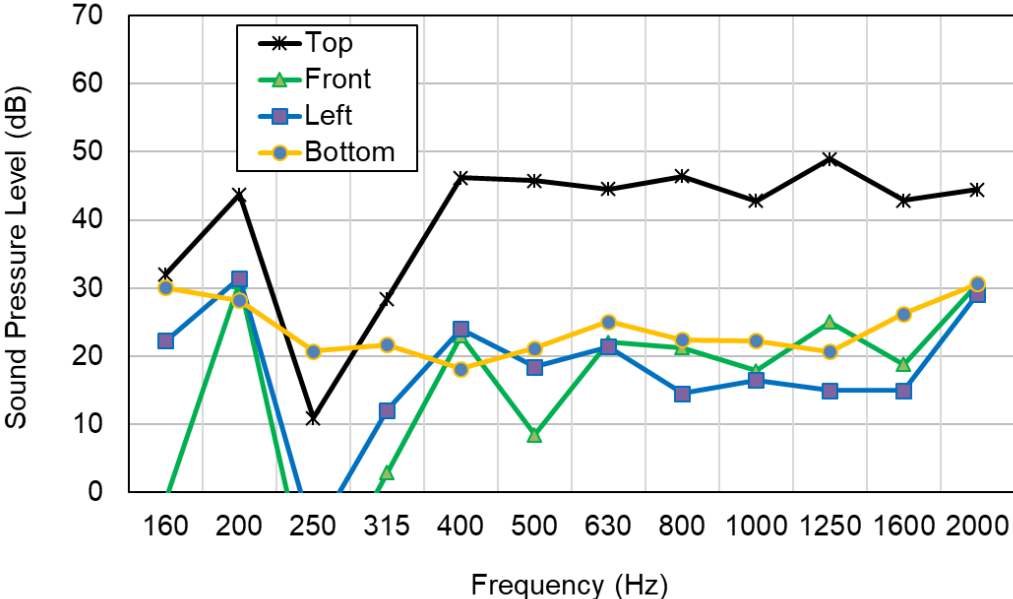

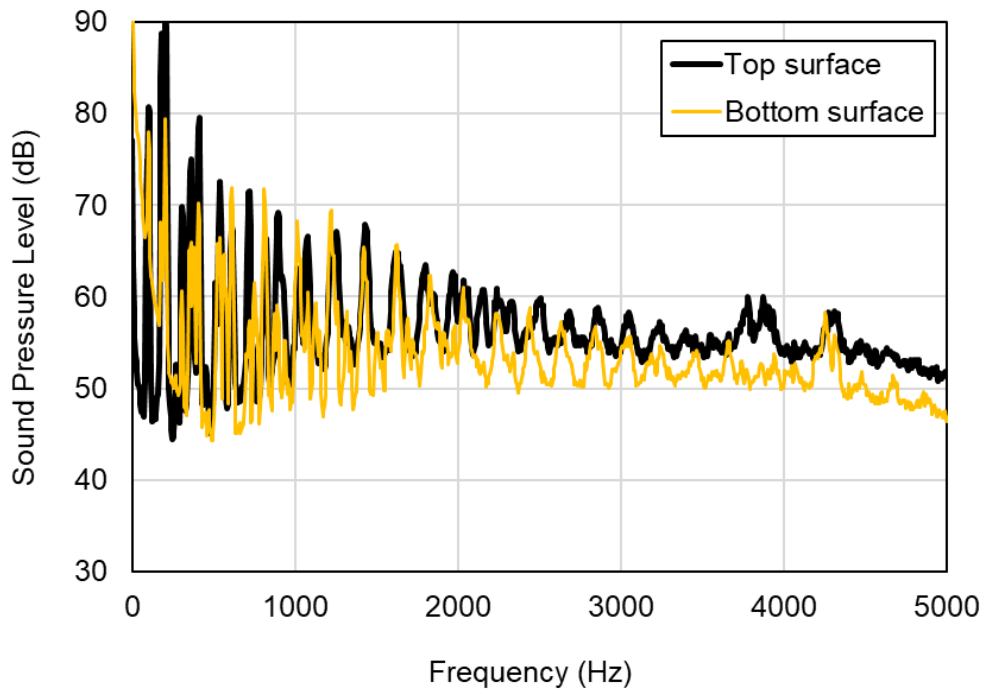Figure 5.7 Sound pressure contributions for UAV

Figure 5.8 Sound Pressure of top and bottom surface of the UAV

Possible reasons for the difference include the directional character of the sound sources and that the acoustic impedances above and below the UAV are very different.   The mismatch of the impedance (Clinton, 1950) may be caused by the airflow around the UAV. Impedance measurements above and below the UAV were performed with PU-probe in the hemi-anechoic chamber.   In the measurement shown in Figure 5.9, the UVA hovered at a height of 1.5 m with layers of sound absorbing lining stacked on the floor. Then sound absorption on the floor served to reduce reflections of the floor.
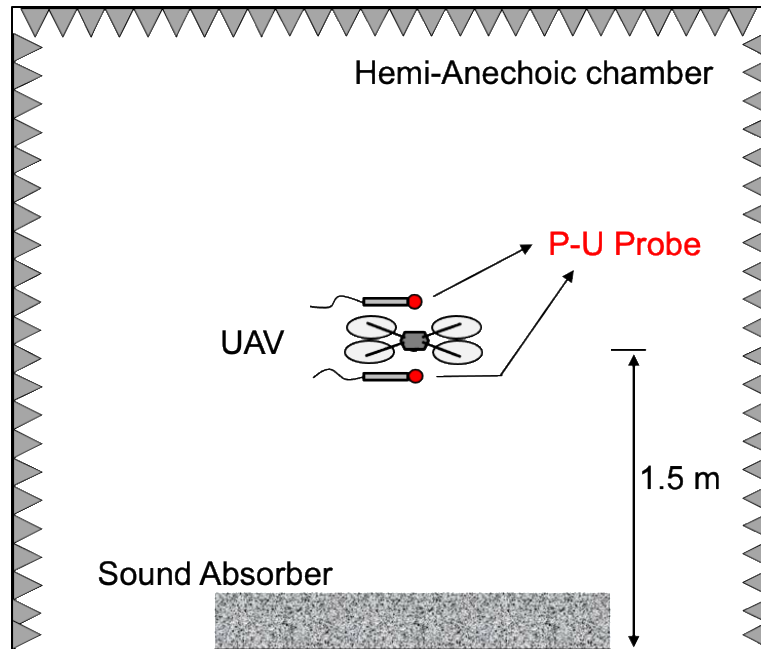
Figure 5.9 Experiment Layout for Acoustic Impedance measurement

The impedance can be expressed as

$$Z = \frac{p}{u_n} \tag{5.3}$$

The impedance results in Figure 5.10 illustrate that the acoustics impedance is much higher on the bottom surface than the top surface. This impedance difference is almost certainly produced as a result of the flow but the rationale is not well established. Figure 5.11 (b) to Figure 5.14 (b) show particle velocity contours. It can be observed that the particle velocity is much higher on the top rather than the bottom side.

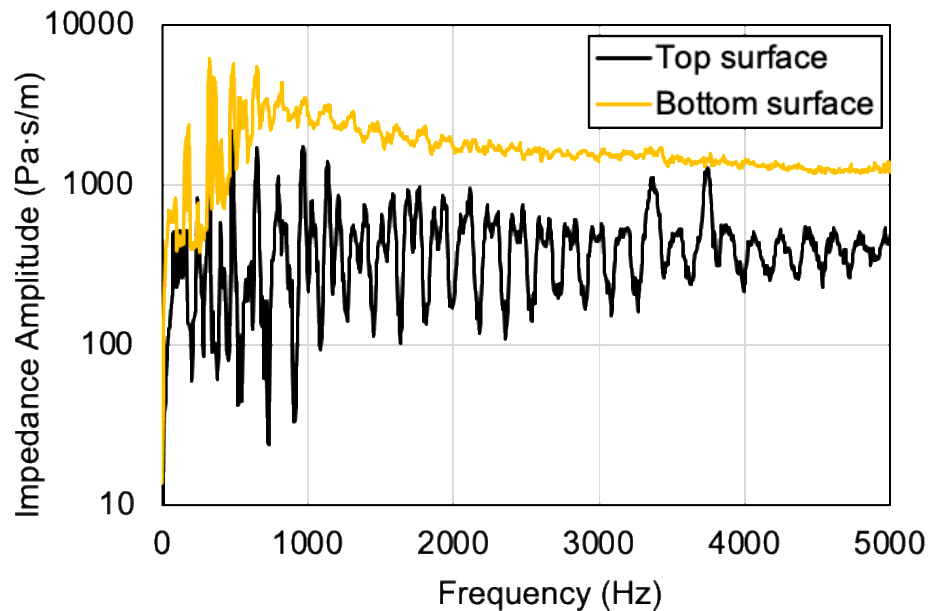Figure 5.10 Acoustic Impedance of top and bottom surface of the UAV

5.6   Use of the P-U Probe to Identify the Noise Signature

The P-U Probe is a very suitable type of sensor to identify the noise sources for hovering UAV because the particle velocity sensor is insensitive to frequency components of other strong sources that are not in the direction measured. Since the weight is not equally distributed, the front pair of blades rotates at slightly different RPM compared to the rear pair. Since the noise emitted by the UAV is mainly caused by the rotational components, the different RPM of the blades will result in different noise components in the frequency domain. Particle velocity measurements can differentiate between fore and aft propeller sources. In Figure 5.1, it can be observed that for the 1st harmonic component, there are two peaks close to each other around 190 Hz. One peak is at 185 Hz, while the other one is at 200 Hz.

The contours of sound intensity, particle velocity amplitude, and phase on the top surface are shown in (a), (b), and (c) from Figure 5.11 to Figure 5.14 respectively. On both sound intensity and particle velocity amplitude contours, it can be observed that the 185 Hz component is due to the rear pair of blades.

Figure 5.12 and Figure 5.14 show that the 200 Hz component is produced by the front pair of blades.

Identifying these noise components from the rotational blades is very critical in UAV design. Because if the two frequencies components are too close in frequency to each other, it may result in noise modulation phenomenon, which sometimes brings uncomfortable noise concern for communities.
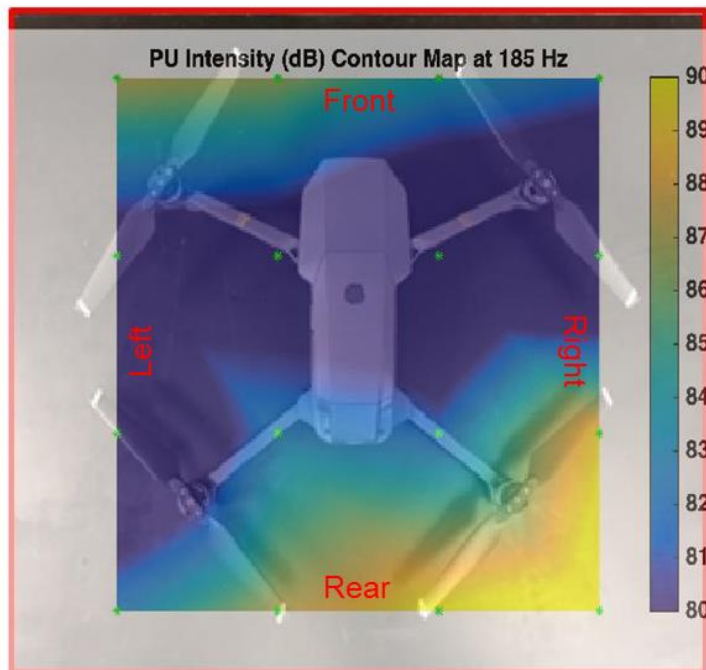
(a) Sound intensity contour
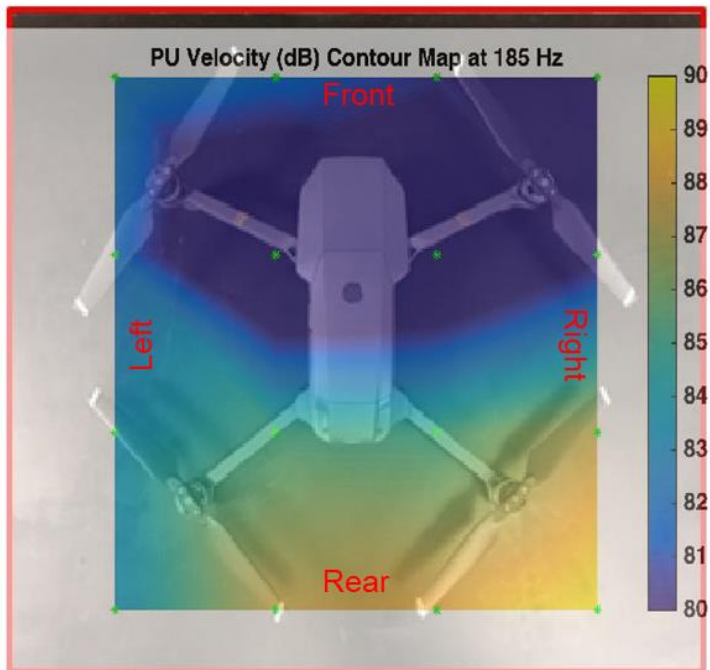
(b) Particle velocity amplitude contour
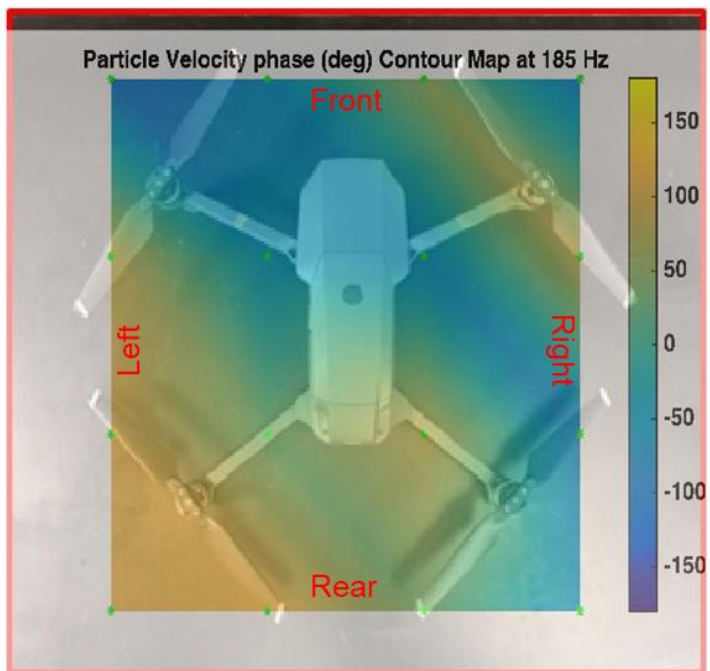
(c) Particle velocity phase contour

Figure 5.11 Sound Intensity and Particle Velocity contour on top surface at 185 Hz

(a) Sound intensity contour

(b) Particle velocity amplitude contour

(c) Particle velocity phase contour

Figure 5.12 Sound Intensity and Particle Velocity contour on top surface at 200 Hz
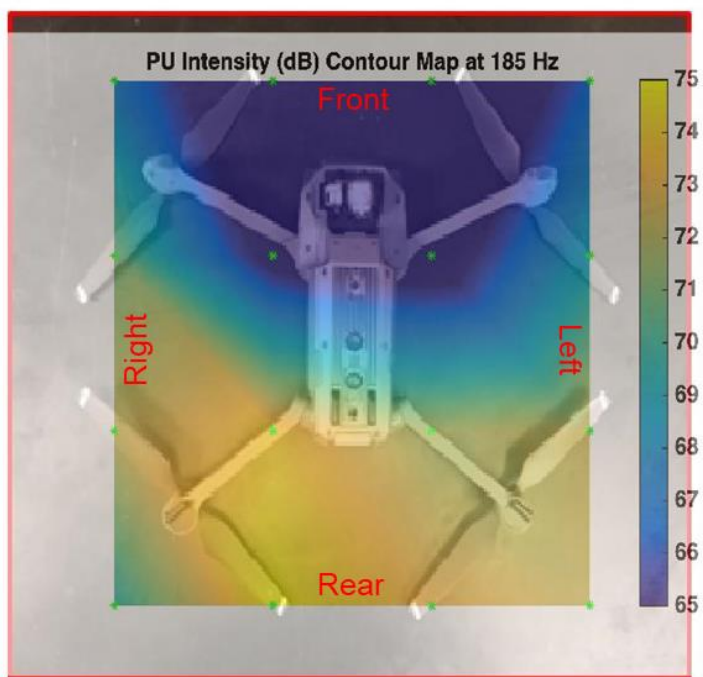
(a) Sound intensity contour
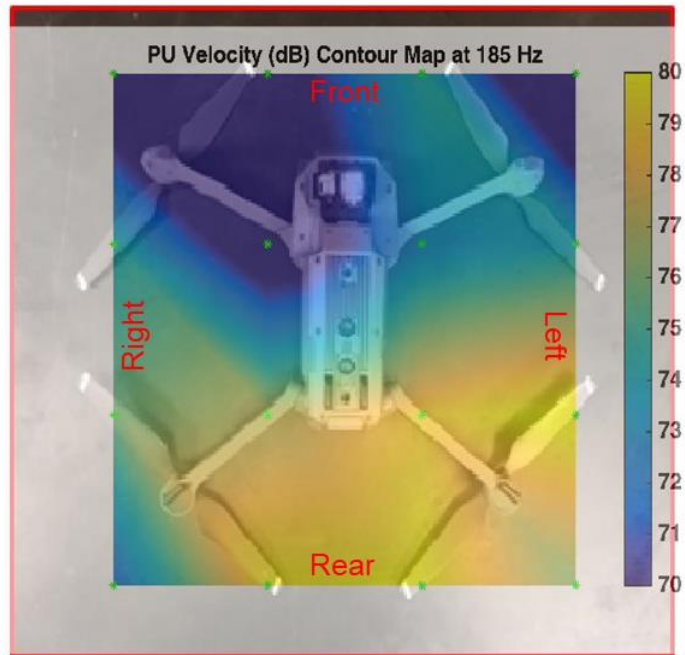
(b) Particle velocity amplitude contour
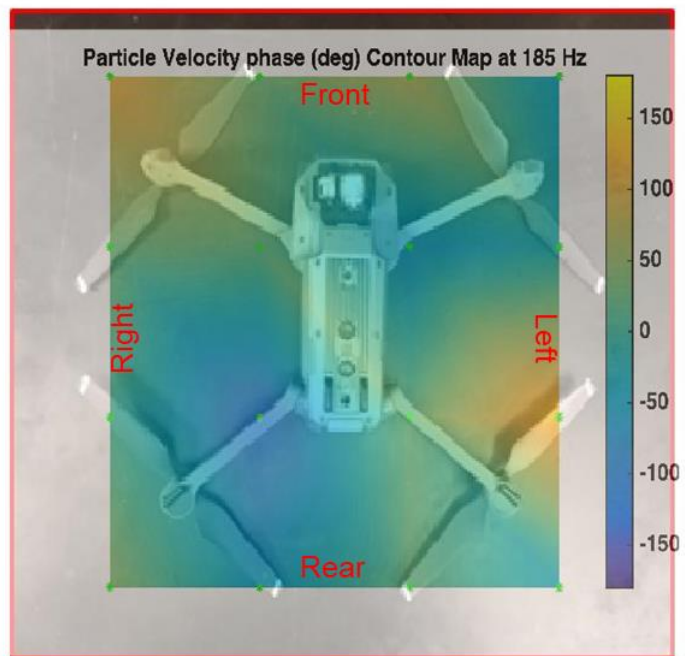
(c) Particle velocity phase contour

Figure 5.13 Sound Intensity and Particle Velocity contour on bottom surface at 185 Hz

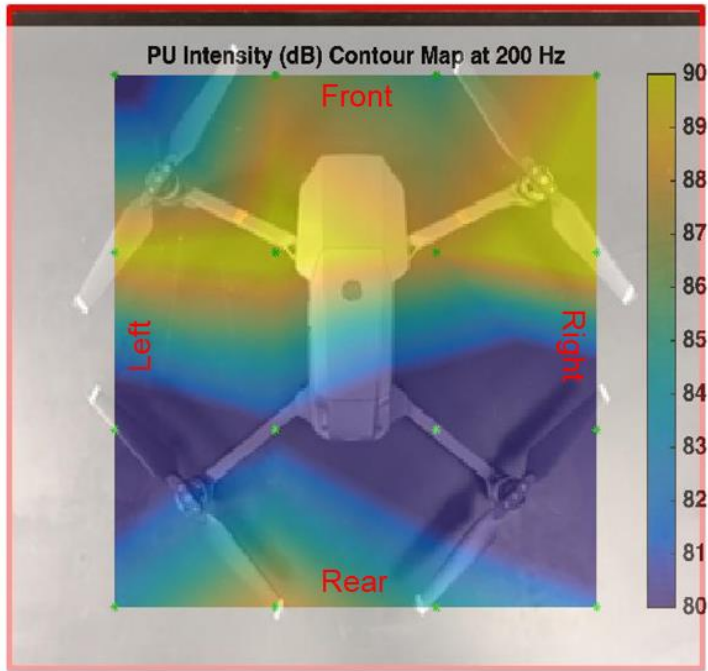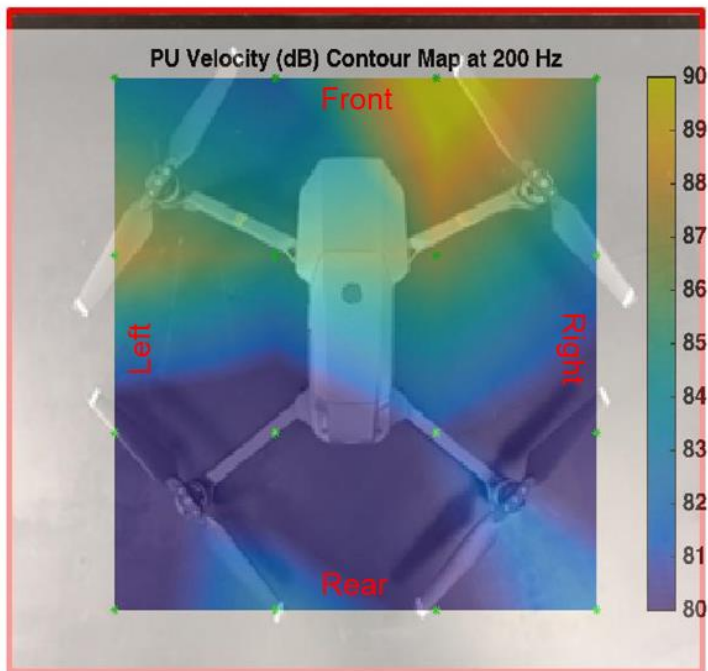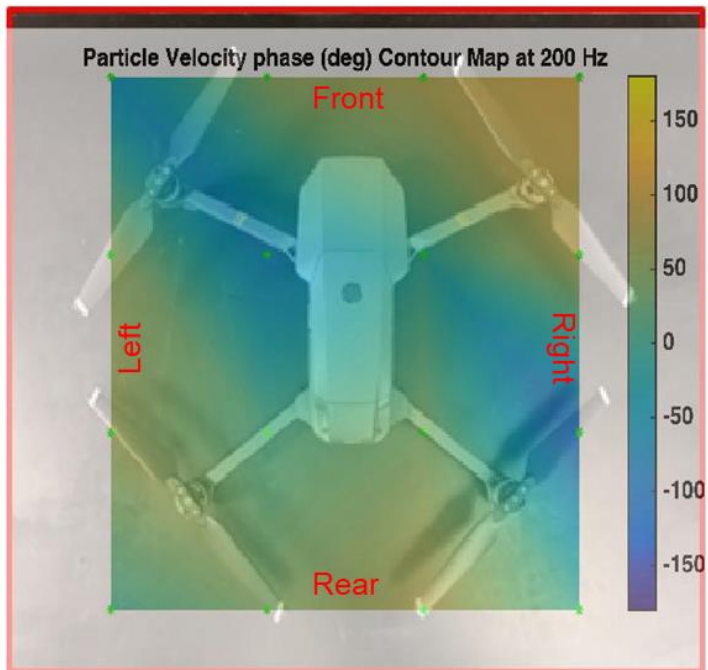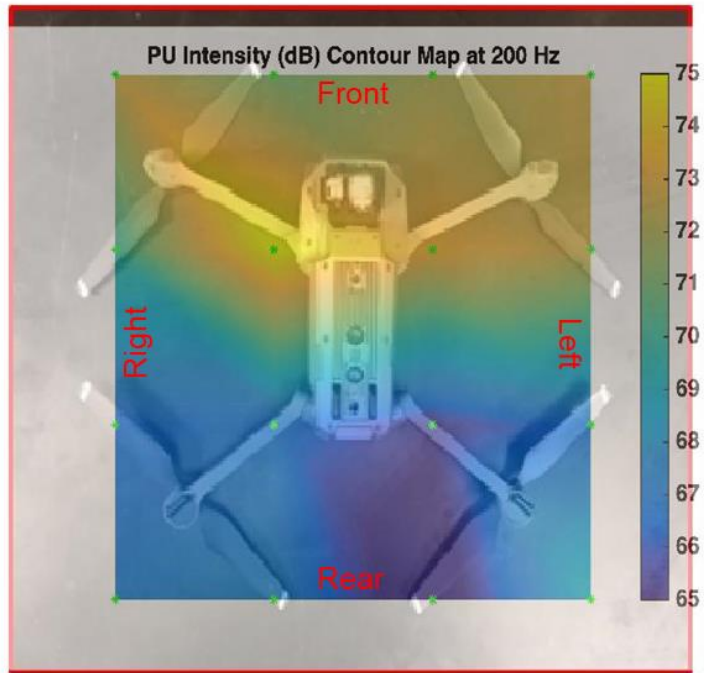(a) Sound intensity contour
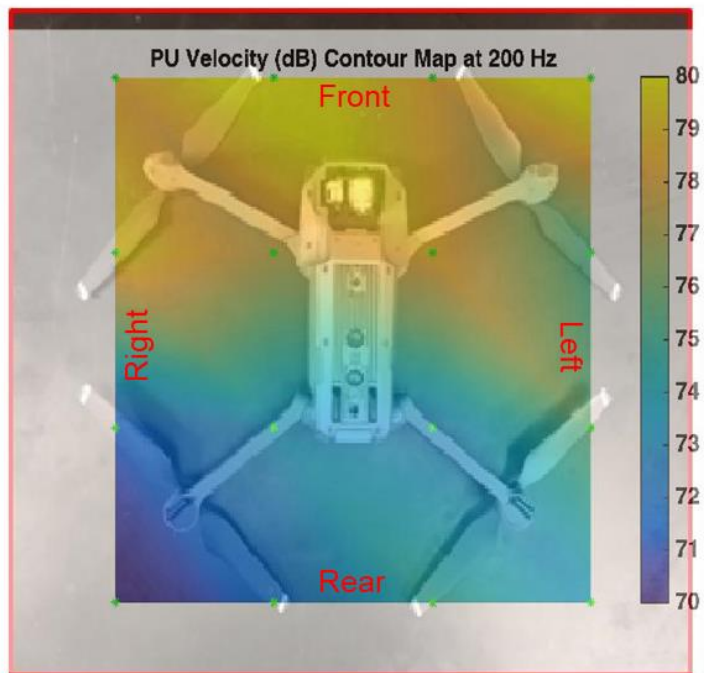
(b) Particle velocity amplitude contour
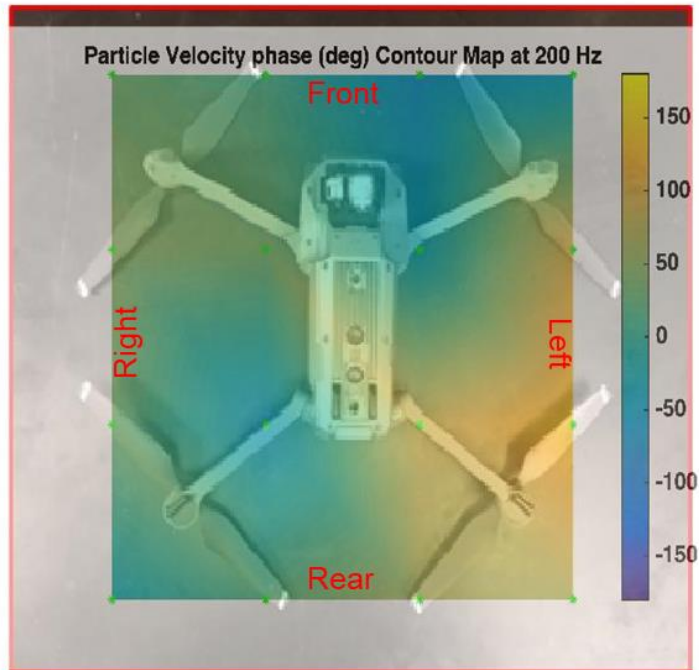
(c) Particle velocity phase contour

Figure 5.14 Sound Intensity and Particle Velocity contour on bottom surface at 200 Hz

5.7 Summary

PCA was used to predict the noise radiation from a small UAV. The receiver location was located 5.5 m away from the source in a hemi-anechoic chamber. Transfer functions were measured reciprocally between patches on an imaginary rectangular cuboidal surface and the receiver location with the UAV suspended from a frame. After which, the volume velocity for each patch was determined using the P-U Probe. Particle velocity, sound pressure, and sound intensity were measured simultaneously by the P-U Probe. Using this data, sound pressure level at the receiver point was estimated with good agreement compared to direct measurement. The contribution from each surface of the imaginary rectangular

cuboidal was compared. The primary contribution was from the top surface of the UAV. The explanation of the dominant top surface is that the acoustic impedance has been influenced by the air flow, therefore the sound radiation for the top and bottom surface are quite different with each other. In order to identify the noise components of the UAV, the sound intensity and particle velocity contours were also plot. From the P-U Probe contours, it was found that for the hovering status, the front pair of propeller had different blade pass frequency with the rear pair.

Chapter 6   CONCLUSIONS AND FUTURE WORK

The objective of this research was to combine panel contribution analysis (PCA) with scale modeling to predict the sound pressure emissions from complicated, real world machinery. The main steps in PCA are to a) discretize the structure, b) measure the volume velocity while running, c) measure transfer functions between the source and a position in the field, and d) then compute sound pressure in the field by multiplying the transfer functions by the volume velocity.

6.1   PCA in Exterior Radiation Application

PCA was used to determine the noise emissions from a generator set. The sound pressure in the field was determined using both correlated and uncorrelated sources. Volume velocities were measured using a combination sound pressure and particle velocity probe or P-U-probe. The sound pressure level at the receiver locations was predicted using both full scale and half scale transfer functions with good agreement. In addition, PCA was used to determine the effect of barrier treatments. The method used permits sound emissions to be predicted prior to locating the equipment. Moreover, sound mitigation measures can be considered prior to siting.

The main contributions of this study were to demonstrate that:

1. PCA can be combined with scale modeling to accurately predict noise emissions for exterior problems.

2. Treatments can be considered using scale model transfer functions.

3. A simple point source developed at the University of Kentucky is appropriate for PCA.

4. The P-U probe can be used to measure the volume velocity and sound intensity for each panel, and that the sound pressure level can be predicted using both uncorrelated and correlated source assumptions.

5. The contributions from different components may be assessed using the procedure.

6.2 PCA in Room Acoustics Application

In the next study, PCA was applied with scale modeling to rank noise sources and assess treatments in a large bakery. This is an interior case where both the direct and reverberant sound fields are important. The noise sources were three identical air handler units. Each unit was discretized into patches and transfer functions were measured reciprocally on both the full-scale case and a 1/10-scale model. Transfer functions were adjusted in the scale model so that the air attenuation was properly included in the calculations. Surface vibration and sound intensity were measured simultaneously by a P-U Probe while the machine was operating. PCA was then applied assuming correlated and uncorrelated sources. Barrier and sound absorptive treatments were then assessed using the combination of PCA and scale modeling.

The main contributions of this study were to demonstrate that:

1. PCA can be combined with scale modeling to accurately predict noise emissions for interior problems.

2. Acoustic transfer functions measured using the scale model can be corrected to include the effect of air dissipation. This will be especially important for large room environments.

3. Sound absorptive treatments can be included properly in the scale models.

4. The contributions from different sources can be accurately assessed using the strategy.

6.3   PCA in UAV Noise Prediction

PCA was then used to predict the noise emission from a small UAV. The receiver location was 5.5 m away from the source. Reciprocal transfer functions were measured between UAV surface and the receiver location with the UAV suspended. The volume velocity for each patch was obtained by the P-U Probe. Particle velocity, sound pressure, and sound intensity were measured simultaneously. With this data, sound pressure level at the receiver location was reconstructed with good agreement compared to direct measurement. The contribution from each surface of an imaginary box encompassing the UAV was compared. The primary contribution was from the top surface of the UAV. The sound intensity and particle velocity contours of the top and bottom surface were also measured.

The main contributions of this study were to demonstrate that:

1. PCA can be combined with scale modeling to accurately predict noise emissions from a complicated aeroacoustic source.

2. The contribution to the sound pressure level from the different sides of the encompassing box can be computed using PCA.

123

3. Particle velocity and sound intensity measurements can be successfully procured from a stationary hovering UAV.

6.4 Future Work

While PCA is well-established, little work has been performed on developing best practices for the method. It is recommended that future research should answer the following questions.

1. What is the effect of changing the patch size on the accuracy of the results?

2. How closely does a reciprocal measurement of the vibro-acoustic transfer function correlate with the exact result?

3. What is the best way to measure the surface vibration using a P-U probe and how close to the surface should the sensor be?

4. How does the vibration pattern effect the measurement of volume velocity?

5. When should the correlated or uncorrelated assumptions be used?

In addition. Future work should look into whether scale models can be 3D printed.

Appendix: Barrier Treatment Configuration Layout

Figure A.1 Schematic showing dimensions for barrier Treatment 1 (all dimensions are in m)

Figure A.2 Schematic showing dimensions for barrier Treatment 2 (all dimensions are in m)

Figure A.3 Schematic showing dimensions for barrier Treatment 3 (all dimensions are in m)

Figure A.4 Schematic showing dimensions for barrier Treatment 4 (all dimensions are in m)

Figure A.5 Schematic showing dimensions for barrier Treatment 5 (all dimensions are in m)

Figure A.6 Schematic showing dimensions for barrier Treatment 6 (all dimensions are in m)
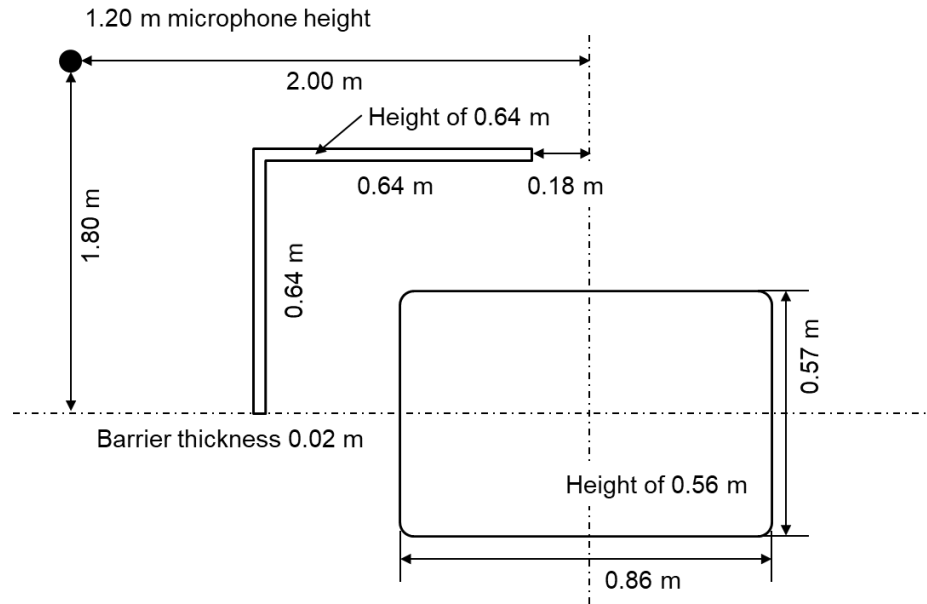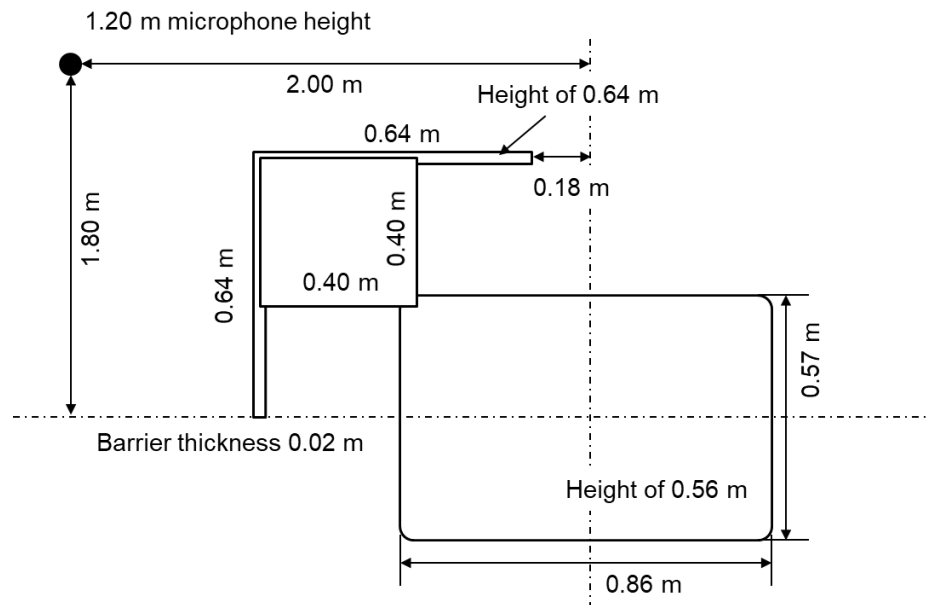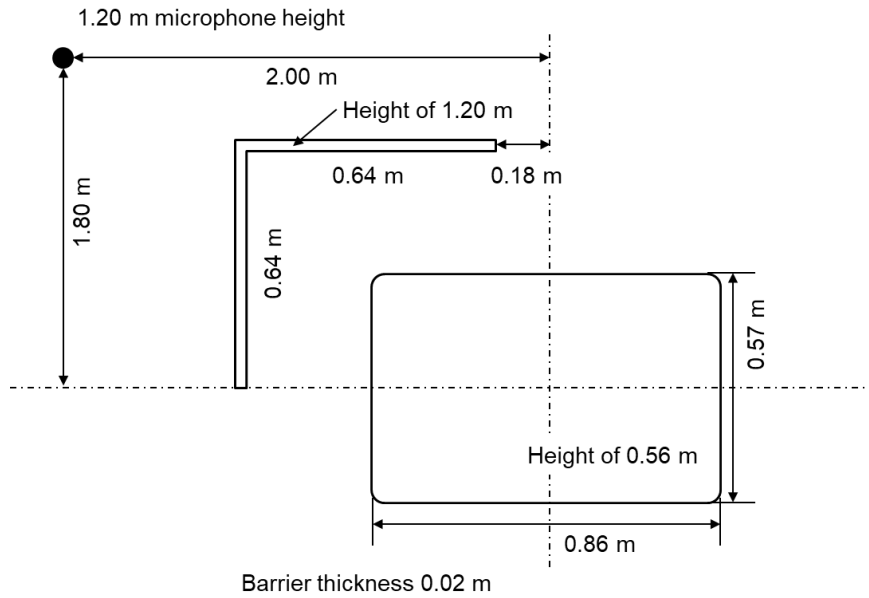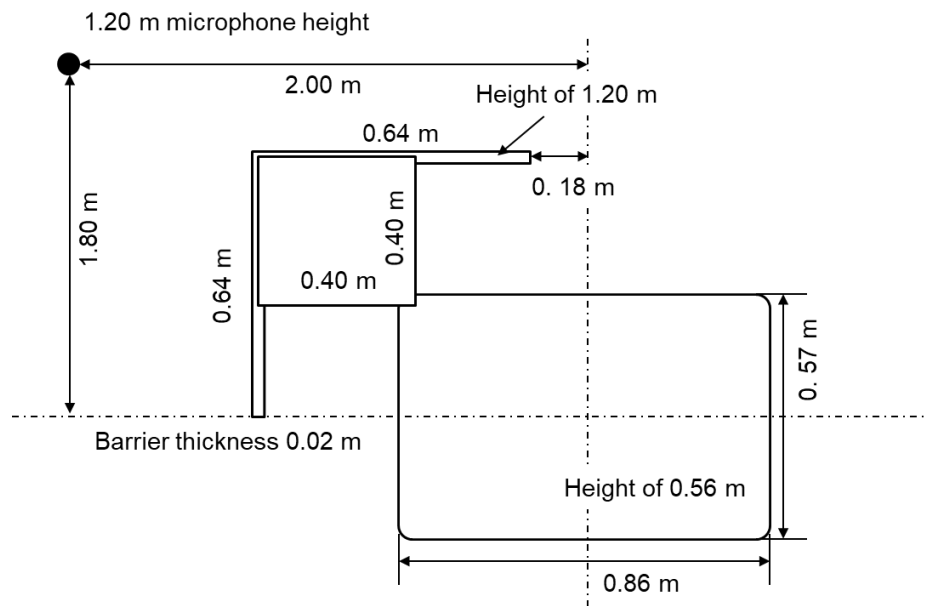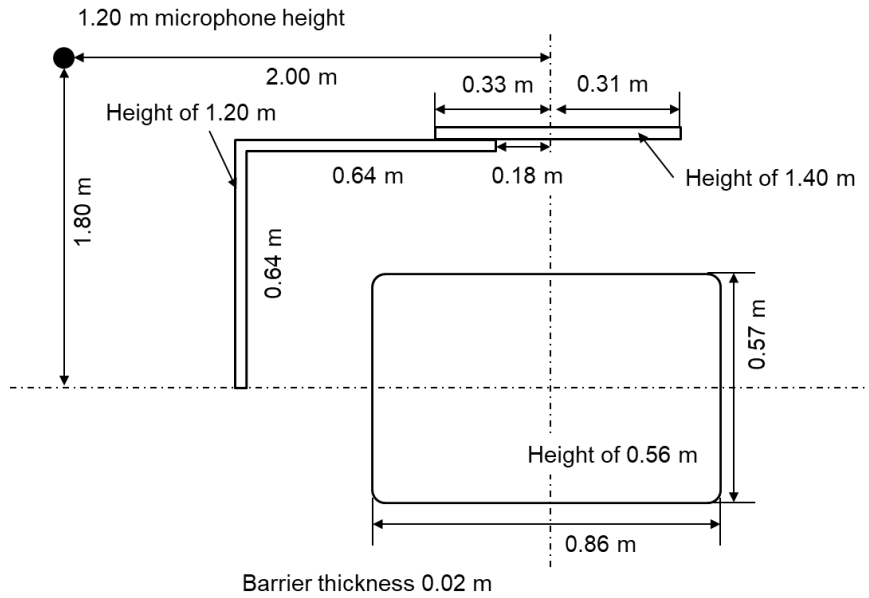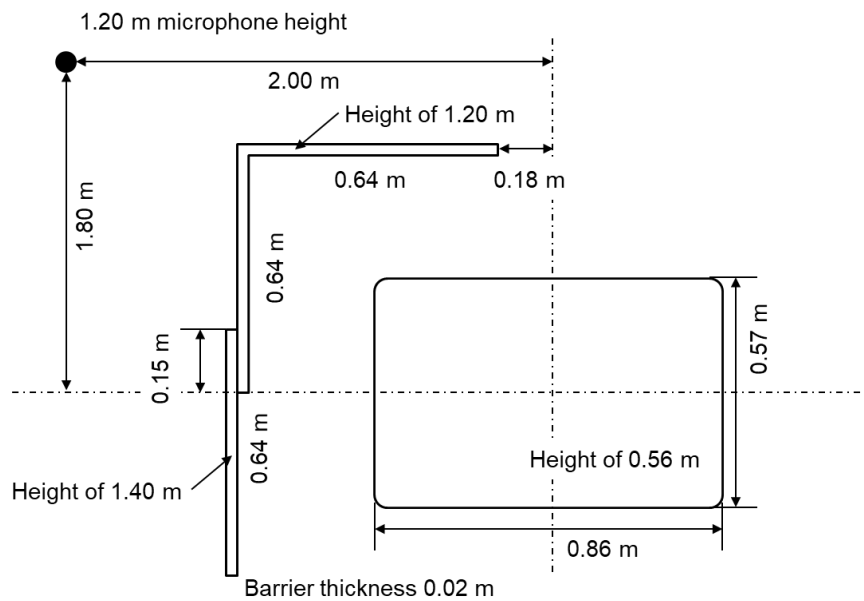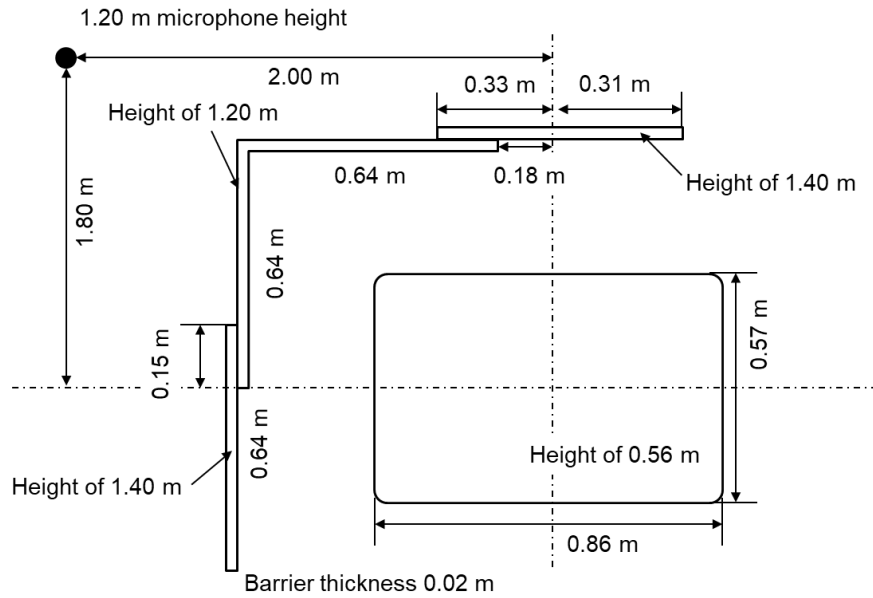
Figure A.7 Schematic showing dimensions for barrier Treatment 7 (all dimensions are in m)
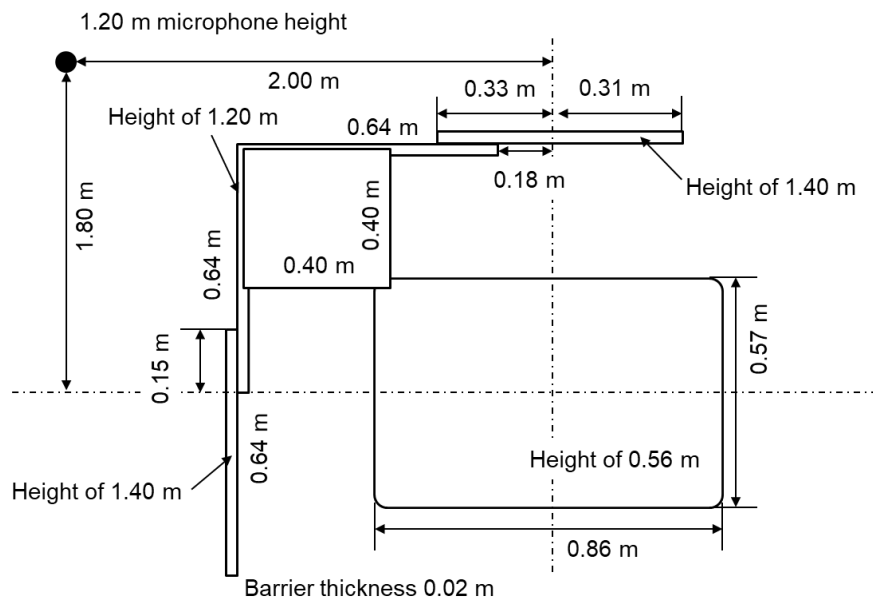
Figure A.8 Schematic showing dimensions for barrier Treatment 8 (all dimensions are in m)

REFERENCES

Anderson, K. and Gaston, K. J., "Lightweight Unmanned Aerial Vehicles will Revolutionize Spatial Ecology," Frontiers in Ecology and the Environment, vol. 11, no. 3, pp. 138146, Apr, (2013).

ANSI/ASA S1.26, "American National Standard Methods for Calculation of the Absorption of Sound by the Atmosphere," (2014).

ASTM C384-04, Standard test method for impedance and absorption of acoustical materials by impedance tube method, (2016).

ASTM C423, Standard test method for sound absorption and sound absorption coefficients by the reverberation room method, (2009).

ASTM C522-03, "Standard Test Method for Airflow Resistance of Acoustical Materials," (2016).

ASTM C522-09, Standard Test Method for Airflow Resistance of Acoustical Materials, American Society for Testing and Materials, 2009.

ASTM E1050-12, "Standard Test Method for Impedance and Absorption of Acoustical Materials Using a Tube, Two Microphones and a Digital Frequency Analysis System," (1998).

Bai, M. R. and Lee, J., "Industrial Noise Source Identification by Using an Acoustic Beamforming System," J. Vib. Acoust 120(2), 426-433 (1998).

Berglund, B., Lindvall, T., and Schwela, D. H., "Guidelines for Community Noise," Guidelines for Community Noise, ed: OMS, (1999).

Bies, D. A., Hansen, C. H., and Howard, C. Q., "Engineering Noise Control," 5th edition, CRC Press. (2017).

Burleson, C., "Aviation Leadership, Economy and Security," Commercial Aviation: A New Era, Workshop hosted by the National Academy of Engineering, ed. A. Akay, G. G. Fleming, R. D. Hellweg, G. C. Maling, Jr., and E. W. Wood, (2017).

Cannard, M., Joseph, P., Kim, J. W., and Paruchuri, C. C., "Slitted leading-edge profiles for the reduction of broadband interaction noise: physical mechanisms and performance," 25th AIAA/CEAS Aeroacoustics Conference, 2019, p. 2511, (2019).

Chaitanya, P., "Aerofoil geometry effects on turbulence interaction noise," PhD Thesis, University of Southampton, UK, (2017).

Cheng, G., Herrin, D. W., Liu, J. and Stencel, J., "Determination of Acoustic Emissions using Panel Contribution Analysis and Scale Modeling," Applied Acoustics, Volume 155, Pages 63-74, (2019).

Chiariotti, P., and Martarelli, M., "Acoustic beamforming for noise source localization – Reviews, methodology and applications," Mechanical Systems and Signal Processing, Volume 120, 2019, Pages 422-448, (2019).

Cho, Y. T., Roan, M. J. and Bolton, J. S., "A comparison of near-field beamforming and acoustical holography for sound source visualization," Proceedings of the Institution of Mechanical Engineers, Part C: Journal of Mechanical Engineering Science, 223(4), pp. 819–834, (2009).

Comesaña, D. F., de Bree, H. E., and Dolores, E., "Helicopter cabin interior noise assessment using Scan & Paint Transfer Path Analysis," 38th European Rotorcraft Forum 2012, ERF 2012. 2. (2012).

Comesaña, D. F., Holland, K., Wind, J., and de Bree, H. E., "Comparison of inverse methods and particle velocity based techniques for transfer path analysis," In Acoustics 2012, (2012).

Cremer, L., and Heckl, M., "Structure Borne Sound -Structural Vibrations and Sound Radiation at Audio Frequencies," Second Edition, Springer-Verlag, (1987).

Croker, M.J., "Handbook of noise and vibration control," John Wiley & Sons, (2007).

de Bree, H. E., "The Microflown: An Acoustic Particle Velocity Sensor," Acoustics Australia, Vol. 31, No. 3, pp. 91-94, (2003).

de Bree, H. E., Basten, T., Tijs, E., and Voogdt, J., "Fast in-flight cabin interior sound source localization," (2007).

de Bree, H. E., "An overview of Microflown Technologies," Acta Acustica, 89, 163-172 (2003).

de Bree, H. E., Druyvesteyn, W. F., Berenschot, E., and Elwenspoek, M., "Three-Dimensional Sound Intensity Measurements Using Microflown Particle Velocity Sensors," In Proceedings of the IEEE International Conference on Micro Electro Mechanical Systems, 124-129, (1999).

d de Bree, H. E., and Basten, T., "Low sound level source path contribution on a HVAC," SAE Technical Paper 2008-36-0505, (2008).

de Bree, H. E., Leussink, P., Korthorst, T., Jansen, H. etc., "The Microflown: a novel device measuring acoustic flows," Sensors and Acuators A, Physical, vol. SNA054/1-3, 552-557, (1996).

de Bree, H. E., and Druyvesteyn, W., "A particle velocity sensor to measure the sound from a structure in the presence of background noise," Forum Acusticum Budapest 2005: 4th European Congress on Acustics, (2005).

de Bree, H. E., "The Microflown," Ph.D. thesis, ISBN 9036509262, 7 February (1997).

Dunn, I. P., and Davern, W. A., "Calculation of Acoustic Impedance of Multi-layer Absorbers," Applied Acoustics 19(5):321–334, (1986).

Fahy, F. J., "The Vibro-Acoustic Reciprocity Principle and Applications to Noise Control," Acustica, Vol. 81, pp. 544-558, (1995).

Fahy, F. J., "Some Applications of the Reciprocity Principle in Experimental Vibro-Acoustics," Acoustical Physics, Vol. 49, No. 2, pp. 217-229, (2003).

Farassat, F., and Succi, G. P., "A review of propeller discrete frequency noise prediction technology with emphasis on two current methods for time domain calculations," Topics in Catalysis, (1980).

Geerlings, A. C., Thompson, D. J., and Verheij, J. W., "Model-Based Acoustic Substitution Source Method for Assessing Shielding Measures Applied to Trains," Applied Acoustics, Vol. 62, pp. 979-1000, (2001).

Grosso, A., and Hake, W., "Fast Panel Noise Contribution Analysis on a Running Train," In 10ème Congrès Français d'Acoustique, (2010).

Gur, O., and A. Rosen., "Design of Quiet Propeller for an Electric Mini Unmanned Air Vehicle," Journal of Propulsion and Power 25 (2009): 717-728, (2009).

Hald, J. and Mørkholt, J., "Panel Contribution Analysis in a Vehicle Cabin using a Dual Layer Handheld Array with Integrated Position Measurement," SAE Int. J. Passeng. Cars – Mech. Syst. 2(1):1458-1469, (2009).

Hasheminejad, S. M., Chong, T. P., Joseph, P., and Lacagnina, G., "Effect of Leading-Edge Serrations on Trailing-Edge-Bluntness Vortex-Shedding Noise Radiation," 25th AIAA/CEAS Aeroacoustics Conference, 2019, p. 2437, (2019).

HEWLETT PACKARD, "Sound Power Measurements," Application Note 1230

Holland, K. R. and Fahy, F. J., "An area-integrating volume velocity transducer for vibroacoustic reciprocity applications in vehicles" (ISVR Technical Report, 267) Southampton, GB. University of Southampton 35pp, (1997).

Intravartolo, N., Sorrells, T., Ashkharian, N., and Kim, R., "Attenuation of Vortex Noise Generated by UAV Propellers at Low Reynolds Numbers," 55th AIAA Aerospace Sciences Meeting, (2017).

ISO 140-4:1998, "Acoustics - Measurement of Sound Insulation in Buildings and of Building Elements - Part 4: Field Measurements of Airborne Sound Insulation between Rooms," (1998).

ISO 10534-2, "Acoustics-Determination of sound absorption coefficient and impedance in impedance tubes - Part 2: Transfer-function method," (1998).

ISO 3745:2003, "Acoustics - Determination of Sound Power Levels of Noise Sources using Sound Pressure - Precision Methods for Anechoic and Hemi-anechoic Rooms," (2003).

Jacobsen, F., and de Bree, H. E., "A Comparison of Two Different Sound Intensity Measurement Principles," J. Acoust. Soc. Am., Vol. 118, No. 3, pp. 1510-1517, (2005).

Jacobsen, F., and Jaud, V. A., "Note on the Calibration of Pressure-velocity Sound Intensity Probes," Acoustical Society of America. Journal, 120(2), 830-837. (2006).

Jacobsen, F., "Sound field indicators: Useful tools," Noise Control Eng. J. 35, 37–46, (1990).

Karan, G., "Comparative Study and Design of Economical Sound Intensity Probe," Open Access Master's Report, Michigan Technological University, (2019).

Kim, B. S., Kim, G. J., and Lee, T. K., "The Identification of Tyre Induced Vehicle Interior Noise," Applied Acoustics, Vol. 68, pp. 134-156, (2007).

Kim, G. J., Holl, K. R., and Lalor, N., "Identification of the airborne component of tyre-induced vehicle interior noise," Applied Acoustics - APPL ACOUST. 52. 141-156. (1997).

Kloet, N., Watkins, S., and Clothier, R., "Acoustic signature measurement of small multi-rotor unmanned aircraft systems," International Journal of Micro Air Vehicles, 9(1), 3-14, (2017).

Liu, J., Zhou, L., and Herrin, D. W., "Demonstration of Vibro-Acoustic Reciprocity including Scale Modeling," SAE Noise and Vibration Conference, Grand Rapids, MI, May 16-19, Paper No. 2011-01-1721, (2011).

Lord Rayleigh, "Some General Theorems Relating to Vibrations," Proceedings London Mathematical Society, Vol. 4, pp. 357-368, (1873).

Lyamshev, L. M., "A Question in Connection with the Principle of Reciprocity in Acoustics," Soviet Physics Doklady, Vol. 4, pp. 406, (1959).

Lyamshev, L. M., "A Method for Solving the Problem of Sound Radiation by Thin Elastic Shells and Plates," Soviet Physics Acoustics, Vol. 5, pp. 122-124, (1959).

Mason, J. M., and Fahy, F. J., "Development of a Reciprocity Technique for the Prediction of Propeller Noise Transmission through Aircraft Fuselages," Noise Control Engineering Journal, Vol. 34, No. 2, pp. 43-52 (1990).

Malcolm J. Crocker, "Handbook of noise and vibration control," John Wiley and Sons, INC. (2007).

Marte, J. E., and Kurtz, D. W., "A Review of Aerodynamic Noise from Propellers, Roters, and Lift Fans," NASA, Jet Propulsion Laboratory, Technical Report 32-1462, (1970).

Mason, J. M., and Fahy, F. J., "Application of reciprocity technique for the determination of the contributions of various regions of a vibrating body to the sound pressure at receiver point," Proc. Inst. Acoust., 12 (part 1) 469-76, (1990).

McAuliffe, C., "The Influence of High Speed Air Flow on the Behavior of Acoustical Element," Master Thesis, Massachusetts Institute of Technology, (1950).

Microflown Ebook 4A Standard Calibration Techniques

Microflown Regular P-U Probe Specification Sheet

Nielsen, T. G., "A field calibrated real time system for intensity measurements," Proceedings of Inter-Noise 88, Avignon, France, 1988, pp. 123–126. (1988).

Ning, Z., Wlezien, R. W., and Hu, H., "An experimental study on small UAV propellers with serrated trailing edges," In 47th AIAA Fluid Dynamics Conference (p. 3813), (2017).

PCB PIEZOTRONICS, "Model 377B02, Precision Condenser Microphone Installation and Operating Manual,"

Putner, J., Lohrmann, M., and Fastl, H, "Analysis of the contributions from vehicle cabin surfaces to the interior noise," In Inter-Noise 2013, Innsbruck, Austria, (2013).

Schuring, D. J. "Scale Models in Engineering," Pergamon Press, (1977).

Self, R. H., "Propeller Noise," Encyclopedia of Aerospace Engineering, online published in Wiley Online Library, December 15, (2010).

Sinibaldi, G., Marino, L., "Experimental analysis on the noise of propellers for small UAV," Applied Acoustics 2013, (2013).

Tijs, E., Wind, J., and Comesaña, D. F., "Fast, High Resolution Panel Noise Contribution Method," SAE Technical Paper 2011-01-1594, (2011).

Wallin, H. P., Carlsson, U., Abom, M., Boden, H., and Glav, R., "Sound and Vibration," Stockholm, (2011).

Wolde, T. T. "Reciprocity experiments on the transmission of sound in ships," (Doctoral dissertation, Waltman), (1973).

Wolde, T. T., Verheij, J. W., and Steenhoek, H. F., "Reciprocity method for the measurement of mechano-acoustical transfer functions," Journal of Sound and Vibration, 42(1), 49-55, (1975).

Wolff, O., and Sottek, R., "Panel Contribution Analysis - An Alternative Window Method," SAE Technical Paper 2005-01-2274, (2005).

Wolff, O., "Fast panel noise contribution analysis using large PU sensor arrays," Inter-Noise, (2007).

Wu, S. F., "Analyzing panel acoustic contributions toward the sound field inside the passenger compartment of a full-size automobile," The Journal of the Acoustical Society of America 137, 2101, (2015).

van Honschoten, J. W., Krijnen, G. J. M., Svetovoy, V.B., de Bree, H. E., Elwenspoek, M. C., "Optimization of a two-wire thermal sensor for flow and sound measurements," MEMS Interlaken (2001).

Ver, I. L., and Beranek, L. L., "Noise and vibration control engineering principles and applications," 2th Edition, John wiley and sons, INC. (2006).

Verheij, J. W., "Inverse and Reciprocity Methods for Machinery Noise Source Characterization and Sound Path Quantification. Part 1: Sources," International Journal of Acoustics and Vibration, Vol. 2, No. 1, pp. 11-20, (1997).

Verheij, J. W., "Inverse and Reciprocity Methods for Machinery Noise Source Characterization and Sound Path Quantification. Part 2: Transmission Paths," International Journal of Acoustics and Vibration, Vol. 2, No. 3, pp. 103-112 (1997).

Xiang, H., and Tian. L., "Development of a Low-cost Agricultural Remote Sensing System Based on an Autonomous Unmanned Aerial Vehicle (UAV)," Biosystems Engineering, vol. 108, Issue 2, February 2011, Pages 174-190, (2011).

Zheng, J. H., Anderton, D., and Fahy, F. J., "Determination of Sound Transmission from an Engine Test Cell to a Control Room Using an Acoustic Reciprocity Technique," Inst. Mech. Engineers, London. Paper C487/037 (1994).

Zheng, J. H., Fahy, F. J., and Anderton, D., "Application of a Vibro-Acoustic Reciprocity Technique to the Prediction of Sound Radiated by a Motored IC Engine," Applied Acoustics, Vol. 42, pp. 333-346, (1994).

VITA

Gong Cheng was born in Anhui, China. He received his Bachelor's Degree in Physics from Jilin University, China in 2007, and obtained a Master's Degree in Acoustics from Jilin University, China in 2010. After graduation, he worked in China First Automotive Works (FAW), R&D Center for noise and vibration research on vehicle design.

In August 2012, he enrolled in the Ph. D program of vibration and acoustics in the Department of Mechanical Engineering at University of Kentucky. During his study, he published 1 journal article, 8 conference proceeding articles. Additionally, he has 1 journal article under review. In the year of 2019, he received the Leo Beranek Student Medal award from INCE-USA. He has been working at Tesla in California since 2019, engaged in noise and vibration design on electric vehicles.

Gong Cheng